A STUDY ON SINTERING BEHAVIOUR OF PRASEODYMIUM DOPED CERIA BASED SOFC ELECTROLYTES
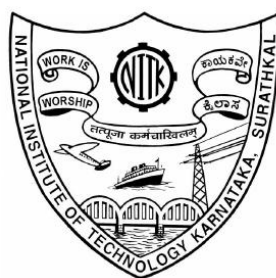
Thesis
Submitted in partial fulfillment of the requirements for the
degree of
DOCTOR OF PHILOSOPHY
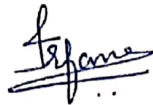
By
IRFANA SHAJAHAN

DEPARTMENT OF CHEMICAL ENGINEERING
NATIONAL INSTITUTE OF TECHNOLOGY KARNATAKA
SURATHKAL, MANGALURU-575025
March – 2021

DECLARATION

By the Ph.D. Research Scholar

I hereby *declare* that the Research Thesis entitled **A Study on Sintering Behaviour of Praseodymium Doped Ceria Based SOFC Electrolytes** which is being submitted to the **National Institute of Technology Karnataka, Surathkal** in partial fulfilment of the requirements for the award of the Degree of **Doctor of Philosophy** in **Chemical Engineering Department** is a *bonafide report of the research work* carried out by me. The material contained in this Research Thesis has not been submitted to any University or Institution for the award of any degree.

165070 CH16F02, IRFANA SHAJAHAN

Department of Chemical Engineering

National Institute of Technology Karnataka, India

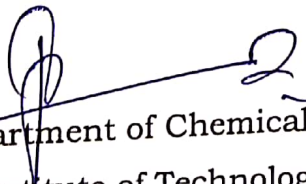Place: NITK-Surathkal

Date: 6 April 2021

CERTIFICATE

This is to *certify* that the Research Thesis entitled **A Study on Sintering Behaviour of Praseodymium Doped Ceria Based SOFC Electrolytes** submitted by **IRFANA SHAJAHAN** (Register Number: 165070 CH16F02) as the record of the research work carried out by her, is *accepted as the Research Thesis submission* in partial fulfilment of the requirements for the award of degree of **Doctor of Philosophy**.

Dr. Hari Prasad Dasari

Associate Professor

Research Guide

Chairman - DRPC

Department of Chemical Engineering

National Institute of Technology Karnataka, India

HEAD OF THE DEPARTMENT
CHEMICAL ENGINEERING
National Institute of Technology Karnataka, Surathkal
P.O. Srinivasnagar - 575 025, D.K., Mangalore

ACKNOWLEDGEMENTS

Dedication

To my family, my teachers, and my friends

ABSTRACT

The present study explores the sintering kinetic behaviour of the Praseodymium doped ceria (PDC, $Ce_{0.9}Pr_{0.1}O_2$) based Solid Oxide Fuel Cell (SOFC) electrolyte materials synthesized by various methods like the EDTA-citrate method, Microwave assisted co-precipitation method (using solvents like ethanol, water and iso – propyl alcohol) and room temperature co-precipitation method and are characterized by X- Ray Diffraction (XRD), Raman Spectroscopy, Scanning Electron Microscopy (SEM), Transmission Electron Microscopy (TEM) analysis and Dilatometer studies. By synthesis approach, the sintering temperature of the PDC electrolyte materials is drastically decreased from 1500°C to 1100°C by achieving unimodal shrinkage rate behaviour at a much lower temperature from 1460°C to 765°C and successfully achieved single-phase cubic fluorite PDC solid-solution. Two sintering models (Constant Heating Rate (CHR) method and Dorn method) were successfully implemented to identify the mechanism for early stages of sintering and found that grain boundary diffusion mechanism (m ~ 2) is dominating in PDC pellets synthesized by the MWCOP-ISP method. The effect of liquid additives such as Li, Co, Fe and Mg on the sintering kinetic behaviour of PDC pellets synthesized by MWCOP-ISP is further studied and decreased the sintering temperature from 1100°C to 850°C with the Li liquid additive as a sintering aid. The two sintering models further suggested that the Li-PDC pellets also follow the grain boundary diffusion model (m ~ 2) during the early stages of sintering. The 10PDC, 1Li-PDC, 3Li-PDC, 3Co-PDC, 3Fe-PDC and 3Mg-PDC nano-structured samples exhibited a thermal expansion co-efficient of 15.3×10^{-6} / °C, 18.2×10^{-6} / °C, 14×10^{-6} / °C, 15.2×10^{-6} / °C, 13.8×10^{-6} / °C and 15.7×10^{-6} / °C respectively.

Keywords: Praseodymium doped ceria; Sintering additives; Sintering mechanism; Solid oxide fuel cells; Dilatometer; Solid oxide electrolyte

TABLE OF CONTENTS

LIST OF FIGURES

LIST OF TABLES

ABBREVATIONS

Abbreviation	Description
a	Lattice constant
ASR	Area Specific Resistance
BET	Brunauer–Emmett–Teller
COP	Co-Precipitation
CHR	Constant Heating Rate
d	Interplanar distance
D	Crystallite size
E_a	Activation Energy
EDTA	Ethylenediaminetetraacetic acid
EDS	Energy Dispersive x-ray Spectroscopy
GDC	Gadolinium Doped Ceria
HT	High Temperature
ISP	Iso-Propyl Alcohol
IT - SOFCs	Intermediate Temperature Solid Oxide Fuel Cells
LT	Low Temperature
MIEC	Mixed Ionic Electronic Conductor
MWCOP	Microwave Assisted Co-Precipitation Method

(Cont.)

NDC	Neodymium Doped Ceria
OCV	Open Circuit Voltage
PDC	Praseodymium Doped Ceria
Pr	Praseodymium
RE	Rare Earth
RTCOP	Room Temperature Co-Precipitation Method
SDC	Samarium Doped Ceria
SEM	Scanning Electron Microscopy
SOFCs	Solid Oxide Fuel Cells
SOECs	Solid Oxide Electrolysis Cells
CTE	Coefficient of Thermal Expansion
TEM	Transmission Electron Microscopy
TGA	Thermogravimetric analysis
TMO	Transition Metal Oxide
TPB	Triple Phase Boundary
XRD	X-ray Diffracion
YC	Young Cutler
YDC	Yttrium Doped Ceria
YSZ	Yttrium Stabilized Zirconia

(Cont.)

ε	Lattice strain
ϕ	Degree of agglomeration

UNITS AND NOTATIONS

Symbol	Description
%	Percentage
°C	Degree celsius
F	Faraday Constant
Å	Armstrong
a.u.	Arbitratry unit
dL/L_0	Linear Shrinkage
dL/dt	Shrinkage Rate
e^-	Electrons
i	Current Density
$V_o^{\cdot\cdot}$	Oxygen Ion Vacancy
S/cm	Siemens Per Centimeter
m^2/g	Square meter per gram
min	Minutes
h	Hours
σ	Ionic Conductivity
nm	Nanometer
θ	degree

(Cont.)

λ	Wavelength
μm	Micrometer

CHAPTER 1

INTRODUCTION

1.1. BACKGROUND

Global energy demand has been increasing continuously due to increasing industrialization and population and is expected to double by 2050 (Gadonneix et al. 2013). This growing energy demand is problematic as the production methods pose large environmental issues. Most of the power generation methods are mainly based on the combustion of fossil fuels that cause emission of carbon dioxide and other air pollutants into the environment. One of the major challenges is to confine the global temperature rise below 2ºC by reducing greenhouse gas emissions. Increasing greenhouse gas emissions, energy crisis and climate change has been forced to find an alternative power generation source with high efficiency and minimal environmental impact (Upadhyaya et al. 2004). Fuel cells are considered to be the promising alternative energy source to replace the fossil fueled engines (Welaya et al. 2011).

A fuel cell is a ceramic electrochemical reactor that converts a gaseous fuel to electrical energy and heat with high conversion efficiency and low environmental impact, especially for hydrogen-fuelled fuel cells; where, the final product is electricity, heat, and water (Badwal and Foger 1996; Ruiz-Morales et al. 2011). Fuel cell offers a high-efficiency power generation mechanism when compared to other conventional energy production mechanisms, where the chemical energy of fossil fuel is converted to electrical energy after several steps that involve energy losses. The energy efficiency of a fuel cell is generally between 40–60%, or up to 80% efficient in cogeneration if waste heat is captured for use, which is higher than diesel or gas engines (Arsalis 2008).

The main component of the fuel cell system includes a dense electrolyte membrane in contact on both sides with two porous electrodes, cathode and anode. Fuel is oxidized at the anode to form positive ions which pass through the electrolyte and react with O_2 to give water as a product while at cathode oxidant is reduced by accepting electrons from the external circuit. The ionically conducting and electrically insulating electrolyte facilitates the transport of charged species. The fuel cell can produce electricity, as long as the fuel is supplied (Kalra et al. 2015).

Fuel cells are categorized based on the electrolyte materials used mainly, Molten Carbonate Fuel Cell (MCFC), Alkaline Fuel Cell (AFC), Phosphoric Acid Fuel Cell (PAFC), Polymer Electrolyte Membrane Fuel Cell (PEMFC), and Solid Oxide Fuel Cell (SOFC). Low-temperature fuel cells that operate below 300ºC include PEMFC, AFC, PAFC, and high-temperature fuel cells that operate above 600ºC, include MCFC and SOFC. There is an increasing trend in reducing the operating temperature of SOFC to develop Intermediate Temperature SOFCs (500ºC – 700ºC) to avoid material degradation problems (Murray et al. 1998). Hence, improvements in the design of existing materials and cells are extensively investigated to obtain better performance at an intermediate temperature. The merits of high-performance IT - SOFCs is currently the topic for more research and development (Bonamartini Corradi et al. 2006; Chen et al. 2007).

Among the different types of fuel cells, SOFCs exhibit higher conversion efficiency, fuel adaptability, promotes internal reforming, and non-precious catalyst materials for electrodes can be used as they operate at high temperatures (Stambouli and Traversa 2002). Therefore, IT- SOFCs has attracted many researchers to shift their studies to renewable and clean energy generation. The present research work is related to the development of electrolyte material for the application of Intermediate Temperature SOFCs (IT - SOFCs).

1.2. SOLID OXIDE FUEL CELLS

Solid oxide fuel cells (SOFCs) are mainly characterized by oxide ion-conducting ceramic compound known as the electrolyte material, usually metal oxide. The main components of SOFC include a gas-tight dense electrolyte membrane, a cathode, and an anode. At the cathode side (air electrode), oxidant (oxygen in the air) is reduced to oxide ions. The difference in oxygen chemical potential between fuel and air is the driving force for these oxides, pass through the oxide ion-conducting electrolyte and react with fuel (H_2) at the anode (fuel electrode) to form water and liberate electrons. The electrons flow through an external circuit between anode and cathode, producing a continuous electric current as long as fuel and oxidant are supplied (Stambouli and Traversa 2002).

The half-cell reactions (Ravi Chandran and Arjunan 2015) occurring at the electrodes when hydrogen is used as fuel can be expressed as:

Cathode Reaction:

$$\frac{1}{2}O_2 + 2e^- \rightarrow O_2^-\qquad\qquad(1.1)$$

Anode Reaction:

$$H_2 + O_2^- \rightarrow H_2O + 2e^-\qquad\qquad(1.2)$$
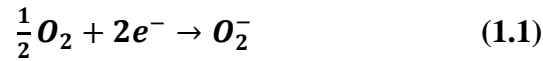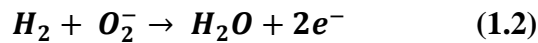
The overall cell reaction is

$$H_2 + \frac{1}{2}O_2 \rightarrow H_2O\qquad\qquad(1.3)$$
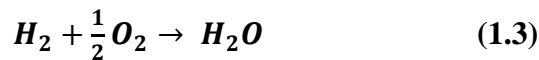
Where, O_2^- is the oxygen ion in the electrolyte.

One of the important features of SOFC is fuel adaptability, i.e., without external reforming, hydrocarbons, CO, bioethanol, etc. can be used as fuels (Lu et al. 2002). The high operating temperature of SOFC allows the internal reforming of the fuels.

The electromotive force (emf) generated by the electrochemical cell as a function of the ideal standard open circuit potential (E°) given by the Nernst equation (Chakraborty 2018),

$$\mathbf{E_{emf}} = \mathbf{E}° + \frac{RT}{nF} \ln \left(\frac{P_{H2}\, P_{O2}^{0.5}}{P_{H2O}} \right) \qquad (1.4)$$

Where, F is Faraday's constant, n is the number of electrons, R is the gas constant, T is the operating temperature, and P_{H2}, P_{O2}, P_{H2O} represents oxygen partial pressures in the cathode air and anode fuel electrodes, respectively.

Equation 1.4 describes the system is under equilibrium conditions. The actual voltage of a SOFC (V) is affected by polarisation losses associated with the cathode (η_c) and the anode (η_a), as demonstrated by **Equation 1.5**

$$\mathbf{V} = \mathbf{E_{emf}} - \mathbf{IR} - \mathbf{\eta_c} - \mathbf{\eta_a} \qquad (1.5)$$

Where E_{emf} is the Nernst potential of the reactants, I is current, R is the ohmic resistance, and η_c and η_a are the cathodic and anodic polarization losses.

The three types of irreversible losses that cause deviate from the ideal performance can be broken down into various resistances caused by activation polarisation, ohmic polarization, and concentration polarization (Kalra et al. 2015).

Activation polarization refers to the voltage loss accounting for the activation energy to make or break chemical bonds at both the cathode and anode. It dominates at low current density region where the activation energy barrier for the reactions is greater. At the electrode surface, the rate of the electrochemical reaction is controlled by kinetics. The chemical energy barrier must be overcome to promote the reactions. At the cathode, the activation polarisation is much higher than the one on the anode because the cathode facilitates the dissociation of the oxygen molecules to oxygen ions and transport the

oxygen ion, simultaneously. For IT-SOFCs, activation polarisation is one of the most significant voltage losses due to their higher operation temperature

The ohmic overpotential is due to the resistance to the flow of ionic and electronic charge carriers, in the electrolyte, the electrodes, the interconnect plates, and the external circuit. The electrolyte resistance typically dominates the ohmic resistance and can be reduced by decreasing the thickness of the dense electrolyte or by enhancing the ionic conductivity of the dense electrolyte. The ohmic resistance decreases with an increase in operating temperature. Ohmic polarization is described by Ohm's law (Barbir 2013) and is expressed as

$$\eta_{ohm} = IR, R = (R_{el} + R_i + R_c) \tag{1.6}$$

Where, R_{el}, R_i, and R_c represents the resistance of the electrodes, the solid electrolyte, and the electrode-electrolyte contact, respectively.

Concentration polarization is the voltage loss to diffusion limitations in the electrodes at high current densities because the formation of product water and excess humidification will block the reaction sites. The diffusion of gas from gas channels to the electrodes, diffusion of reactants to the triple-phase boundary through the electrodes, and diffusion of product away from the electrolyte interface are the three principal sources of the concentration polarization. By using thinner electrodes with high surface areas, the concentration polarisation was minimized as this shortens the gas diffusion paths to the reaction sites (Shimada et al. 2016).

1.3.   MATERIALS FOR SOFCs

1.3.1   Anode Materials

The anode in SOFC facilitates the electrochemical oxidation of the fuel, fuel gas diffusion, and transport of by-products of the electrochemical reaction and transport of electrons to the external circuit. Therefore, the anode material should follow the following basic requirements (Jiang San Ping and Hwa Chan 2004; Tsipis and Kharton 2008; Zhu and Deevi 2003) :

1) Mixed electronic and ionic conductivity

2) Stability in reducing environment

3) TEC comparable to other components

4) Porous structure and

5) High electrocatalytic activity

Among the transition metals, Nickel (Ni) is considered as the best choice for anode material since it exhibits the highest catalytic activity for H_2 oxidation (Ravi Chandran and Arjunan 2015; Setoguchi et al. 1992) and is cheaper when compared to other noble metals. The low melting temperature, higher sinterability of Ni, and performance degradation of fuel cells are the limitations to use Ni alone as the anode material (Prakash et al. 2014). Ni/ 8mol%YSZ (Ni – 8YSZ) cermets are the most commonly used anode materials. The YSZ is an ionic conductor and facilitates the transport of ions from electrolytes, thereby extend the triple-phase boundary (TPB). Direct exposure to hydrocarbon fuels leads to the deposition of carbon in the anode, which would give rise to the performance degradation of the fuel cell on repeated use (Koh et al. 2002). Cu–Ni, Cu–Co metal alloys were used with YSZ as an alternative cermet anode to overcome this limitation (Hari Prasad et al. 2009; Prasad et al. 2011, 2012a; Venugopal et al. 2007).

1.3.2   Cathode Materials

The role of the cathode in SOFC is a reduction of oxidant, transport of oxygen ion to the electrolyte, to provide sufficient thermal and chemical stability at high-temperature in air.

It should have high electronic and ionic conductivity. Cathode operates in an oxidizing environment of air involves in the oxygen reduction reaction (ORR) and is manufactured as a porous structure to facilitate the transport of molecular oxygen from the gas phase to the air electrode/electrolyte interface.

Numerous oxide materials have been studied as cathode materials for SOFC. Lanthanum manganese oxide doped with strontium (LSM) based perovskite was widely used for SOFC cathodes (Jiang 2008). LSM is found to be an electronic conductor and show appreciable ionic conductivity only at high overpotentials (Skinner and Kilner 2003). $LaMnO_3$ is an intrinsic p-type conductor, and the electronic conduction arises due to the small polaron hopping of an electron-hole between the 3+ and 4+ valence states of manganese, the maximum electronic conductivity was obtained for x = 0.5 (Jiang 2008). The ORR is strictly limited to the electrolyte - electrode - air triple-phase boundary (TPB) in LSM cathode where oxygen-reduction reactions on mixed-conducting electrodes with high enough ionic conductivity can occur along the entire cathode surface (An et al. 2010).

Other cathode materials investigated include Lanthanum cobaltite, $LaCoO_3$, and Lanthanum manganite, $LaMnO_3$, based perovskites (Adler 1998; Jiang 1998) and the other alternatives include Gd-based perovskites and the compositions $Sm_{1-x}Sr_xCoO_{3-\delta}$ (SSCs), which can operate at temperatures as low as 500°C (Skinner and Kilner 2003).

1.3.3 Electrolyte Materials

Electrolyte, an ion-conducting ceramic, is the principal component of SOFC. The electrolyte material is the component of the fuel cell responsible for ion transportation between electrodes, for the separation of the reacting gases, and the internal electronic conduction blocking, forcing the electrons to flow through the external circuit (Laosiripojana et al. 2009). For satisfactory performance, requirements of electrolytes include (Arunkumar et al. 2012):

1) High oxide-ion conductivity at the operating temperature

2) Negligible electronic conduction

3) High density to promote gas impermeability

4) Thermodynamic stability over a wide range of oxygen partial pressure

5) Compatibility with electrodes and other cell materials

6) Negligible chemical interaction and comparable thermal expansion coefficient (TEC) with other components

The operating temperature of SOFCs is determined by the temperature required to achieve sufficient ionic conductivity in the electrolyte. High oxygen ionic conductivity is exhibited by fluorite related structures with the general formula of AO_2, where A is a tetravalent cation (Inaba and Tagawa 1996). This structure is a face-centered cubic arrangement of cations with anions occupying all the tetrahedral sites, leading to a large number of octahedral interstitial voids. Thus, the structure is a rather open one, and rapid ion diffusion might be expected (Singhal and Kendall 2003).

Popular oxide electrolyte materials include zirconia-based oxides, ceria-based oxides, lanthanum gallate-based oxides, and bismuth-based oxides (Ishihara et al. 2006; Kharton et al. 2004). Zirconia (ZrO_2) stabilized with yttrium known as yttrium-stabilized zirconia (YSZ) is considered a state of art material used as electrolyte material in SOFC, which has a high ionic conductivity at high temperature. Application of doped ceria materials is of particular interest for potential use in intermediate and low-temperature SOFC due to a higher ionic conductivity to stabilized zirconia and a lower cost in comparison with lanthanum gallate-based phases (Kharton et al. 2001). Ceria-based electrolytes have higher ionic conductivity than YSZ at a lower temperature due to its lower activation energy for oxide ion migration (Hui et al. 2007). Sr^{2+}, Mg^{2+} doped $LaGaO_3$ (LSGM) are other class of electrolyte material which has higher conductivity than YSZ and doped ceria. Nevertheless, the drawback of this electrolyte is the difficulty in obtaining pure single-phase LSGM, Ga evaporation at low-oxygen partial pressure, and is expensive than ceria-based electrolytes.

As the solid electrolyte is the most important component in solid oxide fuel cell device, considerable effort has been directed towards the identification of novel materials for oxide ion conduction, as discussed above. Rigorous operating regimes mean that few materials have the appropriate set of electrical, chemical, and mechanical properties to produce a successful material that can compete with the established electrolytes. One of the main drawbacks of doped ceria-based electrolyte materials is the use of very high sintering temperatures (above 1500°C) to obtain highly dense and single-phase ceramic samples when the solid-state reaction method is used. For the practical application of SOFC electrolyte material, it is essential to fabricate a dense (> 90%) electrolyte layer at processing temperatures below 1300°C to minimize undesired reactions with other components as well as fabrication costs of LT-SOFCs (Joh et al. 2016). Hari Prasad et al. (2010) reported the synthesis of nano-crystalline GDC powders with a relative density of 97% at a lower sintering temperature of 950°C (Hari Prasad et al. 2010). High sintering temperature does not allow co-firing of doped ceria with the adjoining cell components, causes high energy costs. The lower- sintering temperature offers the possibility for obtaining ceramics with submicron grain size since conventional solid-state reaction usually results in the coarsening of the grains (Fergus et al. 2009). Apparent grain boundary conductivities and calculated true grain boundary conductivities were significantly higher for sub-micron grain size (Christie and Van Berkel 1996).

Therefore, the recent trend of SOFC operation at intermediate temperatures is to obtain less demanding operating conditions to reduce the constraints on materials selection. To reach this goal, significant experimentation is required to achieve better stability of new electrolyte materials with high density (>90%) for its use in LT/ IT – SOFCs.

1.4.   SINTERING

Sintering is the heat treatment step in the formation of a ceramic where the powder is converted into dense solids. The driving force for densification or sintering is mainly due to the reduction in the surface free energy of the sintering compact in the system. The objective of sintering studies is to understand the influence of powder properties such as particle size and surface area temperature, composition, and sintering atmosphere on the microstructure produced, which defines the desired properties of the material.

Solid-state sintering is divided into three idealized stages, described in terms of the microstructure and the dependence of the relative density of the ceramic material on the sintering time is shown in **Figure 1.1**. The three stages of the sintering are characterised by the microstructure of the ceramic material and are described as follows: (Gupta 1971)

1) In the initial stage, powder particles grow together, and sharply concave necks are formed between the individual particles, and rearrangement of the particle occurs at this stage. The shift of the curvature gradient from covex to concave which directs the mass flow is the driving force of sintering at this stage. During the initial stages of sintering, the sharp curvature gradients will be reduced.

2) In the intermediate stage, the interpenetrating network of solid particles and pores is formed. This stage is considered valid to 90 – 95 % density, hence covers most of the densification process. Grain growth (coarsening) becomes significant at this stage. The elimination/ decrease in the surface energy is the driving force of sintering at this stage.

3) In the final stage, pores break down into closed voids as the sintering proceeds. The pores are assumed to shrink during this stage and finally leads to the closure of the pores together which leads to the 100% theoretical density of the material. There is a decrease in the surface area and the gradient of curvature at the final stage of sinteing which leads to a slower rate of sintering during the final stage. For a polycrystalline ceramic to be

considered highly dense for electrolyte applications, a relative density greater than 95% is required i.e., when there is no remaining open porosity.

Vapour diffusion, surface diffusion, grain boundary diffusion, dislocation motion and lattice diffusion are the several mechanisms involved in the sintering of crystalline materials. Solid vapour interface between spherical particles with high surface energy will transfer between particles in contact with one another with the application of heat energy. Vapour diffusion, surface diffusion, and lattice diffusion leads to neck growth and coarsening of the particles without densification. Grain boundary diffusion to the pores causes deformation of the particle and permits neck growth, which will lead to the formation of grain boundaries having lower energy than the particle surface (Gupta 1971).
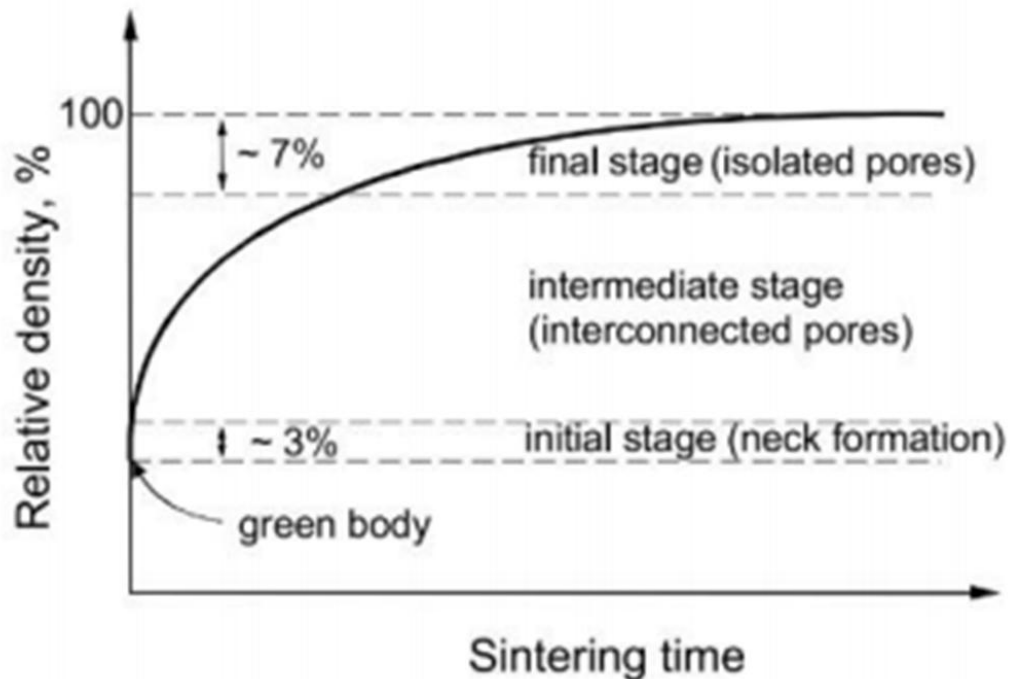
Figure 1.1: Schematic diagram of solid state sintering (Gupta 1971)

Most of the porosity is removed in the densification stage as the interstitial vacancies migrate to the grain boundaries. Thus, sintering is considered an effective process to

reduce porosity and enhances properties such as electrical conductivity, strength, translucency, and thermal conductivity. Using sintering, very high levels of purity and uniformity in starting materials are obtained, even controlled, and uniform porosity among materials is observed. The final stage of sintering involves grain growth and the overall reduction of the grain boundary. Atoms or ions diffuse less than an interatomic distance to new positions resulting in grain growth. The homogeneity of the green body is a significant factor to be considered during sintering. Uneven shrinkage during the sintering process creates enormous stress within the green body and leads to rapid propagation of a crack during thermal treatment (Kuczynski 1956; Rahaman 1996).

The study on grain growth and the densification is important inorder to obtain the excellent sintering behaviour of the ceramic material. The grain boundary diffusion mechanism is an important mechanism for the densification process. The grain boundaries that are formed with in the neck area (interparticle) results in the mass flow of the material with an activation energy (intermediate) between the volume diffusion and surface diffusion. According to the grain boundary diffusion model, the mass (along the grain boundary) is deposited on the neck surface and the densification proceeds as the atoms move along the grain boundary. It was reported that the grain boundary diffusion mechanism is the most dominant mechanism in most of the ceramics, metals and other compounds (Kuczynski 1956). There are only few reports that has mentioned in the literature about the sintering mechanism and the activation energy for the early stages of sintering in doped ceria based materials. Therefore, one of the goal of the present work is to identify the sintering mechanism of PDC for the initial stages of sintering and to calculate the activation energy of sintering process.

In a SOFC, the co-sintering/ co-firing of the entire unit cell reduce processing times and cost and are very difficult to accomplish. The electrolyte layer must be dense to perform its functions. On the contrary; the electrodes must be porous, and each component of the unit cell requires different microstructures to perform their functions, leading to high-temperature processing to complete all three sintering stages. At high processing

temperature, undesired migration of electrode materials through the electrolyte interface, which adversely affects the functional properties of the materials, in turn, leads to the degradation of the cell's electrochemical performance, which is the main drawback of high-temperature processing.

Liquid phase assisted sintering is another method used for reducing the sintering temperature of a ceramic material. The sintering additive will form a grain boundary liquid phase when it is heated, assuming that the liquid fully wets the solid surfaces, separates the particles by a liquid bridge, and also results in the formation of pores within the liquid. The grain boundary liquid phase will provide a pathway for transport of the matter and reduce interparticle friction. The driving force for densification is the reduction in the liquid/vapour interfacial area (German et al. 2009).

Figure 1.2 represents the schematic of the microscopic evolution in the liquid phase sintering. Firstly, the densification of the liquid phase sintering is influenced by the particle size, liquid content and the solubility. Smaller particle size enable the full densification at lower temperature or in a shorter sintering time. Three overlapping events namely rearrangement, solution precipitation and solid state sintering occurs during the liquid phase sintering process. The three overlapping stages described are as follows: (German et al. 2009)

1) In the initial stages of sintering, after the formation of liquid, rearrangement of the particle occurs. The liquid will wet the surface of the particles and the capillary stress created causes a greater rearrangement of the particles at this stage and will continue till a stable configuration is attained.

2) Densification by solution precipitation involves the diffusion of material at solid/ vapour interface and the precipitation of the material on the particles, with higher and lower chemical potential respectively.

3) Densification by solution precipitation is followed by Ostwarld Ripening. The densification at this stage is slow due to the microstructure coarsening (results in increase in the diffusion distance).
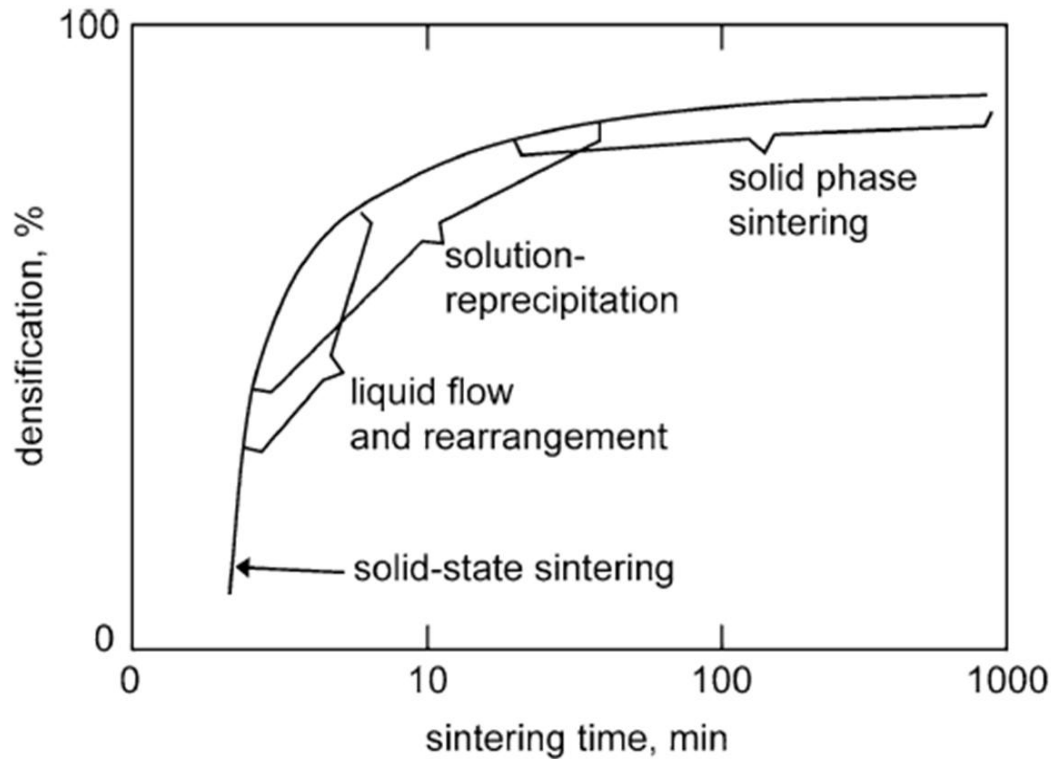
Figure 1.2: Schematic diagram of the microscopic evolution in the liquid phase sintering (German et al. 2009)

1.5.   SCOPE AND OBJECTIVE

The advantages of lowering the operating temperature of SOFCs have attracted considerable interest worldwide inorder to avoid material degradation problems. The high operating temperature posses various challenges such as an increase in the fabrication cost of the cell, poor chemical compactibility of the electrode and electrolyte, difficulty in the selection of proper sealents and interconnects and inter-diffusion between the electrode-electrolyte interlayer at high temperature which causes the degradation of the stack. One of the significant barriers to decrease the operating temperature is the ohmic loss of the electrolyte. Emphasis is placed on the approach to reduce the operating temperature of SOFCs and increase the performance of electrolyte material in IT range by developing new electrolyte material. Several advantages are obtained with the reduction in operating temperature which includes; they are less exposed to thermal and mechanical stress, a wide range of materials selection, short start-up time, easy maintenance, better thermal management, and much more economical, reduced effect of thermally activated processes. Researches have shifted towards the development of LT/ IT- SOFCs to make SOFCs commercially available.

High sintering temperature (~1500°C) to obtain fully dense material is one of the drawbacks of ceria based electrolyte materials. The high sintering temperature of the electrolyte material results in a rapid grain growth which leads to poor mechanical stability of the material. Therefore, one of the critical challenges that the SOFC electrolytes have is their poor densification behaviour and to obtain fully dense electrolyte; the sintering temperature has to be raised to 1500°C (cerai based electrolyte material) depending on the material system. The high sintering temperature could also result in several other disadvantages such as partial reduction of Ce^{4+} to Ce^{3+}, undesirable chemical expansion, high energy cost, and failure of co-firing with other SOFC components, phase diffusion and chemical interaction between the components which in turn affect the electrochemical performance of the cell. The ceria based materials at high sintering temperatures above 1500°C results in the partial reduction of ceria which leads

to the deteriorated properties of the cell; therefore it is necessary to reduce the sintering temperature in order to develop highly dense and high performance electrolyte material. Decreasing the sintering temperature of electrolytes would greatly facilitate the fabrication technique since the electrolyte can be co-fired with the electrodes without changing their microstructures much at relatively low temperatures. As a result, it is needful to reduce the sintering temperature since the electrode materials are sintered at a lower temperature compared to that of the electrolyte material.

Enhanced densification kinetics and overall sinterability of the electrolyte at lower sintering temperature can be achieved by controlling the nano-particle size and choosing suitable sintering aids. However, most of the studies decreased the sintering temperature down to 1200°C by either controlling the particle size or choosing suitable sintering aids. The emphasis of the current work is to put on the effect of decreasing the sintering temperature of the PDC electrolyte material to reduce the fabrication cost, which also provides better reliability, portability and operational life.

Therefore, the scope of the present work is to synthesize praseodymium doped Ceria (PDC) based electrolyte materials and to study the sintering behaviour of the as-synthesized metal oxides. The variation in the shrinkage behaviour of PDC material with the dopant addition is analyzed.

The specific objectives of the present study are:

1. Synthesis of Praseodymium doped ceria electrolyte material for IT-SOFCs using various synthesis methods.

2. Study of physical characteristics of Praseodymium doped ceria nano-crystallites using X-ray diffraction, Raman spectroscopy, SEM with EDS, and TEM to find the phase, nature, agglomerate nature, and nano-particle size.

3. To study the multi dopant effect (Liquid sintering aid dopants) in Praseodymium doped ceria based material.

4. To study the dilatometric and shrinkage behavior of the as-synthesized Praseodymium doped ceria electrolyte membrane.

5. To reduce the sintering temperature of the as-synthesized nano-powder by adding suitable dopants by varying the synthesis methods to $< 1000°C$.

1.6.   ORGANIZATION OF THE THESIS

The rest of the thesis is organized as follows:

Chapter 2 provides the literature review of various electrolyte materials that are used for SOFC applications. Co-doped and doubly co-doped ceria based electrolyte materials for SOFCs that were previously reported are also reviewed in this section. The effect of transition metal oxide doping and the mechanism for initial stages of sintering is also discussed in this chapter.

Chapter 3 contains the methodology and the methods that are adopted for the synthesis of PDC electrolyte material, characterization techniques that are used, and the sintering conditions of the samples.

Chapter 4 explains the synthesis of PDC electrolyte material by EDTA – citrate method and the nature of solubility of praseodymium ceria solid solutions with an increase in heat-treatment temperature from 800°C to 1200°C. The chapter discuss the reason for the high sintering temperature of the prepared PDC sample, formation of solid solution of PDC material and the phase stability studies of the PDC sample.

Chapter 5 deals with the effect of the synthesis methods (Microwave-assisted co-precipitation method using different solvents, i.e., ethanol, water and isopropyl alcohol, room temperature co-precipitation method, and EDTA-Citrate method) on the sintering behaviour of PDC electrolyte material and the sintering mechanism for the initial stages of sintering has also been discussed. The main focus of the chapter is to analyse the linear shrinkage, shrinkage rate and the mechanism and the activation energy for the early stages of sintering.

Chapter 6 deals with the dilatometer results of various liquid additives (Li, Co, Fe, and Mg) as co-dopants to praseodymium doped ceria at up to 3 mol% synthesized by microwave-assisted co-precipitation method using isopropyl alcohol. The chapter also

explains the sintering kinetic study of the samples, linear shrinkage and shrinkage behaviour of the pellet. The activation energy calculated from CHR and Dorn method has also been discussed in the chapter.

Chapter 7 concludes the summary and conclusion of as-synthesized praseodymium doped ceria based materials on the sintering kinetic behaviour for the application of IT-SOFCs and provides scope for future studies.

CHAPTER 2

LITERATURE REVIEW

The background for the literature review of various electrolyte materials used for SOFC applications and various objectives of the study is outlined. Reported literature for co-doped and doubly co-doped ceria based electrolyte materials is discussed in this chapter. The literature review is sub-categorized under different themes, namely:

I. Ceria based electrolyte materials for IT- SOFCs.

II. Praseodymium doped ceria based electrolyte material for IT-SOFCs.

III. Effect of synthesis methods on sintering temperature of doped ceria based materials.

IV. Ceria-based electrolyte material doped with transition metal oxides.

V. Sintering mechanism for the early stages of sintering of doped ceria based materials

The literature survey carried out under this theme is presented in the following sections.

2.1.   CERIA BASED ELECTROLYTE MATERIAL FOR IT-SOFCs

Fluorite-structured oxide materials such as yttria-stabilized zirconia (YSZ), rare earth doped ceria (Gadolinium doped ceria (GDC), Praseodymium doped ceria (PDC), Samarium doped ceria (SDC)), and rare earth doped bismuth oxide have been widely investigated as electrolyte material for a solid oxide fuel cell (Singhal 2000). High sintering temperature (~1500°C) to obtain fully dense material is one of the drawbacks of ceria-based electrolyte materials (Chen and Chen 1996; Kleinlogel and Gauckler 2001; Li et al. 2002). The high sintering temperature of the electrolyte material results in a rapid grain growth, which leads to the poor mechanical stability of the material. The high sintering temperature could also result in several other disadvantages such as partial

reduction of Ce^{4+} to Ce^{3+}, undesirable chemical expansion, high energy cost, and failure of co-firing with other SOFC components, phase diffusion, and chemical interaction between the components which in turn affect the electrochemical performance of the cell (Gil et al. 2006; Lewis et al. 2001; Yoshida and Inagaki 2006). The ceria-based materials at high sintering temperatures above 1200°C result in the partial reduction of ceria, which leads to the deteriorated properties of the cell; therefore, it is necessary to reduce the sintering temperature to develop highly dense and high performance electrolyte material (Dong et al. 2010). The high operating temperature posses various challenges such as an increase in the fabrication cost of the cell, inter-diffusion between the electrode-electrolyte interlayer at high temperature, causes the degradation of the stack. Therefore it is needful to reduce the sintering temperature since the electrode materials are sintered at a lower temperature than that of the electrolyte material (Pound 1992). Therefore, the need to reduce the overall cost of the system and maintain an optimum trade-off between performance and lifetime of the stack led to the development of fluorite-type oxide electrolytes $Ce(Re)O_{2-\delta}$ (Re: rare-earth or alkaline-earth cations).

Doped cerium oxides are considered a promising electrolyte for IT-SOFCs because of high ionic conductivity at lower temperatures when compared to the traditional electrolyte material Yttrium stabilized zirconia (YSZ) (Bellon et al. 1998). The main drawback of this solid solution (Doped cerium oxides) is the high sintering temperature when prepared by solid-state reactions (VanHerle et al. 1997). An intensive investigation has been done to reduce the operating temperature of SOFC down to 800 - 500°C has been found that densification occurs at elevated temperature (>1500°C). It is assumed that the main factors that affect ionic conductivity are the powder synthesis and sintering process (Ding et al. 2010; Pérez-Coll et al. 2010; Reis et al. 2011). Tian et al. (2000) reported that Yttria-doped ceria (YDC) prepared at lower sintering temperatures with the smaller grain size exhibited much higher overall conductivities than those sintered at 1500°C (Tian and Chan 2000). Powder morphology and powder size are the two factors that affect the sintering behaviour results in varied grain size and homogeneity in the grain size at identical sintering conditions (Ding et al. 2010). Herring et al. (1950)

reported that smaller particle size allows densification to occur via grain-boundary diffusion instead of lattice diffusion at a lower sintering temperature (Herring 1950).

2.2. PRASEODYMIUM DOPED CERIA BASED ELECTROLYTE MATERIAL FOR IT-SOFCs

Praseodymium doped ceria materials (PDC) have been reported as a good candidate for electrolyte materials for SOFCs (Esther Jeyanthi et al. 2015; Kuru et al. 2011). Pr cation in the ceria lattice can exist in variable valence states (+3, +4) at atmospheric pressure and promotes oxygen vacancies (Reddy et al. 2009). The praseodymium dopant increases the oxygen ionic conductivity of electrolyte by altering the grain boundary behaviour of oxides by increasing the oxygen vacancies (Ji et al. 2005). Due to the variable valence state of praseodymium in the ceria lattice, the density of anion vacancies is lower when compared to other dopants like gadolinium and samarium (Sadykov et al. 2006). A massive increase in chemical expansion upon heating is another critical anomalous behaviour of PDC (Bishop et al. 2014), which can cause stoichiometric or phase change expansion. Ftikos et al. (1993) investigated the thermal expansion of PDC, found that low thermal expansion coefficient and good electrical conductivity which makes these ceramics suitable candidates for electrolyte material. The sintering temperature was found to be 1550°C for PDC ceramics to obtain a fully dense ceramic pellet, which is very high when compared to GDC and SDC (Ftikos et al. 1993).

Shuk and Greenblatt (1999) pointed out that the uniformly small particle size in the range 35 - 50 nm allows sintering of the PDC samples into highly dense ceramic pellets at 1300°C, which is lower compared to the samples prepared by solid-state techniques, which require sintering temperature 1600 - 1650°C to obtain fully dense material. The maximum total conductivity was 1.4×10^{-2} S cm^{-1} at 700°C (Shuk and Greenblatt 1999). Nauer et al. (1994) reported that cerium - praseodymium oxide forms fluorite-type solid solutions for all samples up to 30 mol% PrO_{2-x} (Nauer and Steele 1994) while M. J. Chen et al. (Chen et al. 2007) obtained a single-phase fluorite solid solution up to 35 mol%.

The incorporation of 20 mol% praseodymium into CeO_2 lattice caused a decrease in cell parameter of 0.0014nm, indicates the solid solubility of Pr in CeO_2 is restricted for the solid solution formation (Wang et al. 2002). Shuk and Greenblatt (1999) also observed two phases when the concentration of PrO_{2-x} exceeds 30 mol%, one with CeO_2 fluorite phase and another phase with PrO_{2-x} fluorite with a larger lattice parameter, which is in good agreement with the results reported by Nauer et al. (1994). Wang et al. (2000) investigated on carbonate-derived PDC solid solutions and found out that low sintering temperature of 1200°C can produce 99% dense ceramic material via pressureless sintering for 4h. The densification temperature reported by Wang et al. (2002), is at least 400°C lower than that used for powders processed via solid-state reactions (Wang et al. 2002).

The introduction of the addition of alkaline-earth metals improves the sintering properties and relative density of $La_{0.2}Ce_{0.8}O_{2-\delta}$ from 68% at sintering temperature 1700°C to 91% at a lower temperature (1580°C) and increases samples conductivity, decreasing at the same time the activation energy of total conductivity in the air was reported by Pikalova et al. (Pikalova et al. 2008). Chen et al. (2007) synthesized PDC materials by pechini method using citric acid as a chelating agent and sintered at 1500°C for 14h in the air to form dense pellet (Chen et al. 2007). The optimal conductivity of 6.7×10^{-2} S cm^{-1} was observed at 700°C in the air on PDC doped with 30% Pr, which is five times higher than the PDC material synthesized by Shuk and Greenblatt.

Spridigliozzi et al. (2019) has investigated the effect of praseodymium doping in GDC on the sintering behaviour and electrical properties of the electrolyte material. It was reported that the relative density of Pr co-doped samples ($Gd_{0.2-x}$ Pr_x $Ce_{0.8}$ $O_{1.9}$) are high when compared to that of undoped samples (Spiridigliozzi et al. 2019). **Figure 2.1** represents the shrinkage rate and linear shrinkage of Pr co-doped samples as function of temperature. It can be seen from the figure, that the densification of all the samples starts at around 700°C and a second densification step occurs at around 1000°C (for 2Pr and 4Pr) and 1100°C (for 8Pr and 10Pr).
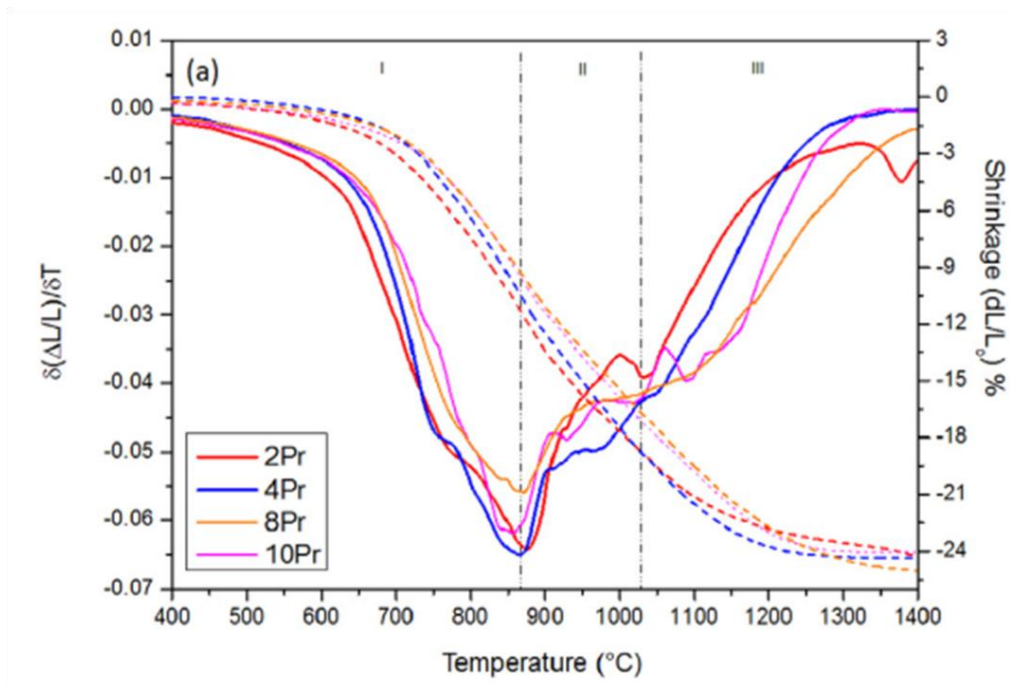
Figure 2.1: Shrinkage rate and Linear shrinkage of Pr co-doped samples as function of temperature (Spiridigliozzi et al. 2019)

It can be seen from the shrinkage rate curve, that all the samples exhibited multiple shrinkage behaviour. The reason for such behaviour is mainly due to the different compaction behaviour of the powder with different agglomerate strength. Thus the appearance of different shrinkage maxima is mainly due to the different inter particle pore size distribution in the green pellet. It was reported that the high densification of the samples were achieved at 1250°C/ 3h which is less than the common sintering temperatures (> 1400°C) without the use of any sintering additives.

Figure 2.2 shows the comparison of linear shrinkage and shrinkage rate of gadolinium doped ceria and praseodymium co-doped ceria. The shrinkage of the 6 Pr doped sample starts at around 700°C and ends at around 1200°C. Multi modal shrinkage behaviour with several maxima and several minima was noticed for Pr doped samples and was reported that this is due to the change in the sintering mechanism of the sample. In case of GDC sample, the maximum shrinkage has not complete even at 1400°C which indicates that

GDC sample requires a sintering temperature greater than 1400°C. whereas, the Pr doped samples requires a sintering temperature of 1200°C. Therefore, it is evident from the thermo-dilatometer studies that the addition of praseodymium has a positive effect on the compaction, density and powder properties when compared to that of simple GDC samples.
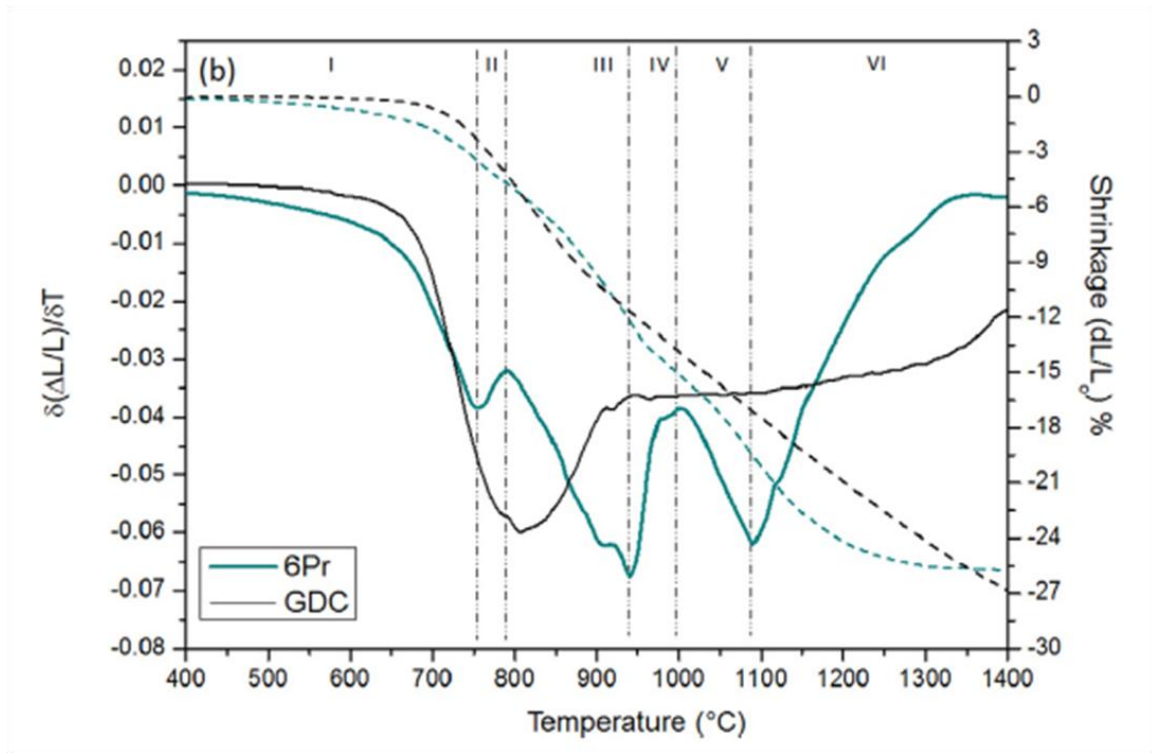
Figure 2.2: Shrinkage rate and Linear shrinkage of GDC and Pr co-doped samples as function of temperature (Spiridigliozzi et al. 2019)

Some of the reports on PDC materials (Liu et al. 2017; Ruiz De Larramendi et al. 2011; Spiridigliozzi et al. 2019; Venkataramana et al. 2017) indicate that it can be a candidate for electrolyte materials for SOFCs since the Pr cation can exist in two oxidation states (Pr^{3+}/Pr^{4+}) and promote oxygen vacancies. Above-mentioned desirable properties discussed in the literature motivated the present study to explore/synthesise PDC nanopowder as an alternative electrolyte material for IT-SOFCs. From this background, the low-temperature synthesis and performance of nanostructured PDC electrolyte for

LT / IT - SOFC applications is to be explored in terms of sinterability and sintering behaviour.

2.3.   EFFECT OF SYNTHESIS METHOD ON SINTERING TEMPERATURE OF DOPED CERIA

Different synthesis methods are adopted for the preparation of ultrafine ceramic powder with high sinterability (Tok et al. 2004; Zhen et al. 2008). Gadolinium doped ceria (GDC) and Samarium doped ceria (SDC) is a promising solid electrolyte material for SOFCs and other solid oxide devices (Fergus 2006; Steele 2000). Ceria is doped with RE^{3+} ions (RE= Gd, Sm) in the crystal structure of ceria, the concentration of oxygen vacancy increases due to the reduction of Ce^{4+} to Ce^{3+}. Citrate complexation, combustion synthesis, hydrothermal synthesis, microwave-induced combustion, co-precipitation, sol-gel, and pechini method are the methods used for synthesizing GDC and SDC. The main advantage of the pechini method, which is a modified sol-gel technique, has the capability of producing ultrafine powders with high purity and homogeneous phase composition at lower temperatures (Arabacı and Öksüzömer 2012). This method produces GDC powder compacts with high density (98% of theoretical value) when the samples are sintered at 1400°C. The ionic conductivity of the as-synthesized dense samples is $3.4x10^{-2}$ S cm^{-1}, the higher total ionic conductivity of the ceramic is due to small grain size, high density, and small grain size and the dopant ion mobility. A.I.Y. Tok et al., reported a lower sintering temperature of 1300°C with 97% relative density with the near maximum for 10 mol% GDC as compared to Arabacı et al., who reported a higher sintering temperature of 1400°C. The results showed that the high sinterability of the as-synthesized powder and could be fully consolidated at 1300°C. After 1300°C there is a decrease in the relative density, which could be due to the reduction of Ce^{4+} to Ce^{3+} (Tok et al. 2006).

Ma et al. (2004) investigated the synthesis of $Ce_{0.8}Gd_{0.2}O_{2-\delta}$ as electrolyte material via conventional mixed-oxide method from high-purity commercial CeO_2 and Gd_2O_3. An

interesting report was that the addition of Gd_2O_3 increases sintering temperature retards densification, and suppresses the grain growth compared with undoped CeO_2. The maximum total conductivity is exhibited by sample sintered at 1550°C for 5h below 500°C, and above 500°C the maximum total conductivity is shown by the sample sintered at 1600°C for 5h. For the samples sintered at 1600°C or above, over 97% relative density is obtained. The sintering temperature has a significant effect on both the grain boundary and the grain interior conductivities. Thus, the total conductivity and the optimum range are found to be between 1550 and 1600°C (Ma et al. 2004).

Huang et al. (1997) prepared SDC, $Ce_{1-x}Sm_xO_{2-x/2}$ (x = 0 - 0.3) by different sol-gel method were successfully sintered at 1400°C into pellets with apparent densities 95% of the theoretical value as compare to other conventional ceramic techniques which require 1600°C for sintering (Huang et al. 1997). The uniformly smaller particle size obtained results in a decrease in the sintering temperature to 1400°C. It was reported that the ionic conductivity of SDC increases with increasing samarium substitution and reaches a maximum at x=0.2. The decrease in conductivity for x > 0.2 is due to the interaction between oxygen vacancy and dopant. Jung et al. (2001) examined SDC with the modified sol-gel method; the gel obtained is treated with high carbon (long-chain, high boiling-point) alcohol of octanol. It was reported that when the samples are sintered to 1200°C the relative density of the powder becomes 92%, on increasing the sintering temperature to 1300°C powder attain near-full relative density (about 98% to the theoretical density) (Jung et al. 2001) which shows better results than reported by Huang et al. (1997). The decrease in sintering temperature is attributed to the reduction in the formation of any chemical bonds between particles during drying which inhibits the formation of hard agglomerates and thus forms soft agglomerate, results in homogeneous shrinkage of ceramic to near full density which is one of the essential characteristics to achieve good sinterability. The higher ionic conductivity of $2.2x10^{-2}$ S cm^{-1} was reported by Dong Ding et al. (2010) for SDC ceramics with a sintering temperature of 1300°C and with a grain size of 0.87μm. With a further increase in sintering temperature, it was found out that the

density remains constant while a significant grain growth was observed. Soft agglomeration and better dispersion of the powders was observed (Ding et al. 2010).

J. Van herle et al. (1996) prepared (Y, Gd, Sm)-doped ceria electrolytes with oxalate co-precipitation allowing a high degree of densification at low temperatures (<1400°C) average particle sizes of 0.5 to 0.7 μm without milling. Using more concentrated oxalic acid solution yields larger sized oxide powders of lower sintering quality. Owing to the high density and chemical homogeneity, high ionic conductivity is exhibited by the as-synthesized doped ceria electrolyte materials. The improved sintering characteristic is due to the dewatering step with ethanol of the resulting oxide powder (Van Herle et al. 1996). Tian et al. (2011) noted that a co-sintering process enhances the sintering process of SDC with a co-pressed NiO-SDC compact. It is showed that electrolytes are dense when they are co-sintered at 1250 - 1450°C with anodic substrates. The SDC compact powder possesses a relative density of 90.7% at 1300°C for 5h, and SDC films sintered with NiO-SDC substrates attains a much higher density of about 99% of the theoretical density. When SDC is sintered at 1300°C, it is found that the conductivity increases with the sintering temperature, and beyond 1300°C, no further improvement in conductivity is found out, the highest ionic conductivity of 1.54×10^{-2} S cm^{-1} at 600°C was achieved (Tian et al. 2011).

Gondolini et al (2013) reported the effect of microwave heating on GDC ($Ce_{0.8}Gd_{0.2}O_2$) samples synthesised by polyol microwave assisted method. **Figure 2.2** and **Figure 2.3** represents the linear shrinkage and the shrinkage rate of the GDC powder synthesised by the above mentioned method and the two commercial GDC powders of the same composition. It can be seen from the figure, that the sintering process of the GDC powder resulted in a multiple shrinkage rate behaviour with a shrinkage maxima at around 610°C and the second shrinkage maxima with a lower shrinkage at a temperature of around 1480°C. The as-synthesised GDC sample sintered at 1400°C/ 6h resulted in a relative density of 93% (Gondolini et al. 2013).
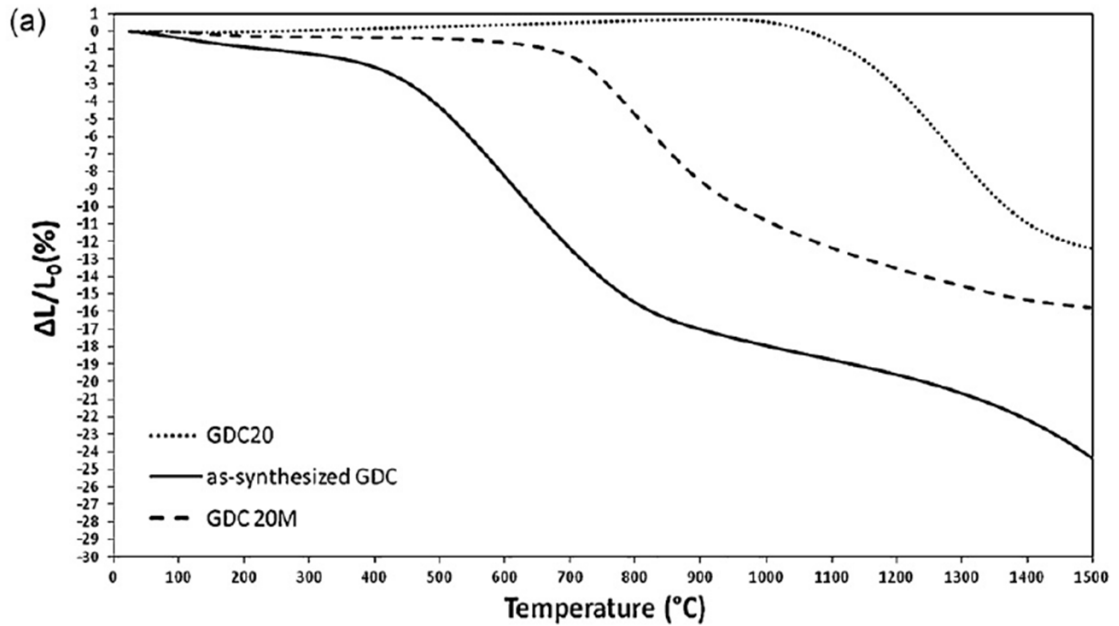
Figure 2.3: Linear shrinkage of GDC20, GDC 20M and as-synthesised GDC powders (Gondolini et al. 2013)
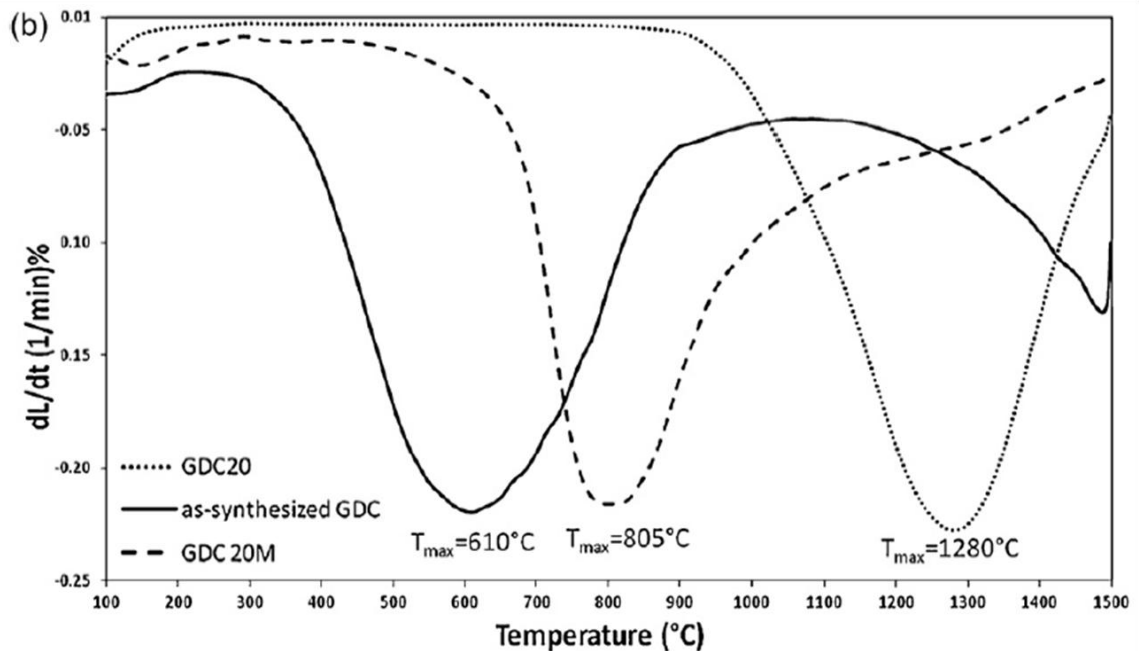
Figure 2.4: Shrinkage rate of GDC20, GDC 20M and as-synthesised GDC powders (Gondolini et al. 2013)

Table 2.1 summarises the effect of different synthesis behaviour on the sintering behaviour and the relativity density. It can be noticed from the **Table**, that synthesis method has a profound influence in the sintering behaviour of the powder. The presence of large pores present in between the hard agglomerate after compacting resulted in high sintering temperature of the samples. The non-homogeneous pore size distribution of the compact resulted in the high sintering temperature of the synthesised powders.

Table 2.1: Effect of synthesis methods on sintering behaviour and density

Sample Studied/Synthesis Method	Sintering Temperature (°C)	Relative Density (%)	Remarks	Reference
GDC / Pechini Method	1400	98	Homogeneous distribution of Gd^{3+} in ceria lattice and its high ionic-mobility	(Arabacı and Öksüzömer 2012)
GDC / Carbonate co-precipitation method	1300	97	Grains were equiaxed and well developed with low porosity	(Tok et al. 2006)
GDC/ Gel Casting Process	1450	96	Powders calcined at lower temperature have a small crystallite size which resulted in a higher density. Gel casting process resulted in a low temperature preparation route with high sinterability	(Cheng et al. 2003)
GDC/ Sol-Gel method using glucose and fructose	1500	-	The sample exhibited two shrinkage maxima indicate the presence of some hard agglomerates in the sample and to decrease these hard agglomerates, glucose, fructose and metal nitrate mole ratios has	(Medisetti et al. 2017)

			to be optimized.	
GDC/ Polyol Method	1400	93	The increase in the specific surface area of the powders resulted in an increase of powder reactivity and the sintering process takespalce at a lower temperature	(Gondolini et al. 2013)
GDC/ Hydrothermal method	1100	96	Low temperature synthesis methods result in a material with lower grain size and better reactivity	(Himri et al. 2016)
GDC/ Soft chemical route	1300	96	Higher contents of gadolinium oxide limited the grain growth. The synthesis methods and the calcination conditions control the initial particle size	(Esposito et al. 2007)
GDC/ Glycine Nitrate Method	1200	97	Decrease in the sintering temperature is due to the formation of softer agglomerates	(Prasad et al. 2010)
SDC/ acrylamide polymerization process	1350	99	Acrylamide polymerization synthesis allows preparing uniformly doped ceria powders resulted in an excellent sintering activity	(Yingping et al. 2010)

SDC / Sol-Gel Method	1400	95	Uniformly small particle size was obtained	(Huang et al. 1997)
SDC / Modified Sol Gel Method	1300	98	Gel treatment with octanol inhibits the formation of hard agglomerates	(Jung et al. 2001)
SDC/ Modified homogeneous precipitation method using alcoholic solvents	1200	93	Powders prepared with different mixtures of water/alcohol exhibited different densification behaviors and these differences are due to the varying degree of agglomeration of the powder particles.	(Camilo de Souza and Muccillo 2019)
SDC / Carbonate coprecipitation method	1300	98	Homogeneous sintering occurs, which indicates soft agglomeration of the SDC particles	(Ding et al. 2010)
YDC/ GDC/ SDC/ Oxalate co-precipitation	1300	97	Improved sintering characteristics are due to the dewatering step with ethanol of the resulting precipitate	(Van Herle et al. 1996)

2.4. CERIA BASED ELECTROLYTES DOPED WITH TRANSITION METAL OXIDE

Fabrication of ceria based electrolytes with relative density > 0.90 requires sintering temperatures >1500°C. The incorporation of Transition metal oxide (TMO) as sintering additives is an alternative method for reducing the sintering temperature of ceria-based materials. The sintering additives will form a grain boundary liquid phase upon heating that fully wets the solid surfaces and provide a pathway for enhanced matter transport and reduce the interparticle friction. The presence of a liquid phase during sintering creates capillary forces that compact particles, close porosity, also increases diffusivity in the material and enhances both surface and lattice diffusions at lower temperatures (Esposito et al. 2009). NiO, MnO_2, Mn_2O_3, Ga_2O_3, Co_3O_4, CoO, and Fe_2O_3 were used as sintering aids in ceria-based electrolytes, which have been shown to effectively promote densification (Kleinlogel and Gauckler 2000; Kondakindi and Karan 2009; Yoshida and Inagaki 2006).

Kleinlogel et al. (2000) reported that nano-crystalline $Ce_{0.8}Gd_{0.2}O_{2-x}$ material could be sintered to lower temperatures below 900°C yields 99% dense samples using a dopant concentration of 1mol% of Co_3O_4. **Figure 2.3** depicts the variation in linear shrinkage rate as a function of temperature for different cobalt concentrations (0–2 mol%). The sintering temperature decreases from above 1300°C for pure GDC to below 1000°C with an increasing dopant concentration from 0-2 mol% Co_3O_4 where a density above 98% theoretical density is achieved (Kleinlogel and Gauckler 2000). GDC doped with 1 mol.% cobalt a three-fold shrinkage rate is observed compared to undoped GDC, and the densification process is finished within a temperature range of about 50°C. Zhang et al. (2004) reported the effect of the TMOs, such as MnO_2, Fe_2O_3, and Co_3O_4 for the densification of ceria-based electrolytes. It was found that MnO_2 and Fe_2O_3 have a very similar effect on the densification and microstructural evolution. The sintering temperature decreases from above 1250°C for GDC without TMOs to 1100°C for TMO-pure GDC and promotes densification. The maximum shrinkage temperature changes

with the type of dopants are as follows: $T_{Max}^{Undoped}$ (~ 1505°C) $> T_{Max}^{Fe/Mn}$ (~1355°C) $>$ T_{Max}^{Co} (~1278°C). These results indicate that TMOs can reduce sintering temperature significantly. The microstructural observation also confirms that the TMO-doped samples also have much larger grain size than the undoped GDC (Zhang et al. 2004). Zhang et al. (2004) claimed that viscous flow sintering occurred in the TMO-doped ceria during sintering, which is contradictory to remarks of Kleinlogel et al. (2000). The additions of Fe and Mn oxide had minimal effect on the grain boundary behaviour, while the addition of Co oxide exhibited a slight decrease in the grain boundary conductivity compared to pure CGO. This indicates a small reduction in the lattice conductivity, probably due to the dissolution of TMOs in CGO crystallites (Zhang et al. 2004).
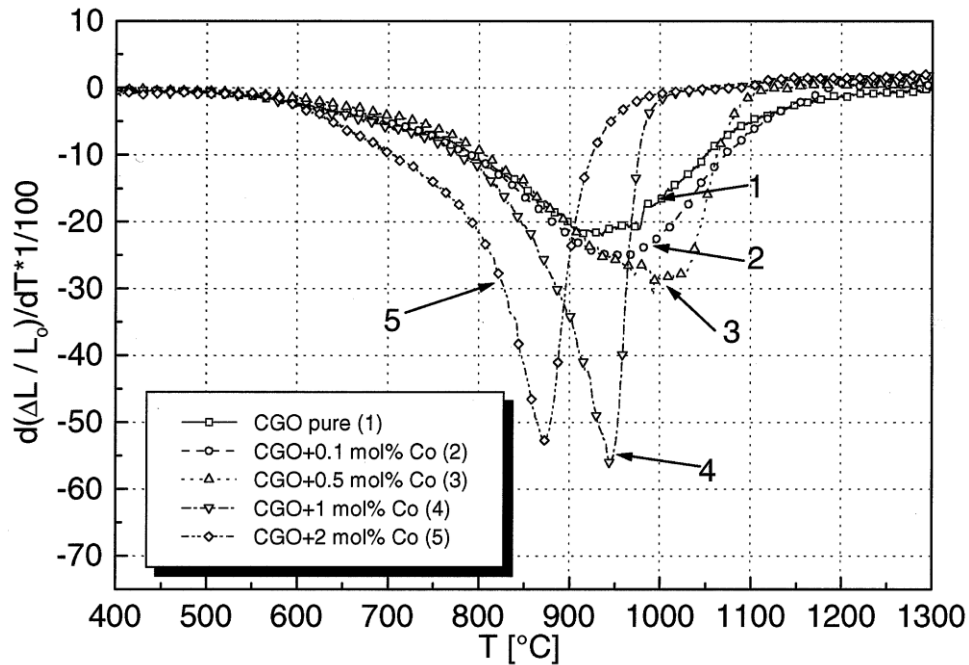
Figure 2.5: Linear shrinkage rate(d($\Delta L/L_0$)/dT) as a function of temperature and Co$_3$O$_4$ concentration (Kleinlogel and Gauckler 2000)

Lewis et al. (2001) reported that a theoretical density > 95% could be achieved in 1 cat.% Co additive doped in YSZ at a lower temperature as 1195°C (Lewis et al. 2001). The reduction in sintering temperature does not affect the conductivity of the doped material, and the conductivity of the doped sample is equal to that of YSZ sintered at the higher temperature without Co additive. Dong et al. (2009) made a comparative study on the sintering characteristics of both CGO10 and 8YSZ doped with 1 at% Fe. A reduction in sintering temperature of 110°C for the 8YSZ with 1 at% Fe-doped was achieved compared with a reduction in sintering temperature of 200°C for 1 at% Fe-doped GDC10 (Dong et al. 2009).

In the case of samarium doped ceria, Mn_2O_3 and Co_3O_4 were found to be sintering promoters. Sintering at 1500°C with additives like Ga, Co, and Mn showed initiation of grain growth and yielded sufficient density. An interesting observation made by Yoshida et al. (2006) is that Mn_2O_3 and Co_3O_4 promoted grain growth of SDC even at the initial stage of sintering, while Ga_2O_3 promoted rearrangement of particle first. It was observed that the conductivity of SDC with Co additive sintered at 1400°C is 8.7×10^{-2} S cm^{-1} at 800°C, which is almost equal to that of SDC sintered at 1600°C (8.9×10^{-2} S cm^{-1} at 800°C) (Yoshida and Inagaki 2006). On the contrary to the results mentioned above, Ayawanna et al. (2009) reported that the total ionic conductivity of SDC and Y-SDC was improved approximately threefold (Ayawanna et al. 2009).

Machado et al. (2019) has studied the effect of 0, 1, 5 mol% iron oxide doped GDC and has reported that co-doping with Fe^{3+} changes the sintering behaviour of the doped cerium oxide and favours densification at a lower temperature of 1200°C with a relative density of 90% when compared to the conventionally prepared GDC material without any sintering additive. The GDC sample without sintering additives resulted in a porous structure with sub-micron grain size. It was also reported that the addition of Fe increases the activation energy (lattice diffusion) for the sintering which results in a larger grain size when compared to the undoped GDC material (Machado et al. 2019).

Zajac et al. (2009) studied on the applicability of transition metal additives as sintering aids for cerium gadolinium oxide electrolyte. It was reported that the nanosized $Ce_{0.85}Gd_{0.15}O_{1.925}$ material shows already improved sintering properties than previous reports but full sintering is not achieved below 1300°C, whereas Cr, Fe and mainly Cu impregnation allows full sintering at 1300°C. It was also mentioned that for transition metal ions containing materials the improvement of the grain boundary conductivity was observed upon lowering the sintering temperature. Therefore, by the addition of Cr, Fe and Cu, the sintering temperature has been reduced to 1300°C with a relative density of 95% (Zajac et al. 2009).

Jason D. Nicholas et al. (2007) investigated the effect of dopants like Cu, Co, Fe, Mn, Li, and Zn on the sintering temperature of GDC. They introduced the use of Vegard's slope quality factor analysis as a tool to predict the sintering behaviour of the above-mentioned transition metal oxide dopants in GDC. The dopant must segregate to the grain boundaries instead of dissolving in bulk to form a liquid phase. The solubility of a dopant is inversely proportional to the square of its "Vegard's Slope" and for CeO_2, the Vegard's Slope, X, can be described as

$$X = (0.0220r_i + 0.00015z_i) \qquad (2.1)$$

Where r_i is the difference in ionic radii between the dopant and Ce^{4+} in 8-fold coordination, and z_i is the difference in charge between the dopant and Ce^{4+} (Nicholas and De Jonghe 2007). To induce liquid phase sintering dopants in GDC should have an absolute value of the Vegard's Slope greater than zero. A second phase in which CGO is insoluble can form if the |Vegard's Slope| is too large, preventing liquid phase sintering and forcing the system to sinter via the solid-state sintering mechanism observed for the pure material.

The dopants with moderate absolute values of the Vegard's Slope liquid phase sintering in CGO are known to occur. The segregation of dopants with a negative Vegard's slope will introduce oxygen vacancies for charge neutrality and increase the grain boundary

cation mobility, further results in greater densification. Nicholas et al. used this Vegard's slope quality factor analysis tool to predict the sintering behaviour Cu, Co, Fe, Mn, Li, and Zn in GDC.

Table 2.2 summarises the effect of TMOs on co-doped samples on the sintering temperature and relative density. From the above-discussed literature, the effects of transition metal oxide doping on the densification kinetics and sintering behaviour of doped and co-doped ceria materials are discussed and have been considered as an alternative method to decrease the sintering temperature. The addition of the sintering aids helps the densification process by the formation of a liquid phase and the densification occurs due to diffusion of matter under the capillary action on the surface of the grains which result in a lower sintering temperature.

Table 2.2: Sintering additives effect on Sintering temperature and relative density

Sample Studied/ Sintering Additives	Sintering Temperature (°C)	Relative Density (%)	Remarks	Reference
GDC/ Co_3O_4	900	99	Threefold shrinkage is observed for 1 mol% cobalt oxide. Oxygen ion conductivity and electrolytic domain boundary remains unchanged compared to pure $Ce_{0.8}Gd_{0.2}O_{2-\delta}$ material sintered for a longer period	(Kleinlogel and Gauckler 2000)
GDC/ MnO_2, Fe_2O_3 and Co_3O_4	1278	97	Co_3O_4 is the most effective sintering aid and has the highest densification rate. TMOs can reduce sintering temperature; promote densification and grain growth for CGO20 ceramics	(Zhang et al. 2004)
GDC/ Li_2O	950	99	Li^+ ion doping into the GDC lattice may activate the Gd migration during the sintering process. Significant sintering promoting effect using $L_{i2}O$	(Zhu et al. 2014)

			was closely related to the fact that the Li-Gd-Ce-O liquid phase could form at a much lower temperature.	
GDC/ CuO	1000	96	A significant reduction of about 400°C in the densification temperature of $Ce_{0.79}Gd_{0.2}Cu_{0.01}O_{2-\delta}$ was obtained when compared with $Ce_{0.8}Gd_{0.2}O_{2-\delta}$. The addition of a minor amount of CuO does significantly change the sintering mechanism of $Ce_{0.8}Gd_{0.2}O_{2-\delta}$ samples.	(Dong et al. 2011)
GDC/ CuO	1050	97	Ternary phase (Gd_2O_3-CeO_2-CuO) promots a rapid densification due to diffusion of matter under the capillary action on surface of the grains. Liquid phase is promoted by the incorporation of CuO, which has a lower melting point (1326°C) than those of CeO_2 (2400°C) and Gd_2O_3 (2420°C), decreasing the total melting point of the ternary composition.	(Santos et al. 2018)
8YSZ/ Co_3O_4	1195	>95	Co_3O_4 is an effective sintering aid for YSZ and maintained conductivity approximately equal to that	(Lewis et al.

			of YSZ sintered at the higher temperature without additive.	2001)
SDC/ Co_3O_4	1300	92	The addition of only 0.5% Co could reduce the sintering temperature and the total ionic conductivity of the sample by approximately threefold.	(Ayawanna et al. 2009)
SDC/ Fe_2O_3	1450	95	Fe_2O_3 doped samples promotes the densification in SDC due to the viscous flow sintering occurred in the Fe-doped ceria system.	(Zheng et al. 2011)
SDC/ Mn_2O_3 and Co_3O_4	1400	Highly dense	The electrochemical property of SDC with Co_3O_4 sintered at 1400°C was comparable to SDC without additives sintered at 1600°C.	(Yoshida and Inagaki 2006)
SDC/ Li_2O	900	-	For relative density higher than 82%, grain size increased rapidly. The activation energy for densification reached 5.54±0.50 eV, leading to a liquid phase formation in the grain boundary.	(Le et al. 2013)

2.5.　SINTERING MECHANISM FOR THE EARLY STAGES OF SINTERING

The sintering process has been mainly classified into three stages, namely the initial stage, intermediate stage and final stages of sintering. Two different methods (Constant heating rate (CHR method) / Dorn method) have been used to calculate the activation energy and determine the kinetic mechanism in the sintering process. The two different methods used for the sintering experiments to calculate the activation energy for sintering and the sintering mechanism used in the present work are discussed in detail in chapter 3.

Zhang tianshu et al. (2002) had found out the sintering mechanism for undoped ceria to be volume diffusion-controlled sintering whereas; transition metal oxide doping resulted in the transition of mechanism to viscous flow from volume diffusion. Zhang et al. (2002) have studied the early stage sintering mechanism of Fe doped CeO_2 and MnO_2 doped CeO_2 (Tianshu et al. 2002). It was confirmed that the early stage sintering mechanism changes from volume diffusion to viscous flow in the case for pure CeO_2 and Fe/Mn-doped $CeO_{2,}$ respectively. The change in the sintering mechanism is due to the formation of a thin amorphous layer on the particle's surface at a very low temperature, which reduces the friction between the particles and allows the rearrangement of the particles. It was reported in the literature that the transition of the sintering mechanism could also depend upon the amount of dopant added. On the other hand, the activation energy for the viscous flow mechanism should be far smaller than that of the volume diffusion mechanism.

A detailed study on the sintering kinetics for the initial stage of sintering of PDC based materials and liquid additives doped PDC material has not been explored fully. Further research needs to be carried out to make PDC material as a capable electrolyte for SOFC/SOEC applications.Therefore, the current research focuses on the calculation of the activation energy and the sintering mechanism of the as-prepared PDC sample, which exhibits a good sintering activity.

2.6 CONCLUSION

From the literature review, the following inferences are obtained:

- The synthesis method plays a crucial role in controlling the powder characteristics such as crystallite size, morphology, agglomeration, and surface area of the sample.

- Doubly co-doping is considered as an essential pathway for developing potential electrolytes for IT-SOFCs with lower sintering temperature.

- Processing conditions/ synthesis methods have to be altered to achieve nano-particles with a uniform particle size distribution, which leads to uniform shrinkage behaviour and thus decreases the sintering temperature of the sample.

- A detailed study on the effect of liquid additives on PDC material is necessary as per the preliminary literature search. The influence of liquid additives on the sintering behaviour and decreasing the sintering temperature of PDC material has not fully explored for the application of electrolyte material for SOFCs.

- The sinterability of the electrolyte material can be enhanced by the use of a highly diffusive regime, which promotes the densification during the sintering.

- Grain boundary diffusion dominates the sintering mechanism when the particle size is small in the case of ceramics and crystalline materials. As a result, the smaller particles will result in a faster neck to neck growth, which is the driving force for grain boundary diffusion to takes place in the early stages of sintering.

Based on the conclusion from the literature survey, the objectives of the present research are framed. Formulated objectives address the scope of using praseodymium doped ceria based materials as electrolyte material for LT/ IT - SOFCs and are presented in **Chapter 1**. The synthesis methods, characterization techniques adopted for analyzing the synthesized samples, and the sintering studies experimental procedures are discussed in detail and are outlined in the next chapter.

CHAPTER 3

MATERIALS AND METHODS

The praseodymium doped ceria based electrolyte materials in the present study are synthesized using microwave-assisted co-precipitation method using ethanol, water, and isopropyl alcohol as solvents, room temperature co-precipitation method, and EDTA Citrate complex method. Further, the synthesized metal oxides are characterized using various characterization techniques, and the shrinkage behaviour and the mechanism for initial stages of sintering have been studied.

3.1. SYNTHESIS OF CERIA-BASED ELECTROLYTE MATERIALS

3.1.1 EDTA – CITRATE METHOD

In the present work, ceria-based electrolyte materials are synthesized using EDTA Citrate complex method(Prasad et al. 2012b). The advantage of this synthesis method is that EDTA is a versatile non-ion selective chelating agent; it usually forms 6 5-membered rings with most metal ions. The chelating reaction is fast, complete, and in one single step without any cumulative reaction. The intrinsically strong 5-membered ring structure in this complex is typically highly stable even under heat, light, and pH extremes. EDTA forms a more stable complex with a wide range of metal ions than citric acid, one of the most used chelating agents in the Pechini method. The metal ions likely form the main complex with EDTA in the EDTA–citrate–metal complexing process. EDTA forms a cage-type complex with most ions at a 1:1 ratio, which would effectively eliminate the difference between the various metal ions and help the molecule level mixing of the metal ions in the precursor.

On the other hand, citric acid can form a complex with multiple metal ions, or multiple citric acids can form a complex with a single metal ion. Furthermore, the presence of the

OH group in the citric acid's structure makes the polymerisation reaction becomes possible between citric acids or between citric acid and EDTA. The secondary chelation between metal ions and citrate together with the availability of polymerization between the acids could immobilize the metal–EDTA complex and effectively preserve the molecule level mixing of metal ions by homogeneously dispersing the metal–EDTA complex within the citric matrix. Depending on the results obtained, suitable synthesis method can be identified further.

Stoichiometric amounts of metal nitrates were pre-dissolved in deionized water and mixed into an aqueous solution at room temperature. EDTA (ethylenediamine-tetraacetic acid, Sigma Aldrich Chemicals) and citric acid (Sigma Aldrich Chemicals) were used as chelating agents. The necessary amount of EDTA dissolved in NH_4OH (Spectrum reagents) for complete dissolution was then dropped to the mixed metal nitrate solution. Solid citric acid was added under stirring to the resulting mixture, and the citric acid is allowed to dissolve completely to obtain a clear solution. The required amount of NH_4OH solution was added to the clear solution to maintain the pH to the desired value. The mole ratio of total metal ions to EDTA and citric acid used was 1:1:1.5. The excess water and nitrate gases from the resulting final solution were removed by heating this mixture at 100°C under a stirring condition to obtain a thick, viscous gel. The gel obtained is kept in the hot air oven for 24h at 150°C temperature to convert into a solid precursor. The solid precursor was then ground and calcined at 350°C/ 24h to get the final product. A schematic representation of the synthesis method, physical characterization and dilatometric studies are shown in **Figure 3.1.**
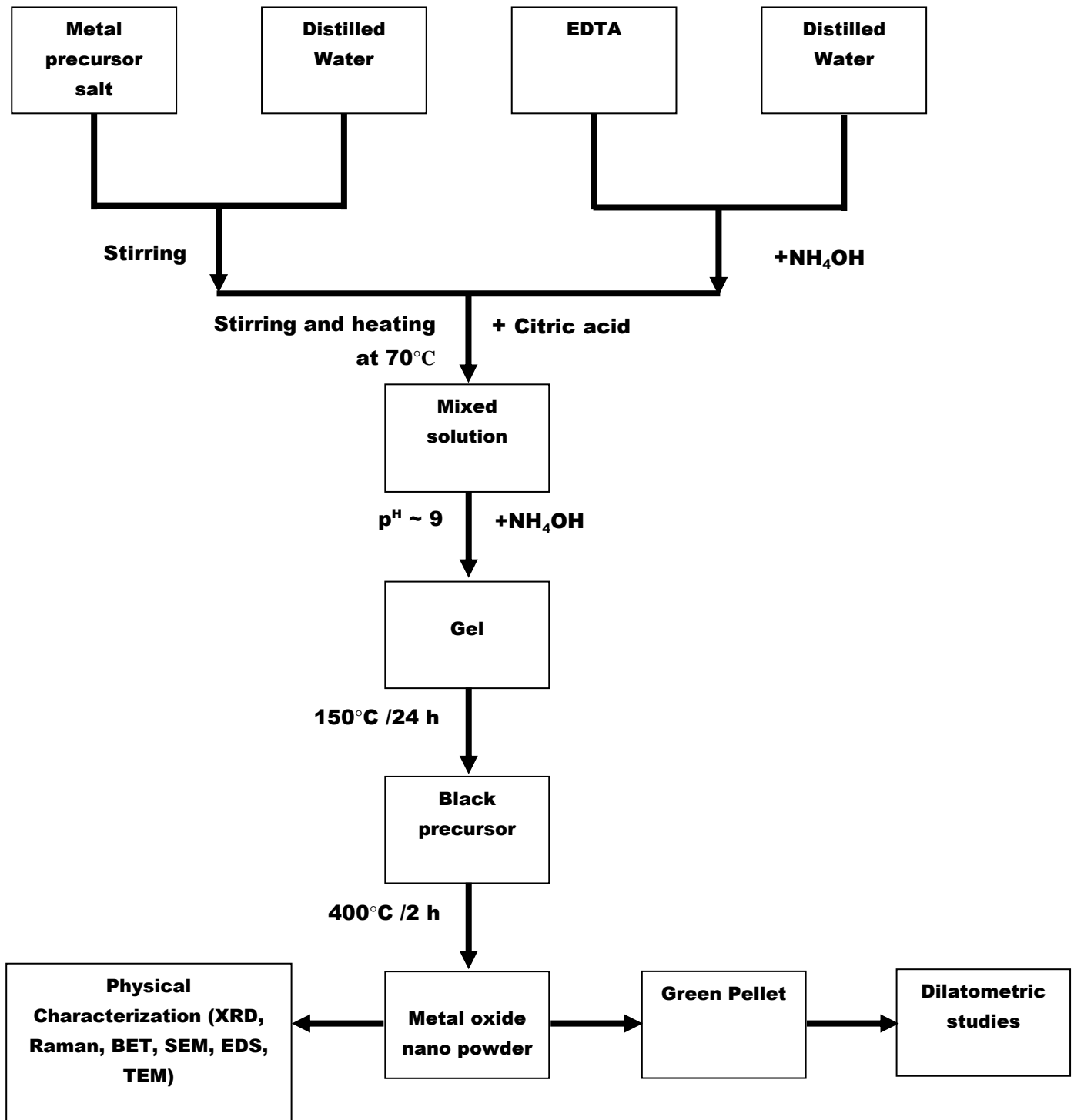
Figure 3.1: EDTA-Citrate method Synthesis procedure, Physical Characterization, and Dilatometric studies

3.1.2   Microwave-assisted co-precipitation method

The co-precipitation method is one of the commonly used methods for the synthesis of ceramic oxides. The advantages of this method include uniform particle size distribution with soft agglomerates, the relatively low reaction temperature when compared to other synthesis methods and homogeneity of the particle distribution. In this method, inorganic salts are used as precursors and are dissolved in any solvent to form a homogeneous solution with the metal ions. The pH of the solution is maintained at ~9 to precipitate the salts as hydroxide, oxalates, or hydrous oxide. The concentration of the salt, pH, and temperature affects the agglomeration and crystal growth. The microwave-assisted heating provides a rapid environment for the formation of nano-particles when compared to other conventional heating methods due to the heating effects of microwave irradiation. The solid mass after precipitation is washed, dried, and calcined to get the final product.

In this work, microwave-assisted co-precipitation synthesis describes the synthesis of PDC material in which the stoichiometric quantities of metal nitrates are dissolved in different solvents such as water, ethyl alcohol, isopropyl alcohol, and acetone. Ammonium hydroxide was added dropwise to this mixture under continuous stirring to complete the precipitation under controlled pH around 9, and the suspensions were treated in a microwave system with a controlled power of 540 W and a temperature of 150ºC for 30 minutes and are allowed to settle. After the synthesis reaction, the precipitates were washed to completely remove all the ammonium nitrate formed and the gel was dried in a hot air oven at 100ºC for 24h. The precursor was then calcined at 350,400 and 450ºC/ 2h to get the final product.

3.1.3   Room temperature co-precipitation method

In this method, isopropyl alcohol was used as solvent to investigate the formation of PDC nano-powder. Solutions of stoichiometric quantities of metal nitrates were dissolved in the solvent. Ammonium hydroxide was added drop wise to this mixture under continuous

stirring to complete the precipitation under controlled pH (~9) is transferred to a bowl and was washed to completely remove all the ammonium nitrate formed and was then filtered. The precipitate was then dried at room temperature for 72h.

3.1.4 Synthesis of Liquid additives doped PDC

A stoichiometric amount of 99.99% pure nitrates (Lithium nitrate, Cobalt nitrate hexahydrate, Ferric nitrate nonahydrate, Magnesium nitrate hexahydrate, Copper nitrate hexahydrate, and Manganese nitrate hexahydrate) were weighed and dissolved in 150ml of ethanol using a magnetic stirrer. The composition of 3mol% of Li assumed was $(Ce_{0.9}Pr_{0.1})_{0.97}Li_{0.03}O_2$. An appropriate amount of nanosized PDC powder synthesized by microwave-assisted co-precipitation method was then added to the solution, and the solvent was then removed by continuous stirring with heating. The powder was then dried in an oven at 130°C for 24h and was then calcined at 400°C/ 2h.

The metal oxide samples synthesized were characterized using various characterization techniques such as X-Ray Diffraction (XRD) to identify phases, confirm crystallinity and calculate crystallite size, the lattice constant and lattice strain, Raman spectroscopy to confirm the phase of the nano-powder and to analyze the presence of functional molecules in the materials. Brunauer-Emmett-Teller (BET) Surface area and particle size analyzer to quantitatively find the specific surface area and calculate particle size. Scanning Electron Microscopy (SEM) with EDS for morphological analysis of the sample and compositional analysis. Transmission Electron Microscopy (TEM) analysis was done to evaluate the morphology and particle size. The PDC powder was uniaxially pressed (150 MPa) to form green pellets with a diameter of 10 mm and a thickness of 12 mm.

3.2 METHODS TO CALCULATE THE ACTIVATION ENERGY OF SINTERING

The two different models used for calculating the activation energy and the sintering mechanism are (1) the constant heating rate method and (2) the Dorn method.

3.2.1. Constant heating rate method (CHR Method)

Woolfrey and bannister (Woolfrey and Bannister 1972) had developed an equation for the isothermal initial stage of sintering and based on the developed equation, Young and Cutler have developed an equation which can be applied to constant heating rate conditions as follows: (YOUNG and CUTLER 1970)

$$\frac{\left(\Delta L/L_0\right)}{T} = A_1 \, exp \left(\frac{-Q}{(m+1)RT}\right) \tag{3.1}$$

Taking natural logarithm on both sides, the equation (1) reduces to

$$\ln\left(\frac{\Delta L/L_0}{T}\right) = \, lnA_1 - \frac{Q}{(m+1)R}\frac{1}{T} \tag{3.2}$$

Where R is the universal gas constant, the exponent m depends on the mechanism of sintering;

m = 0 indicates viscous flow,

m = 1 indicates volume diffusion and

m = 2 indicates grain boundary diffusion.

Therefore the apparent activation energy, Q from **Equation 3.2,** can be calculated under CHR conditions from the slope of ln $[(\Delta L/L_0)/T]$ vs. (1/T) with a slope $[-Q/(m+1)R]$ by determining the value of m (Tianshu et al. 2002). The value of m can be obtained by performing constant heating rate experiments at different heating rates reported by Woolfrey et al., and a relationship between fractional shrinkage and heating rate was established (Woolfrey and Bannister 1972).

$$\left(\Delta L / L_0\right)_T = A_2 C^{\frac{-1}{(m+1)}} \tag{3.3}$$

Taking the natural logarithmic of relative shrinkage vs. heating rate yields a slope of magnitude 1/(m+1). Alternatively, Q can be found out.

3.2.2. Dorn Method

In this method, the apparent activation energy for the initial stage of sintering was determined by giving a rapid heating rate from one isothermal range to another isothermal range so that the microstructure of the sample remains the same (BACMANN and CIZERON 1968). The equation used to determine the apparent activation energy is expressed as follows:

$$Q = \frac{RT_1 T_2}{(T_2 - T_1)} \ln \left[(dY/dt)_2 / (dY/dt)_1\right] \tag{3.4}$$

The present investigation compares the controlled heating rate experiments with that of Dorn's method. The sintering mechanism along with the activation energy was estimated using the CHR model and the Dorn method.

3.3 PHYSICAL CHARACTERIZATION

The various characterization tools that have been adopted in this study are explained here:

3.3.1. X-Ray Diffraction (XRD) Analysis

X-ray diffraction technique is a non-destructive analytical technique for identification and quantitative determination of the various crystalline forms, known as 'phases'. When an incident beam of monochromatic X-rays interacts with a target material, the dominant effect occurs is the scattering of those X-rays from atoms within the target material. The scattered X-rays undergo constructive and destructive interference in materials with a regular or crystalline structure. The diffraction of X-rays by crystals is described by Bragg's Law given in **Equation (3.5).** By this law, the wavelength of electromagnetic radiation is related to the diffraction angle and the lattice spacing of a crystalline sample. The direction of possible diffractions depends on the size and shape of the unit cell of the studied material. The intensities of diffracted waves depend on the kind and arrangement of atoms in the crystal structure. (Warren 1990).

$$\mathbf{2d_{hkl} \sin \theta = \lambda} \qquad \textbf{(3.5)}$$

Where λ is the x-ray wavelength and θ is the Bragg angle relative to the primary x-ray. The generalization is easily performed by just inserting the interplanar spacing d_{hkl} of the crystal lattice under investigation (Mario Birkholz 2006). The lattice strain (ε) of the samples are calculated from the corresponding diffraction peak as given in **Equation (3.6).**

$$\mathbf{\varepsilon = \frac{\beta}{4 \tan\theta}} \qquad \textbf{(3.6)}$$

The x-ray diffraction structural investigations are undergone using the Thomson component of x-rays. XRD measurement was done using XPERT Pro diffractometer with operating parameters of 20-80° 2θ range, 0.02 step size, and 2s as step time at 40 kV and 30 mA. The radiation source used for the X-ray Diffraction (XRD) measurement was Cu Kα (0.154 nm). Debye-Scherrer equation given in **Equation (3.7)** was used to calculate the crystallite size

(D) of the material.

$$D= \frac{0.94\lambda}{\beta \cos\theta} \quad (3.7)$$

Where, λ is the x-ray wavelength, β is the line width in radians and θ is the Bragg angle relative to the primary x-ray.

$$d_{hkl} = \frac{a}{\sqrt{h^2+k^2+l^2}} \quad (3.8)$$

For cubic lattices lattice constant (*a*) is calculated using the above **Equation (3.8)**. This relation is developed based on the consideration that the interplanar spacing (d_{hkl}) depends on the Miller indices (h,k,l) and unit cell parameter *a*.

3.3.2. Raman Spectroscopy Analysis

Raman spectroscopy is a structural characterization technique that relies on inelastic scattering of monochromatic light, known as Raman scattering. The vibrational states in the material are indicated by wave number, and the molecular structure is defined by the width. The intensities can also be compared in the perpendicular and polarized directions to determine the orientation and symmetry of a particular material. Identification of chemical structure and physical form of samples are undergone using Raman spectroscopy, along with that the characteristic spectra features identify the substances of a sample and to calculate the amount of substance quantitatively or semi-quantitatively in a sample.

Raman measurements were performed on a Bruker (Alpha) KBr/ATR in the range of 375–750 cm^{-1} with KBr Optics and high sensitivity DLATGS by using a conventional backscattering geometry with a charged-couple device (CCD) detector consisting of a triple polychromator. The diode laser source used is of the near-infrared 785nm laser with a nominal output of 12.5 mW. As the light interacts with the molecule, virtual sites that are of short-lived states are formed by polarising the electron cloud around the nuclei. These unstable state results in photon re-radiation, and these

energy changes are detected by vibrational spectroscopy (Mukherjee et al. 2017; Smith and Dent 2005).

3.3.3. Scanning Electron Microscopy (SEM) Analysis

The scanning electron microscope (SEM) generates various signals using a focused beam of high-energy electrons at the surface of solid specimens. Signals derived from electron-sample interactions reveal information such as morphology, size, chemical composition, and the crystalline structure. Scanning electron microscopy analysis of the samples is analyzed in a CARL ZEISS SIGMA instrument for the microstructural and compositional analysis of the samples. The Sputtering of the samples was done before the analysis. Secondary electrons and backscattered electrons are frequently used for imaging samples: secondary electrons are especially useful in showing topography and morphology on samples, while backscattered electrons illustrate contrasts in multiphase sample composition. An X-ray is emitted to balance the energy difference created in the atom due to electron vacancy created during the electron ejection from the atom (Voutou and Stefanaki 2008; Zaera and Ma 2006).

3.3.4. Transmission Electron Microscopy (TEM) Analysis

Transmission Electron microscopy is considered to be the most ultrasensitive technique for the evaluation and analysis of the morphology of the sample. A Transmission Electron microscope provides a high-resolution image when the electron beam falls on a very thin specimen and the interaction between the atoms, and the electrons are used for analyzing the crystal structure, grain boundaries, and dislocations. Ultrastructure and crystal defects of the metals can be evaluated using TEM analysis. Diffraction is created during the interaction of electron by crystal, and the crystal lattice information is obtained by the patterns of spots created on the screen during the diffraction. Particle size is calculated from a suitable TEM image by fitting the histogram plot of the particle size and counts by Gaussian peak fitting. To view the inner texture of the particle, the analysis was carried

out using JEM 2100, JEOL TEM (Transmission Electron Microscope) along with SAED (Selective Area Electron Diffraction).

3.3.5. Brunauer-Emmett-Teller (BET) Surface area Analysis

The SMART SORB— 92/93 instrument was used to measure the BET surface area. To remove the residual moisture, the samples were evacuated at 150°C/3 h before the analysis, and nitrogen gas was flushed for 2h. BET analysis provides the surface area of the materials by the nitrogen adsorption measured as a function of relative pressure. To remove the moisture and adsorbed gases, the sample has been regenerated for 60 min at 200°C. The N_2 in the gas mixture gets physically adsorbed on a solid in layers, and the adsorption isotherm is obtained by measuring the gas adsorbed across a wide range of relative pressure at a constant temperature of 77K. To calculate the surface area of the sample, the sample is removed from the nitrogen atmosphere and is heated to desorb the N_2. The volume of nitrogen adsorbed is obtained from the isotherm was used in single-point BET equation (**Equation (3.9))** (Hwang and Barron 1987).

$$\frac{1}{X\left[\left(\frac{P_0}{P}\right)-1\right]} = \frac{1}{X_m C} + \frac{C-1}{X_m C}\left(\frac{P}{P_0}\right) \tag{3.9}$$

Where X is the weight of nitrogen adsorbed at a given relative pressure (P/P_0), X_m is related to the volume of gas adsorbed at STP, which is the monolayer capacity, and C is constant.

Particle size is calculated using the BET surface area is expressed by **Equation 3.10.**

$$\textbf{Particle size from BET surface area} = \frac{6}{\rho \times \textbf{BET Surface area}} \tag{3.10}$$

Where ρ is the density of the metal oxide.

The degree of agglomeration is calculated as the ratio of particle size calculated using BET surface area and crystallite size (D) calculated using the Scherrer equation from XRD analysis (Ayastuy et al. 2010).

$$\Phi = \frac{D_{BET}}{D_{XRD}} \qquad\qquad (3.11)$$

3.3.6. Thermo Gravimetric Analysis (TGA)

The Thermogravimetric analysis was conducted on the fine powder sample using a TGA instrument TGA instrument (TG/DTA 6300) over a temperature range of 30-650°C at 10°C/min heating rate using 100 ml/min flow of air. TGA is a themal analysis technique in which the weight loss of the samle is measured in terms of increasing temperature (CHR) or time (constant temperature). The samples were contained in an alumina crucible and the samples were heated with a heating rate of 5 K/min upto 700°C. The microthermo balance measures the weight change in the sample due to the thermal decomposition, absorption of oxygen or due to any other reactions. All the measurements and the datas are collected with the software.

3.3.7. Dilatometer Studies

The dilatometer is an equipment used to measure dimensional changes in a material as a function of temperature. Dilatometer can be used to provide measurements like sintering temperature, linear shrinkage, shrinkage rate, linear thermal expansion, coefficient of thermal expansion, phase transitions, softening point, shrinkage steps, and decomposition temperature, and glass transition temperature. Dilatometric studies were conducted on samples using a horizontal push-rod type dilatometer (Netzsch, DIL 402, Germany) to study the linear shrinkage and shrinkage rate behavior of the sample and to calculate the activation energy and kinetics of sintering for the initial phases of sintering. The datas of the experiments were collected using Netzsch measurement software. The datas collected were analyzed using the Netzsch Proteus Analysis software.

Sintering behavior of the iso-pressed powder (100MPa) compacts was studied under constant heating rate conditions at 5°C /min, and heated from 33°C to 1500°C to study the shrinkage behavior. In addition to this, constant heating rate experiments at a various heating rate of 5 K/min, 10 K/min, and 15 K/min were carried out from 33°C to 1500°C/

30 minutes to calculate the activation energy of the pellet. The samples were sintered in isothermal conditions as well, where the temperature was held at different levels in the respective temperature range for the sample followed by fast heating (15°C/min) to reach the next isothermal zone.

The relative density of the green pellets and the sintered pellets was measured by using Archimedes method by using the equation;

$$\textbf{Relative density (\%) = (d_m/d_t) x 100} \qquad \textbf{(3.12)}$$

Where d_m is the sintered pellet density measured by using the Archimedes method, and d_t is the theoretical density of the PDC sample (Prasad et al. 2008).

CHAPTER 4

PRASEODYMIUM DOPED CERIA AS ELECTROLYTE MATERIAL SYNTHESISED BY EDTA – CITRATE METHOD FOR IT-SOFCs

Praseodymium-doped ceria (PDC, $Ce_{0.9}Pr_{0.1}O_2$) electrolyte material for intermediate temperature solid oxide fuel cells has been successfully synthesised by EDTA-citrate method. From X-Ray diffraction analysis, fluorite structure along with a crystallite size of 5.4 nm is obtained for PDC nanopowder calcined at 350°C/ 24h. Raman spectroscopy confirmed the structure, presence of oxygen vacancies with the manifestation of the main peak at 457 cm^{-1} and with a secondary peak at 550 cm^{-1}. From Transmission Electron Microscopy analysis, the average particle size is around 7–10 nm and selected area electron diffraction patterns further confirmed the fluorite structure of PDC nanopowder. The PDC nanopowder displayed a BET surface area of 65m^2/g with a primary particle size of ~13 nm (calculated from BET surface area). Dilatometer studies revealed a multi-step shrinkage behaviour with the multiple peaks at 522, 1171 and 1461°C which may be originated due to the presence of multiple size hard agglomerates. The PDC electrolyte pellet sintered at 1500°C displayed an ionic conductivity of $1.213x10^{-3}$ S cm^{-1} along with an activation energy of 1.28eV. Instead of a single fluorite structure, XRD of sintered PDC pellet showed multiple structures (Fluorite structure (CeO_2) and cubic structure (PrO_2).

4.1 SYNTHESIS OF PDC ELECTROLYTE MATERIAL BY EDTA – CITRATE METHOD

The PDC has been synthesised by variety of techniques such as hydrothermal method (Shuk and Greenblatt 1999), sol gel method (Guo et al. 2011), flux method (Bondioli et al. 2000), co-precipitation method (Reddy et al. 2009), combustion synthesis (Esther Jeyanthi et al. 2015) etc. The EDTA-citrate method is used to synthesize a wide variety of oxide materials when compared to other synthesis methods (Shao et al. 2000; Shao and Haile 2004). EDTA and citric acid are used as chelating agents, which forms stable complexes. EDTA citrate method offers the possibility for the synthesis of nano scaled particle size with good compositional homogeneity (Prasad et al. 2012).

This chapter shall discuss the synthesis of praseodymium doped ceria due to the potential in existing in two oxidation states which promotes the oxygen vacancies. Therefore, in the present study, for Pr, a fixed amount of 10 mol% is taken and is synthesised by the EDTA-Citrate complexing method; and physical characterization such as XRD, Raman spectroscopy, SEM and TEM analysis along with the shrinkage behaviour and ionic conductivity measurements of the as-prepared samples were carried out.

In further, the nature of solubility of praseodymium ceria solid solutions for intermediate temperature solid oxide fuel cells synthesised by EDTA – citrate method is analysed. Based on the phase stability study, the sintering temperature of the PDC material can be concluded below the solubility temperature of the PDC material in order to avoid the phase separation issue.

4.1.1   X-ray Diffraction (XRD) and Raman Spectroscopy Analysis

X-ray diffraction patterns and Raman spectra of the PDC powder synthesised by the EDTA - citrate method with the composition of $Ce_{0.9}Pr_{0.1}O_2$ calcined at 350°C for 24h is shown in **Figure S4.1** and **Figure S4.2**. The relatively broad peaks would indicate the presence of a crystalline phase and the formed crystallites was very small. From the XRD pattern, all the major peaks obtained corresponds to the cubic fluorite structure of CeO_2 and agrees well with the JCPDS card data no. 34-0394 (Jamshidijam et al. 2014; Shuk and Greenblatt 1999; Tok et al. 2007). The average crystallite size as calculated by Debye Scherrer's equation of the most intense peak (111) was found to be 5.4 nm.

Table 4.1 shows various physical parameters of PDC nanopowder synthesized by hydrothermal synthesis (Tok et al. 2007), combustion method (Jamshidijam et al. 2014), sol-gel method (Guo et al. 2011). **Table 4.1** is arranged in the increasing order of the calcination temperature (from 100 to 900°C). As it can be noticed that there is an increase in the particle size, decrease in the BET surface area with an increase in the calcination temperature. It is interesting to note that the crystallite size did not follow the similar trend. The crystallite size (5.4 nm) of PDC nanopowder obtained from the current study (EDTA Citrate method, calcined at 350°C/ 24h) is smaller (5.4 nm) than the crystallite size obtained by the hydrothermal method (16.1 nm), calcined at 100°C/ 2h).

It shows that the synthesis method plays a crucial role in controlling the powder characteristics such as crystallite size, morphology, agglomeration and surface area of the PDC nanopowder. Peng et al. (2007) reported that the smaller particle size of the materials allows the sintering of the material into highly dense ceramic pellets at a significantly lower sintering temperature (Peng and Zhang 2007). It was also reported that the powder with highest surface area and smaller particle size allows high sintered density at a lower temperature in a short time (Purohit et al. 2006). Smaller pore requires relatively lower temperature to close the pores whereas larger pores require a higher temperature and longer time to eliminate the pores. Thus the formation of smaller particle

size with soft nature of agglomerates decreases the sintering temperature compared to hard nature of agglomerates with wider pore distribution (Prasad et al. 2010). Thus the powder characteristics affect the densification process during sintering, which will be discussed in-detail in the dilatometer studies in section 4.1.2.

Raman spectra of the PDC powder synthesised by the EDTA - citrate method also confirms the formation of cubic fluorite phase. An intense and sharp peak at 457 cm^{-1} was observed and can be attributed to F_{2g} vibration mode (O-Ce-O) of the fluorite-like structure of pure CeO_2 (Ahn et al. 2012; Esther Jeyanthi et al. 2015). Besides, an additional weak intense peak at 550 cm^{-1} was observed, and it can be associated to a band that could be due to the extrinsic oxygen vacancies present in the solid solution (McBride et al. 1994). The changes in the Raman spectra are related to O vacancies introduced into the cation lattice (multivalent Pr is substituted for Ce^{4+}). Since the radius of Pr^{3+} is larger than Ce^{4+}, it is expected to cause an expansion of the CeO_2 lattice. At higher temperatures, the migration of oxygen ions is facilitated by the presence of oxygen vacancies and thus enhances the ionic conductivity. Since the oxygen vacancies facilitate the migration of oxygen ions through the crystal lattice that also enhances the low temperature densification during sintering (He et al. 2010). Thus, the results from the literature suggest that the ionic conductivity of the sample is enhanced by the presence of high concentration of oxygen vacancies (Li et al. 2009). From the Raman spectroscopy analysis, no indications can be found regarding the presence of an impurity phase even after the calcination step, which is in good agreement with the XRD analysis.

Table 4.1: Comparison of PDC material synthesised by various methods

Synthesis method	Particle Size (nm)	BET Surface area (m^2/g)	Crystallite size (nm)[#]	Calcination Temperature (°C)	Reference
Hydrothermal method	13 ~25[§]	72	16.1	100/ 2h	(Tok et al. 2007)
EDTA Citrate method	13[*]	65	5.4	350/ 24h	[This study]
Combustion method	25[*]	34	17.1	700/ 2h	(Jamshidij am et al. 2014)
Sol-gel method	30 ~50[§]	17	31.3	900/ 4h	(Guo et al. 2011)

* Average particle size calculated from BET data
§ Average particle size calculated from TEM data
# Crystallite size calculated from XRD data

4.1.2 SEM and TEM Analysis

SEM microstructures of the PDC nanopowder are shown in **Figure S4.3**. It is observed that the PDC electrolyte material synthesized is very porous in nature and exhibit particle agglomeration up to a certain extent. **Figure S4.4 (a)** and **4(b)** depicts the TEM image of the PDC nanoparticles. Spherically shaped particles with slight agglomeration were observed. **Figure S4.4 (c)** shows the corresponding selected area electron diffraction

pattern (SAED) patterns of PDC nanopowder. The figure shows concentric rings, which is attributed to (1 1 1), (2 0 0), (2 2 0) and (3 1 1) reflections and these patterns indexed to the cubic fluorite structure of PDC nanopowder matches well with the XRD results.

4.1.3 Dilatometer Studies

The shrinkage rate spectra and linear shrinkage of the PDC pellet is shown in **Figure 4.1**. The sintering process of PDC sample undergoes multiple step shrinkage behaviour is evident from the shrinkage rate curve of the figure. The shrinkage maxima at 522, 1171 and 1461°C indicates the presence of multiple size hard agglomerates after compaction (Prasad et al. 2008). This can be attributed to the shrinkage of different pore sizes in between the hard agglomerates obtained from the non-uniform particle size distribution. **Figure S4.5** shows the non-uniform particle size distribution of calcined PDC powder. From the linear shrinkage of PDC sample as shown in **Figure 4.1**, the shrinkage has not fully completed below 1500°C with a final linear shrinkage of 18%. From dilatometer studies obtained for PDC pellet, it is confirmed that the synthesis method and/ or processing conditions have to be altered to achieve nanoparticles with uniform particle size distribution, which leads to uniform shrinkage behaviour and thus decreases the sintering temperature of the PDC material.
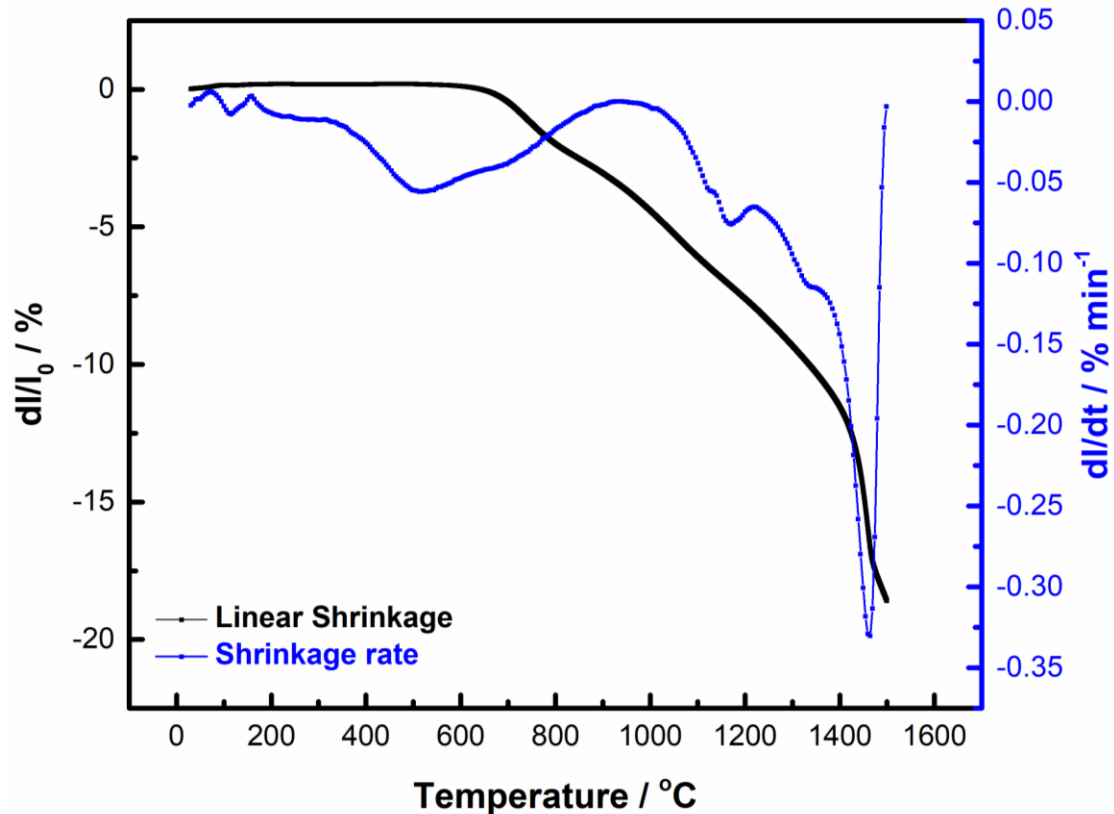
Figure 4.1: Linear shrinkage and shrinkage rate spectra of the PDC pellet

4.1.3. Electrical Conductivity Studies

Figure S4.6 manifests the Arrhenius plot of the conductivity obtained from the PDC pellet sintered at 1500ºC/ 5h in the air. A linear increase in the conductivity is observed with the rise of the operating temperature from 500°C to 800°C. At 700°C, the conductivity is 1.213×10^{-3} S cm^{-1} and is higher than the conductivity of the PDC pellet observed by Shuk and Greenblatt (Shuk and Greenblatt 1999). The activation energy obtained from the Arrhenius plot is around 1.28 eV. **Table 4.2** shows the conductivity of the 10 mol% PDC materials synthesized by various methods. It is noticed that the conductivity is affected by the synthesis method since synthesis method affects the powder properties such as crystallite size, morphology, agglomeration and surface area of

the PDC nanopowder. When compared to the 10 mol% PDC conductivity obtained by M J Chen et al. (Chen et al. 2007) that is 1.1×10^{-2} S cm^{-1} at 700°C, the conductivity observed in the present study is low. For finding out the reasons behind this behaviour, XRD analysis of the sintered PDC pellet is done and depicted in **Figure 4.2**.

From **Figure 4.2**, it is evident that there is a clear phase separation (fluorite CeO_2 + cubic PrO_2) (Dogra et al. 2014). The observed diffraction peaks of ceria agree with the JCPDS card no. 34-0394 and the diffraction peaks of PrO_2 agrees well with the JCPDS card no. 00-024-1006. This phase separation might be the reason for showing a lower conductivity. The conductivity of 10 mol% PDC is one order lower than the 10 mol% GDC electrolyte material (Medisetti et al. 2017), and one of the reasons for such kind of low conductivity might be occurring due to phase separation of PDC material.

Table 4.2: Comparison of Electrical Conductivity of 10 mol% PDC material obtained by various synthesis methods

Synthesis method	Total Conductivity at 700°C (S cm^{-1})	Activation Energy (eV)	Sintering Temperature (°C)	Reference
Hydrothermal Method	6.6×10^{-4}	1.20	1300 / 4h	(Shuk and Greenblatt 1999)
EDTA-Citrate Method	1.2×10^{-3}	1.28	1500 / 5h	[This study]
Pechini Method	1.1×10^{-2}	-	1500 / 14h	(Chen et al. 2007)
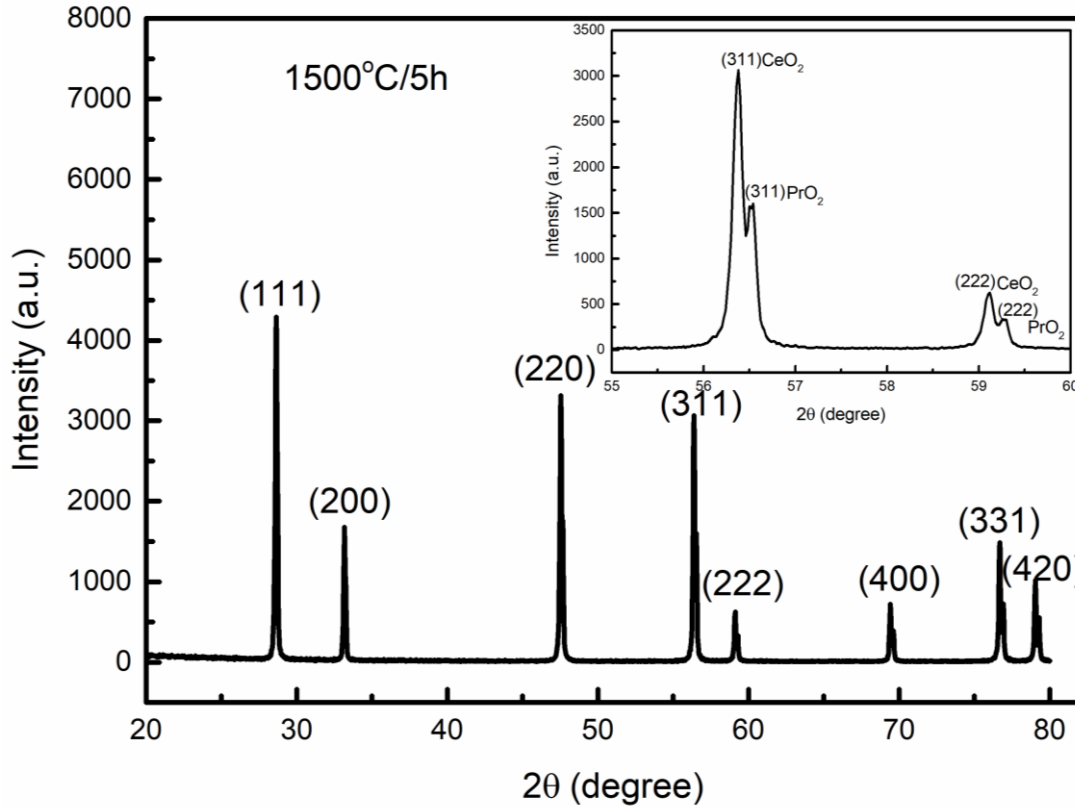
Figure 4.2: XRD analysis of the sintered PDC pellet

Apart from singly doped ceria, several researches have reported the highest ionic conductivity of ceria by doping with two or more dopants. When compared to the results of Sm^{3+}, Pr^{3+} and Nd^{3+} triple doped ceria obtained by Liu et al. (2017) the conductivity of PDC electrolyte material of the present study is lower than the ionic conductivity they have reported (1.25×10^{-1} S cm^{-1} at 600°C). It was reported that the enhancement in ionic conductivity is due to the secondary doping of Pr^{3+} and Nd^{3+} ions which promote the surface ion incorporation and enhance the grain boundary conductivity (Liu et al. 2017). The ionic conductivity of the PDC material of the present study is less than that of nanocrystalline tri-doped ceria ($Ce_{0.76}Pr_{0.08}Sm_{0.08}Gd_{0.08}O_{2-\delta}$) synthesised by sol-gel auto combustion method (total ionic conductivity is 1.86×10^{-2} S cm^{-1}) reported by

venkataramana et al (Venkataramana et al. 2017). The high ionic conductivity of these samples is due to the high concentration of oxygen vacancies in the sample.

From the results obtained in the study, further research focuses on finding new methods (synthesis, processing conditions and dopant modification) to reduce sintering temperature of 1500°C to make PDC materials as an electrolyte material for SOFC applications. Thereby overcoming the phase separation issue, which plays a crucial role in enhancing the ionic conductivity of the PDC electrolyte material for SOFC applications. Thus, identification of the solubility limit of Pr in the ceria lattice plays a key role in enhancing the properties of PDC material and further research was focussed to decrease the sintering temperature of praseodymium doped ceria material below the solubility limit temperature is essential to commercialise PDC as an electrolyte material for IT – SOFCs.

4.2 NATURE OF PHASE STABILITY OF SINTERED Pr DOPED CERIA BASED MATERIAL

The nature of solubility of praseodymium ceria solid solutions, $Ce_{0.9}Pr_{0.1}O_2$ (10PDC) with an increase in heat-treatment temperature from 800°C to 1200°C as oxide ion conductors for intermediate temperature solid oxide fuel cells (IT-SOFCs) were analysed. It was reported that the ceria praseodymium oxide forms fluorite type solid solution up to 30 mol% PrO_{2-x} (Nauer and Steele 1994) while another study reported that single phase fluorite solid solution is formed up to 35 mol% (Chen et al. 2007). However, there is a lack of information reported on the effect of heat treatment on the solubility of praseodymium in CeO_2. The samples were synthesized by EDTA citrate complexing method. Among the various synthesis method, EDTA citrate method is a complex polymerized method used to prepare wide variety of materials oxide (Shao et al. 2000; Shao and Haile 2004). The as-synthesised samples were characterized by XRD, Raman Spectroscopy and SEM analysis. The limited temperature stability of the solid solutions are discussed with respect to the effect of heat treatment in the doped samples.

In the current research, the results of a systematic study of solubility of 10PDC solid solutions by using a variant of EDTA – Citrate complexing method at various heat treatment temperatures are analyzed. The scope of the present work is to develop a PDC based oxide ion conducting material for SOFCs with the aim of enhancing their properties by selecting proper heat treatment conditions (800°C – 1200°C).

4.2.1   X-Ray Diffraction (XRD) Analysis

Figure S4.7 represents the XRD pattern of PDC samples sintered at 800, 900, 1000, 1100, and 1200ºC/ 5h. The XRD pattern revealed the absence of impurity phases up to 1000ºC and exhibited only the reflections of (111), (200), (220), (311), (222) and (400) planes corresponding to the fluorite structure of CeO_2, which indicates the thermally stable solid solution formation in PDC sample. On clear observation of PDC sample sintered above 1000ºC shown in **Figure 4.3** and **Figure S4.8** a distant peak splitting of fluorite CeO_2 and cubic PrO_2 is significantly evident, this is due to the insolubility of praseodymium in to ceria. When compared to sample sintered at 1100ºC and 1200ºC, the number of grains and grain boundaries are high for sample sintered at 800ºC. With the increase in sintering temperature there is an increase in grain size and a decrease in grain boundaries, as a result the smaller ionic radius tries to precipitate out from the matrix (Abbas et al. 2017). This suggests that for the given dopant concentration of praseodymium, the sintering temperature of 1000ºC is sufficiently high enough to ensure the solubility limit of Pr in to ceria system. There is a slight shift in the diffraction peak of PDC sample towards a lower angle when compared to the pure ceria reported in the literature. This is due to the increase of the lattice parameter, which can be attributed to the presence of Pr^{3+} along with Pr^{4+} in the oxide lattice (Reddy et al. 2009).

The crystallite size of the PDC sample is in the range of 15 – 35 nm. The crystallographic data, BET surface area and the lattice parameters of PDC samples sintered at 800, 900, 1000, 1100, and 1200ºC/ 5h are tabulated in **Table S4.1**. There is an increase in crystallite size and lattice parameter, and a decrease in lattice strain is noticed with an increase in the sintering temperature. The increase in the lattice parameter is due to the slightly larger ionic radius of the dopant compared to that of the host ion.
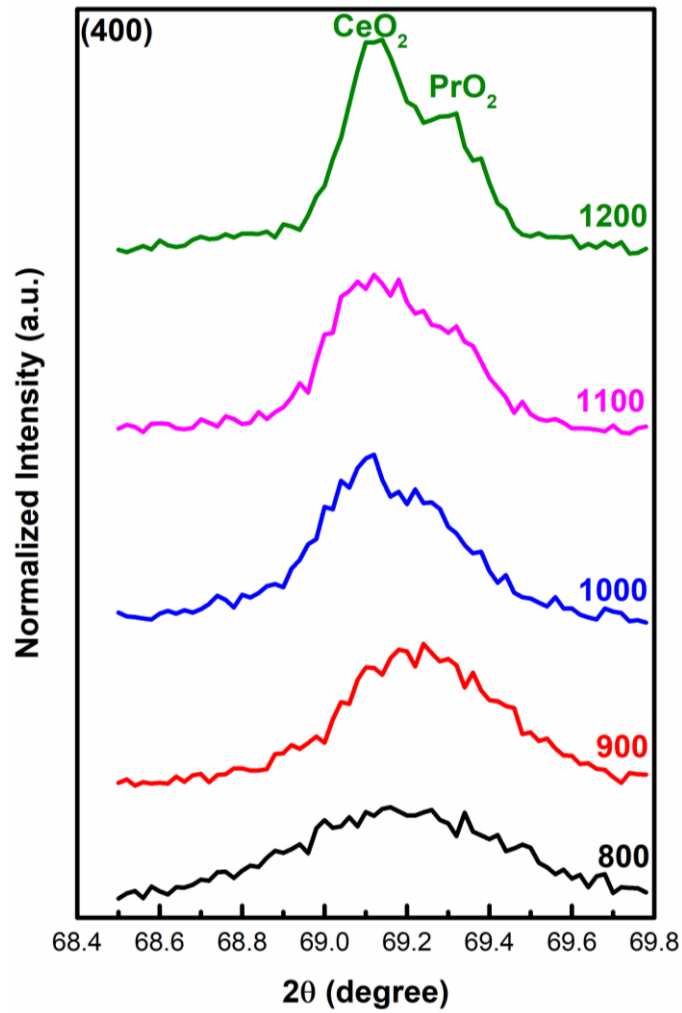
Figure 4.3: XRD pattern of PDC sample sintered at 800, 900, 1000, 1100 and 1200ºC/5h and to peak splitting of (400) peak of sintered PDC sample

4.2.2 Raman Spectra Analysis

The Raman spectra of the as synthesised 10 PDC samples with 785-nm laser lines are shown in **Figure 4.4**. Two main characteristic peaks were observed in the region of 460 – 600 cm^{-1}, and there is no peak corresponding to the individual oxide was observed from the figure. The highest phonon energy corresponds to the peak at 465 cm^{-1}, and it can be related to the F_{2g} vibration mode of the fluorite like structure of pure CeO_2. In addition, the weak Raman band at 580 cm^{-1} is attributed to the formation of oxygen vacancies and the intensity of the peak is related to the concentration of oxygen vacancies (Guo et al. 2011). In case of PDC solid solution, the incorporation of $Pr^{3+/4+}$ leads to the formation of extrinsic oxygen vacancies in addition to the intrinsic oxygen vacancies (Reddy et al. 2011). From the Raman spectroscopy analysis, no indications can be found regarding the presence of an impurity phase even after the sintering at 1000ºC.

4.2.3 Scanning Electron Microscopy Analysis (SEM analysis)

Figure 4.5 (a–e) shows the effect of sintering temperature on surface morphology of the as-synthesised PDC sample. It was found out that the PDC electrolyte material synthesised exhibited foam like agglomeration up to a certain extent and is very porous in nature. It was also observed that the degree of agglomeration increases when the sintering temperature increases to 1200ºC. From **Figure,** it is also evident that trapped porosity inside the grains of materials and enhanced grain growth during sintering process is taking place with the increase in the sintering temperature. During the process of sintering, agglomeration of the particle suppresses the densification process significantly. This can be related to the decreased mobility of cations due to the aggregation of the particle.

The grain growth of the sample and the phase separation of the PDC sample above 1000ºC results in a low conductivity of the sample. Therefore from the results obtained in the phase stability study, further research focuses on to decrease the sintering temperature

of the PDC samples by altering the synthesis method, processing conditions or dopant modification.
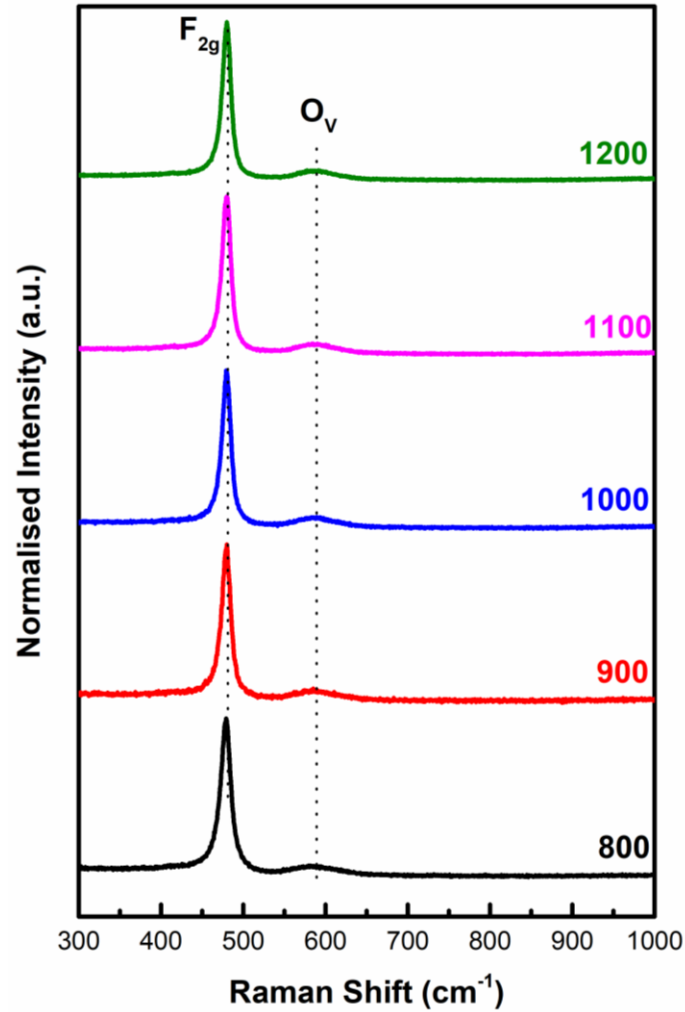
Figure 4.4: Raman Spectroscopy of PDC sample sintered at 800, 900, 1000, 1100 and 1200ºC
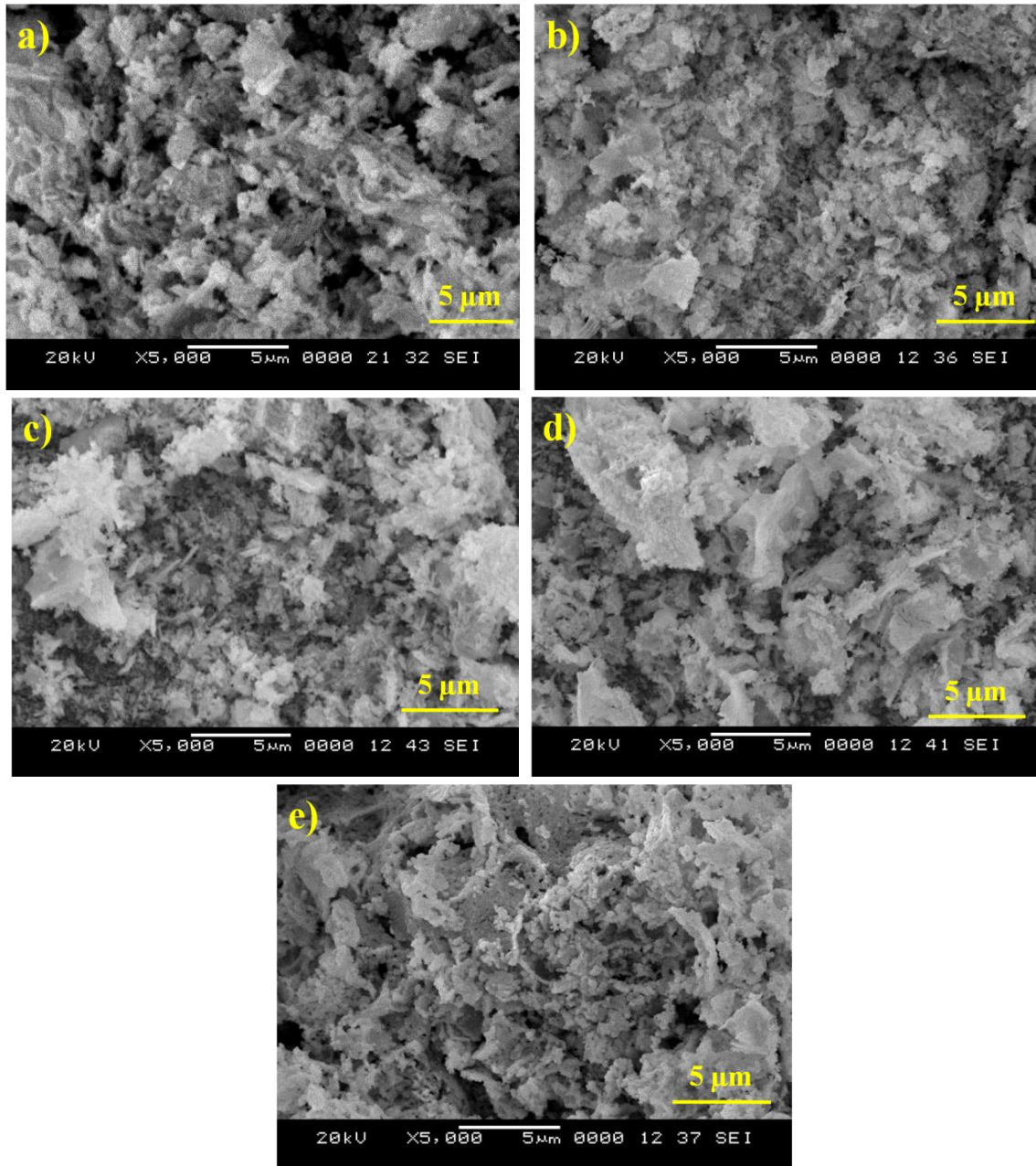
Figure 4.5: SEM micrographs of PDC sample sintered at a) 800, b) 900, c) 1000, d) 1100 and e) 1200ºC

4.3 CONCLUSION

Praseodymium-doped ceria (PDC, $Ce_{0.9}Pr_{0.1}O_2$) electrolyte material for intermediate temperature solid oxide fuel cells (IT-SOFCs) has been successfully synthesised by EDTA-citrate method. From XRD, BET and TEM analysis it can be observed that the calcined sample exhibited a crystallite/particle size of 5–10 nm and from particle size analyser, it is found that the sample displayed an agglomerate size 3.06 μm. Multiple shrinkage behaviour has noticed for the PDC pellet which indicates the presence of multiple size hard agglomerates after compaction and the shrinkage has not fully completed below 1500°C with a final linear shrinkage of 18%. This is due to the presence of multiple size hard agglomerates after compaction.

At 700°C, the sample displayed conductivity of 1.213×10^{-3} S cm^{-1} which is one order lower than the 10 mol% GDC electrolyte material. The phase separation of PDC material could be the reason for the lower ionic conductivity of the material and the XRD of the sintered pellet has been done. A clear phase change of sintered PDC (fluorite CeO_2 + cubic PrO_2) pellet occurs at 1500°C. Therefore, it is necessary to decrease the sintering temperature of the PDC pellet since the phase change has been noticed at 1500°C.

Therefore, further focus is to find out the temperature for the solubility limit of praseodymium in to the ceria lattice. XRD patterns revealed that fluorite-type (F) crystal structure of ceria is confirmed up to sintering temperature of 1000°C, and a clear phase separation of CeO_2 + PrO_2 (biphasic; Fluorite phase + Cubic phase, F + C) is evident at higher heat treatment temperatures above 1000°C, Pr is precipitated in the praseodymium doped ceria system which are in agreement with the phase transitions that occurs in these samples. The assumed phase transition of the synthesized samples may be due to the limited temperature stability of the solid solutions. The grain growth of the sample and the phase separation of the PDC sample above 1000ºC results in a low conductivity of the sample.

Therefore, in order to decrease the sintering temperature of the PDC sample; synthesis method, processing conditions and dopant modification should be altered. The synthesis method and/ or processing conditions have to be altered to achieve nanoparticles with uniform particle size distribution, which leads to uniform shrinkage behaviour and thus decreases the sintering temperature of the PDC material. The results suggests that the PDC based material may be a better electrolyte for the application of electrolyte material of IT – SOFCs with a sintering temperature less than the solubility limit temperature of praseodymium in the ceria lattice.

The next chapter focuses on the effect of synthesis methods on the sintering behaviour of the PDC material. The next chapter also discusses the sintering kinetic mechanism for the early stages of sintering for PDC material. The results obtained are discussed in detail and are outlined in the next chapter.

CHAPTER 5

DILATOMETER STUDIES OF PRASEODYMIUM DOPED CERIA: EFFECT OF SYNTHESIS METHODS ON SINTERING BEHAVIOUR

Praseodymium-doped ceria ($Ce_{0.9}Pr_{0.1}O_2$, PDC), as an electrolyte material for IT-SOFCs, is investigated with respect to the effect of synthesis method and a detailed analysis was carried out to understand the effect on crystallite size, morphology, specific surface area and sintering behaviour. The various synthesis routes such as microwave assisted co-precipitation method, room temperature co-precipitation method and EDTA-citrate complexing method was adopted for the synthesis of praseodymium doped ceria-based nano-materials. XRD pattern confirms the fluorite-type crystal structure of ceria and Raman spectroscopy analysis confirms the structure with the presence of oxygen vacancies. PDC synthesised by microwave assisted co-precipitation method using isopropyl alcohol as solvent exhibited better sintering activity, reduced the sintering temperature and promoted the densification rate when compared to other synthesis methods with uni-model shrinkage behaviour with shrinkage maxima at 765°C. Based on two sintering models (CHR/Dorn method), the initial stage sintering mechanism was investigated in the present study and confirmed that the grain boundary diffusion (m ~ 2) as the dominant mechanism and the activation energy was found to be 116 kJ/mol (CHR model) and 176 kJ/mol (Dorn Method) for initial stages of sintering for PDC material synthesised by microwave assisted co-precipitation method using isopropyl alcohol as solvent.

5.1 EFFECT OF SYNTHESIS METHODS ON SINTERING BEHAVIOUR OF PDC BASED ELECTROLYTE MATERIAL

The synthesis method to be adopted for praseodymium doped ceria based electrolyte material to reduce the sintering temperature has to be studied before the study of sintering additives effect on the sintering behaviour of PDC material. Over the number of years, detailed investigations of the singly doped ceria electrolytes such as GDC, SDC and YDC have been extensively carried out. Although there is sufficient literature reported on the different synthesis techniques of Praseodymium doped ceria nano-powder (Chen et al. 2007; Esther Jeyanthi et al. 2015; Guo et al. 2011; Shuk and Greenblatt 1999; Tok et al. 2007a), only few works has been reported on shrinkage behaviour and decreasing the sintering temperature of $Ce_{1-x}Pr_xO_{2-y}$ (PDC) based electrolyte materials for SOFC applications. It was reported that the ceria praseodymium oxide forms fluorite type solid solution up to 30 mol% PrO_{2-x} for 1550ºC sintered pellet (Nauer and Steele 1994) while another study reported that single phase fluorite solid solution is formed up to 35 mol% for 1500ºC sintered pellet (Chen et al. 2007).

According to our earlier report (Shajahan et al. 2018b), it was found that 10 mol% PDC synthesised by EDTA- citrate method showed a lower ionic conductivity due to the presence of secondary phase at 1500ºC and exhibited a high sintering temperature of 1500°C. From these findings, further research was carried out to find suitable synthesis methods for 10 mol% PDC material to reduce the sintering temperature below 1500°C. The previous chapter results shows that the secondary phase of PDC synthesised by EDTA- citrate method starts at 1000ºC and hence it is mandatory to reduce the sintering temperature below 1000ºC and synthesis approach is followed to overcome the issue. However, there is a lack of information reported on the effect of heat treatment on the solubility of Pr in CeO_2. Therefore, this was the motivation to decrease the sintering temperature below 1000°C by following different synthesis approach.

Therefore, Praseodymium-doped ceria ($Ce_{0.9}Pr_{0.1}O_2$, PDC), as an electrolyte material for IT-SOFCs, is investigated with respect to the effect of synthesis method and a detailed analysis was carried out to understand the effect on crystallite size, morphology, specific surface area and sintering behaviour. The various synthesis routes such as microwave assisted co-precipitation method, room temperature co-precipitation method and EDTA-citrate complexing method was adopted for the synthesis of praseodymium doped ceria-based nano-materials.

TGA, XRD, Raman analysis, BET surface area analysis and dilatometer studies was carried out for all the as synthesised samples to confirm the phase, nature, agglomerate size, particle size, surface area and the sintering behaviour (linear shrinkage and shrinkage rate). XRD pattern confirms the fluorite-type crystal structure of ceria and Raman spectroscopy analysis confirms the structure with the presence of oxygen vacancies. Thermogravimetric analysis of the precursor material was done to find out the decomposition behaviour with the temperature rise.

In further, the linear shrinkage and the shrinkage rate behaviour of the as-synthesised PDC pellets were studied to fix the sintering temperature. The synthesis method (with less sintering temperature) obtained from the present work has been adopted for the further study with the same sintering conditions. Since the powder synthesis methods play a key role in final microstructure of the electrolyte, particle size of the powder and ionic conductivity of the electrolyte (Tan et al. 2003). Therefore, it is necessary to investigate the effect of powder synthesis methods on the microstructure and sintering behaviour of the PDC nano-powder, since the grain size increase with an increase in sintering temperature and dwell time. The obtained results are illustrated and discussed in further.

5.1.1. Thermo gravimetric Analysis (TGA)

The decomposition of PDC black precursor synthesised by MWCOP- Ethanol, MWCOP- Water, MWCOP- ISP, RTCOP and EDTA- Citrate method was analysed by Thermogravimetric analysis before calcination. **Figure 5.1 (a-c)** shows the thermal behaviour of PDC precursor synthesised by microwave assisted co-precipitation method using different solvents, i.e., ethanol, water and isopropyl alcohol respectively. The initial weight loss for all the samples, in the low temperature range (50 – 130°C) is due to the removal of absorbed water molecules in the coordination cycle (Prasad et al. 2008). A small exothermic peak in the same temperature range is detected is mainly attributed to the volatilization of minor impurities. The second weight loss in the temperature range of 150 – 400°C is due to the decomposition of the anhydrous salt/ precursor and an intense exothermic peak can be detected at 270°C (Dudek et al. 2010). The second weight loss can be attributed to the decomposition of nitrate salts, followed by the crystallization of praseodymium ceria based solid solutions.

The weight loss was found to be stable around 450°C for PDC synthesised by water and ethanol as solvents, and 350°C for isopropyl alcohol as solvents, which indicates the formation of phase pure sample at 450°C for water and ethanol and 350°C for isopropyl alcohol as solvents which represents the calcination temperature of the as synthesised powder is to be about 450°C for water and ethanol and 350°C/ 2h for iso-propyl alcohol samples respectively. The weight loss was found to be stable at 400°C for EDTA – citrate method, which implies only the presence of crystalline PDC in all the cases and was confirmed further by the X-ray diffraction analysis.

Figure 5.1 (d) illustrates the thermal behaviour of PDC precursor synthesised by room temperature co-precipitation method using isopropyl alcohol as solvent. TG curve shows two distinct stage of weight loss in two separate steps and DTG curve has two exothermic peaks at 98°C and 255°C. The weight loss in the lower temperature is due to the removal of the superficial and structural water (Prasad et al. 2008). The exothermic peak in the

same temperature range is detected and is mainly attributed to the volatilization of minor impurities. The second weight loss in the temperature range of 240°C – 290°C corresponds to the decomposition of the nitrates (Godinho et al. 2007).

Figure 5.1 (e) represents the TGA graph of pre-calcined PDC sample synthesised by EDTA-Citrate method. Two exothermic peaks at 316 and 350ºC is evident from the DTG curve which indicates the decomposition and combustion of the metal/ nitrate/ citrate/ EDTA complexes in two steps (Prasad et al. 2012). Moisture content in the sample is negligible since only 2% weight loss is evident up to 200°C. The major weight loss in the temperature range of 200-300°C is due to the decomposition of metal chelates of EDTA and citric acid (Prasad et al. 2012). The second exothermic peak at 320ºC – 360ºC is due to the pyrolysis of metal/ nitrate/ citrate/ EDTA complexes with a weight loss of about 32%. After 400ºC no significant weight loss is observed which confirmed the complete removal of impurities from the sample. This confirms that complete decomposition of all the impurities occurs below 450ºC for MWCOP- Ethanol and MWCOP- water; 350ºC for MWCOP- ISP and RTCOP; 400ºC for EDTA- Citrate method; and these temperatures are used for the calcination of the corresponding samples for 2h in air.
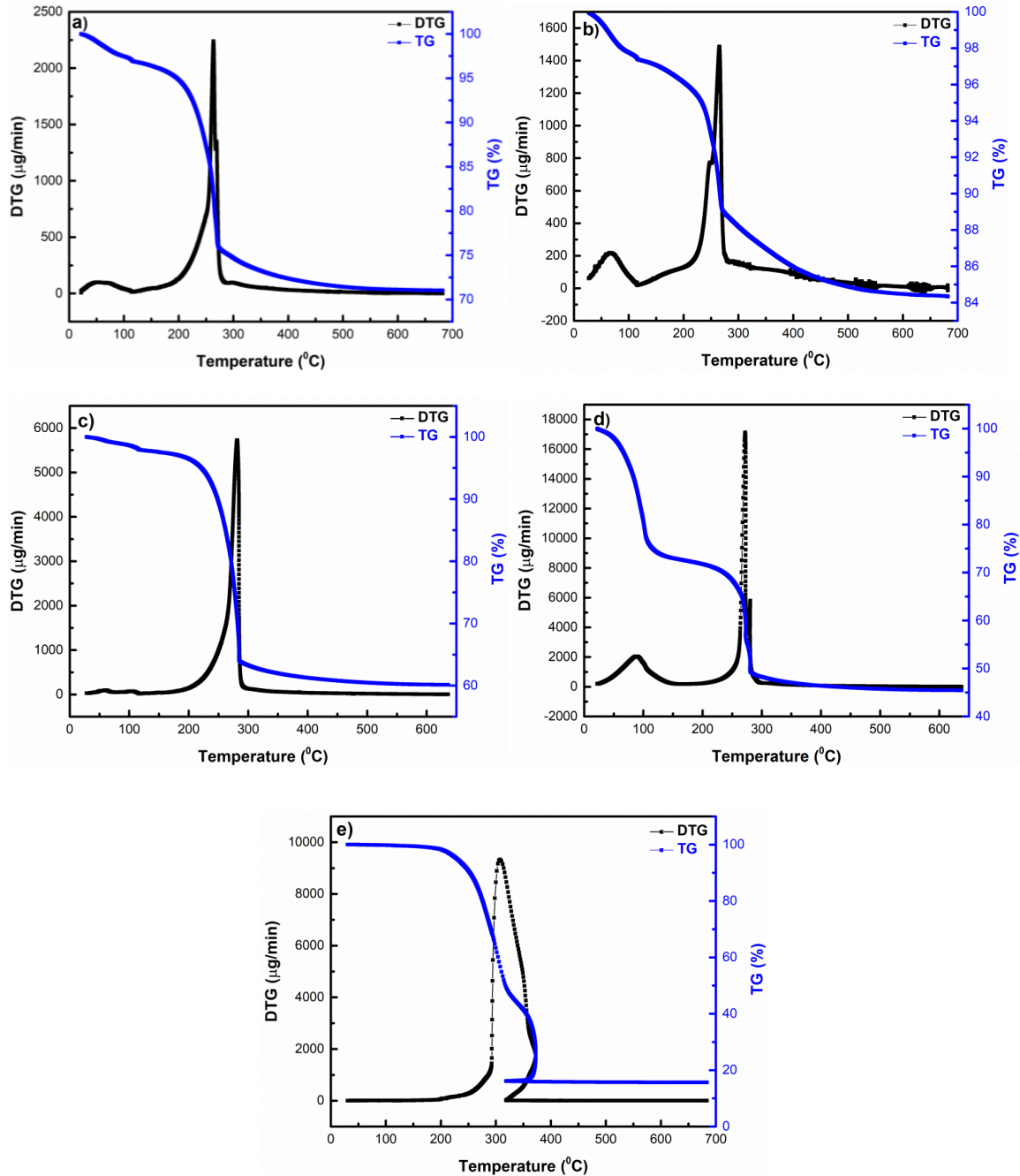
Figure 5.1: TGA Curve of 10 PDC precursor material synthesised by Microwave assisted co-precipitation method using a) ethanol b) water c) Isopropyl alcohol d) RTCOP –ISP e) EDTA- Citrate

5.1.2. X-ray Diffraction (XRD) Analysis

Figure 5.2 displays the XRD diffraction pattern of 10 mol% PDC sample synthesised by microwave assisted co-precipitation method (Ethanol, Water and iso-Propyl alcohol as solvents), room temperature co-precipitation method (Iso-Propyl alcohol as solvent) and EDTA – Citrate method respectively. It can be observed that the diffraction peak of all the as-prepared powder confirms the single phase and the peaks can be indexed to the (111), (200), (220), (311), (222), (400) and (331) planes with a typical cubic fluorite-type crystalline structure of pure CeO_2 (Jamshidijam et al. 2014; Tok et al. 2007b). No additional secondary peaks corresponding to praseodymium oxide were identified in all the samples which indicate the complete incorporation of praseodymium oxide into the lattice of CeO_2. The praseodymium doped ceria appeared to be a single phase for all the synthesis methods.

The average crystallite size obtained by using sherrer's equation and the lattice parameter calculated by using Bragg's equation and other physical properties of the metal oxide is listed in **Table 5.1**. The average crystallite size of the as-synthesized samples varies from 6.6 to 12.2 nm and the lattice parameter was in the range of 5.47 to 5.49A° in which MWCOP-water showed highest crystallite size (12.2 nm) and EDTA-Citrate showed the lowest crystallite size (6.6 nm). The crystallite sizes of all the other samples are within the range. As it can be noticed from **Table 5.1**, that the synthesis methods and calcination temperature plays a key role in powder properties such as crystallite size, surface area, agglomeration and morphology of the as-prepared PDC powder. PDC powder synthesised by using microwave assisted co-precipitation method using different solvents (ethanol and isopropyl alcohol) and room temperature co-precipitation method (isopropyl alcohol as solvent) results in ultrafine particle with uniform crystallite size, can lead to a better sintering behaviour when compared to other methods, and thus the sintering temperature is expected to decrease considerably which will be further discussed in detail in section 5.1.5.

Figure 5.2: XRD pattern of PDC samples synthesised by microwave assisted co-precipitation method, room temperature co-precipitation method and EDTA-citrate method

Table 5.1: Comparison of 10-mol% PDC material synthesised by various methods

Synthesis method		Crystallite size (nm)	Lattice Constant (Å)	Lattice strain (ε)	BET Surface area (m^2/g)	Calcination Temperature (°C)	Degree of agglomeration (Φ)	Composition using EDS (%)	
								Ce	Pr
MWCOP	Ethanol	9.2	5.47	0.0162	61	450/ 2h	1.49	89.30	10.53
	Water	12.2	5.47	0.0122	50	450/ 2h	1.36	90.30	9.68
	Iso-Propyl Alcohol	9.6	5.47	0.0154	71	350/ 2h	1.24	89.55	10.44
Room temperature co-precipitation method		9.7	5.49	0.0153	73	350/ 2h	1.17	89.60	10.36
EDTA - Citrate		6.6	5.47	0.0225	82	400/ 2h	1.53	90.02	9.97

5.1.3. Raman Spectroscopy Analysis

The Raman spectra with an excitation laser line (785nm) of PDC powders synthesised by various methods was done in order to confirm the formation of praseodymium doped ceria solid solutions are presented in **Figure 5.3**. A sharp and intense first order peak was observed at $465cm^{-1}$ is due to the F_{2g} symmetric mode of fluorite type cubic structure of pure CeO_2, which corresponds to the vibration of oxygen ions around cerium ions (Ahn et al. 2012; Shajahan et al. 2018a).

The observed weak and low-intensity second order band observed at 560 cm^{-1} is attributed to the presence of oxygen vacancies (defect peak) in the material. The addition of dopant into ceria lattice results in the generation of defective mode, i.e., in order to maintain charge neutrality oxygen vacancies are generated in the lattice due to the formation of Ce^{3+} (by the reduction of Ce^{4+} to Ce^{3+} ions). As it can be seen from Figure that no other detectable secondary peaks corresponding to praseodymium oxide were noticed which confirms the formation of a CeO_2 based solid solution and is in good agreement with XRD results.

Figure 5.3: Raman spectra of PDC samples synthesised by microwave assisted co-precipitation method, room temperature co-precipitation method and EDTA-citrate method

5.1.4. Scanning Electron Microscopy (SEM) Analysis

The representative SEM micrograph of PDC sample synthesised by various methods are shown in **Figure 5.4 (a)-(e)**. SEM analysis helps in understanding the surface structures of the as-synthesised samples. It can be seen from the figures that sponge-like agglomerated (hard agglomerates) structures are observed for PDC sample synthesised by MWCOP- Water **(Figure 5.4 (b))** and EDTA- Citrate method **(Figure 5.4 (e))** which

could hinder the densification during sintering process. The SEM image of MWCOP – ethanol **(Figure 5.4 (a))**, MWCOP - isopropyl alcohol as solvent **(Figure 5.4 (c))** and room temperature COP **(Figure 5.4 (d))** appeared to consist of weak agglomerates, which could result in a higher sintering activity when compared to the former samples and it agrees well with the extent of degree of agglomeration reported in **Table 5.1**.

The obtained value of the degree of agglomeration (Φ) (ratio of particle size obtained from BET surface area to the crystallite size from XRD) is in the range of 1.17 to 1.53. The maximum agglomeration is observed for PDC powder synthesised by EDTA citrate method and the minimum agglomeration are observed for MWCOP-ISP and RTCOP. The correlation of the degree of agglomeration with the sintering behaviour of the as-synthesised PDC powder will be discussed in detail in the section 5.1.5.

Table 5.1 shows the EDX analysis of PDC powders which confirmed the presence of Ce, Pr and O in the composition which confirms the purity of $Ce_{0.9}Pr_{0.1}O_2$. The EDX composition of all the samples asserts that the theoretical and the actual compositions of all the samples are almost similar.
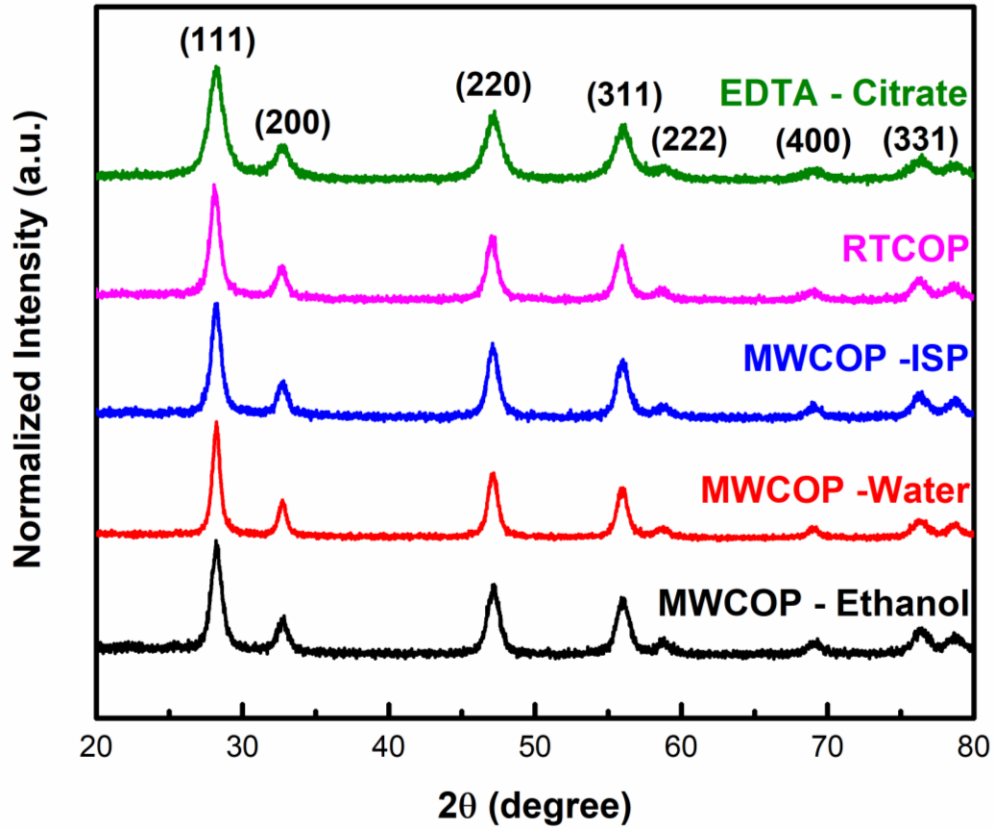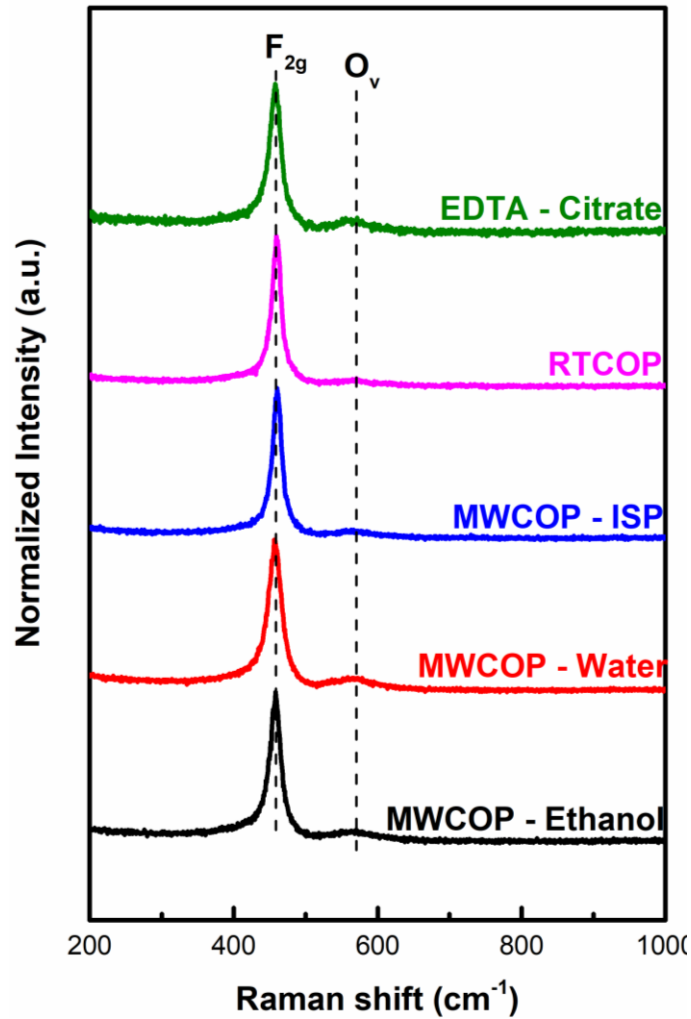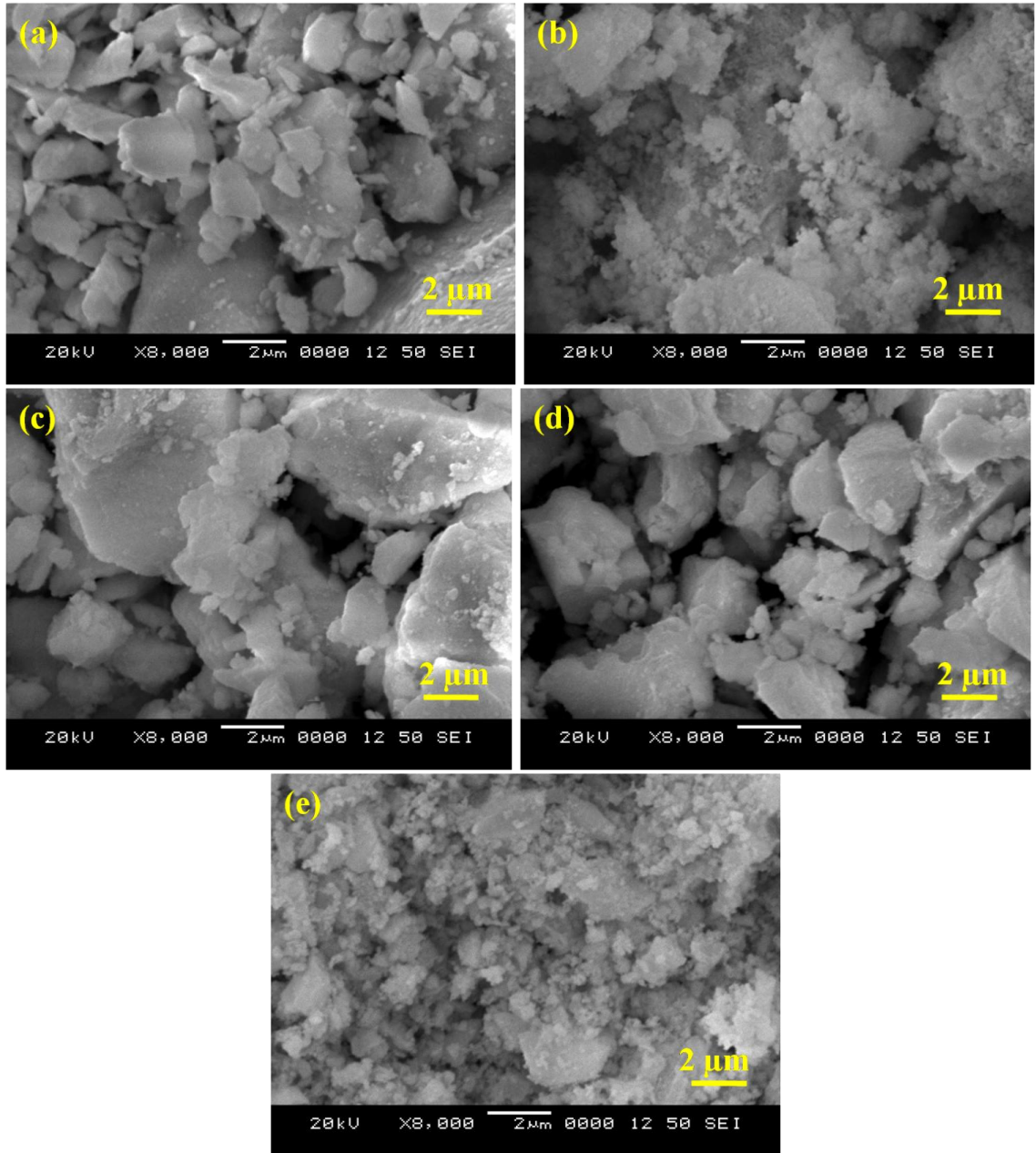
Figure 5.4: SEM micrograph of PDC samples synthesised by microwave assisted co-precipitation method, room temperature co-precipitation method and EDTA-citrate method

5.1.5. Dilatometer Studies

The linear shrinkage and shrinkage rate behaviour of PDC powders obtained from dilatometer studies as a function of temperature at a constant heating rate of 5 K/min are depicted in **Figure 5.5** and **Figure 5.6** respectively. Interestingly, **Figure 5.5** clearly shows that the synthesis method has a profound effect in shifting the onset of the sintering temperature from a higher range to a lower temperature (from ~600ºC for EDTA- Citrate method to ~350ºC for MWCOP- ISP), and significantly enhances the densification phenomena. Most importantly, it has been reported that smaller crystallite size and particle size of the powder could be the reason for such phenomena (Prasad et al. 2010). The smallest crystallite size shown by PDC powder synthesised by EDTA Citrate method (see **Table 5.1**) also had an early onset of sintering but didnot achieve full density at 1500ºC. The reason for this type of behaviour of the sample may be due to the presence of high degree of agglomerates in the starting powder, ie; the presence of large pores present in between the hard agglomerate after compacting.

MWCOP- ISP and RTCOP reached a maximum linear shrinkage of ~16% at a shrinkage temperature of 900ºC, whereas MWCOP- Ethanol has reached a line shrinkage of ~9% at 900ºC. The maximum linear shrinkage of 15% was achieved for MWCOP- ISP and 16% for RTCOP below 900ºC, which indicates that the full densification of the powder can be attained below 900ºC. The higher surface area of the particle provides the driving force for sintering and thereby increases the shrinkage rate of the MWCOP-ISP and RTCOP when compared to MWCOP-Ethanol. Meanwhile, MWCOP-Ethanol has the lowest shrikage rate percentage of ~9% was attributed to the lower grain boundary diffusion of the sample.
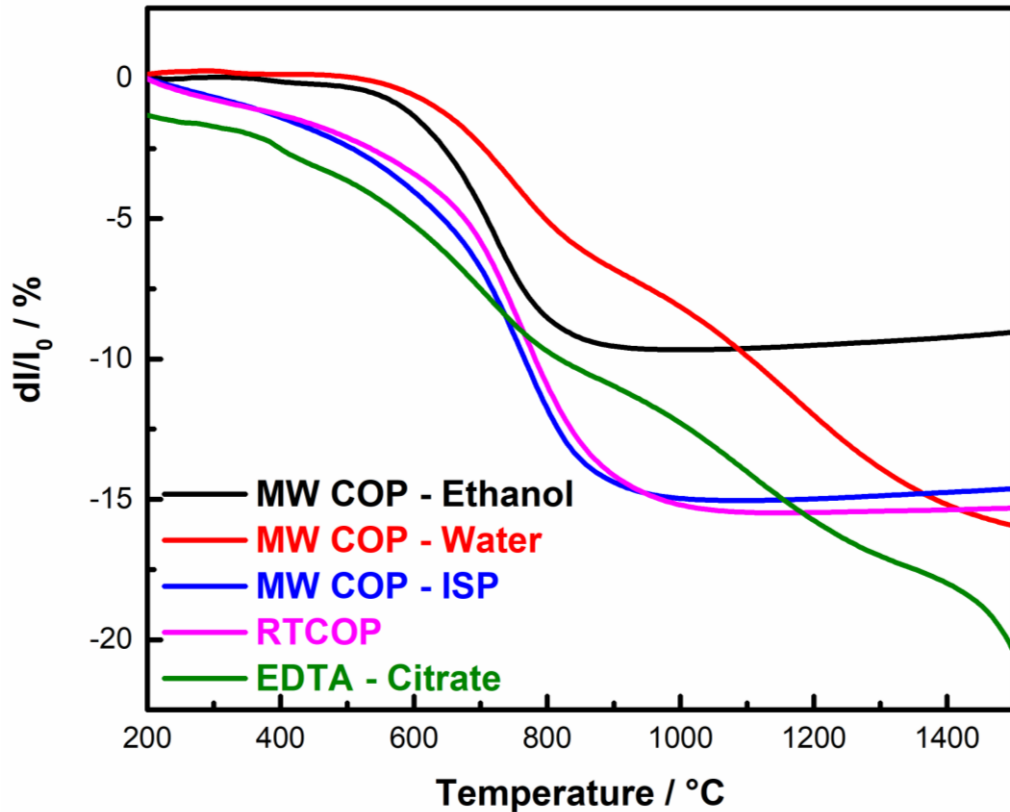
Figure 5.5: Linear shrinkage of PDC green pellets from 200°C to 1500°C

The shrinkage of MWCOP- Ethanol began at 600ºC and is saturated at 900ºC with a single shrinkage maxima at 730ºC. As discussed earlier, the monomodal pore size distribution obtained in the three as-prepared samples indicates the uniform pore population within the compacted powder structure due to the fracturing of agglomerates and the uniform distribution of the same (Ghosh et al. 2008). The rearrangement and the fracturing of the agglomerates results in the high densification of the sample prepared (Ghosh et al. 2008). The pressure applied on the powder should be more than the agglomerate strength inorder to achieve a high green density of the compact, vice-versa results in a bimodal pore size distribution of the sample. Thus the soft agglomerate powder with a uniform pore size distribution results in a single peak in the first derivative

shrinkage curve (shrinkage rate curve). Thus the homogeneous pore size distribution of the present investigation indicates the high sinterability of the as-prepared powders.

It can be seen from **Figure 5.6** that the sintering process of the samples and the temperature of maximum shrinkage rate of as prepared PDC powder changes with the effect of synthesis methods and is in the following order T_{Max}^{RTCOP} (~775ºC) $> T_{Max}^{MWCOP-ISP}$ (~765ºC) $> T_{Max}^{MWCOP-Water}$ (~750ºC,1200ºC) $> T_{Max}^{MWCOP-Ethanol}$ (~730ºC) $> T_{Max}^{EDTA\ Citrate}$ (~700°C,1150ºC). The sintering of MWCOP- Water and EDTA- Citrate showed a multiple shrinkage behaviour, which can be attributed to different size distribution of the agglomerates or due to different particle/pore size distribution, with the shrinkage maxima at (750°C, 1200°C) and (700°C,1150°C) respectively. The reason for such type of behaviour is due to the presence of hard agglomerates even after the compaction of the pellet and these hard agglomerates could not be easily broken even after the compaction which remained as uniform and large size pores in between the hard agglomerates. Specifically, the initial shrinkage is caused by the densification of the highly sinterable nano particle resulting in the first peak of the shrinkage rate at a lower temperature and further heating results in the closing of the larger pores which leads to the second peak of the shrinkage rate a higher temperature in MWCOP- Water and EDTA- Citrate method.

Table 5.2 summarises the calcination temeprature, initial sintering temeprature, sinteing end temeprtaure, maximum shrinkage rate temperature an relative density of the powders synthesised by different methods. It can be seen from the Table that the highest relative density has obtained for MWCOP – ISP and RTCOP samples which indicates the feasibility of using MWCOP – ISP PDC sample as electrolyte material for SOFC.

Table 5.2: Comparison of results of sintering experiments of 10-mol% PDC material synthesised by various methods

Synthesis method		Calcination Temperature (°C)	Relative Density of Green Pellet (%)	Initial sintering temperature (ºC)	Sintering end temperature (ºC)	Maximum shrinkage rate temperature (ºC)	Sintering Temperature (°C)/ 2h	Relative Density of Sintered Pellet (%)
MWCOP	Ethanol	450/ 2h	65 ± 0.27	505	895	730	1100	88 ± 0.35
	Water	450/ 2h	53 ± 0.63	584	>1500	750, 1200	1450	90 ± 0.20
	Iso-Propyl Alcohol	350/ 2h	58 ± 0.33	429	956	765	1100	94 ± 0.20
Room temperature co-precipitation method		350/ 2h	54 ± 0.26	432	1040	775	1100	91 ± 0.25
EDTA - Citrate		400/ 2h	53 ± 0.32	365	>1500	700, 1150	1450	90 ± 0.50

The sintering of MWCOP- Ethanol, MWCOP- ISP and RTCOP exibited a single maximum shrinkage or a uni modal agglomerate size distribution indicating a single densification mechanism is occuring in the samples. The appearance of one strong single shrinkage maxima in the samples indicate the good powder characteristics of the starting material and good homogenity of the powder compact with uniform size of the pore and distribution. The results of the linear shrinkage rate indicates that the sintering behaviour of the initial and final stages of sintering are dependent on the synthesis methods and the powder properties.
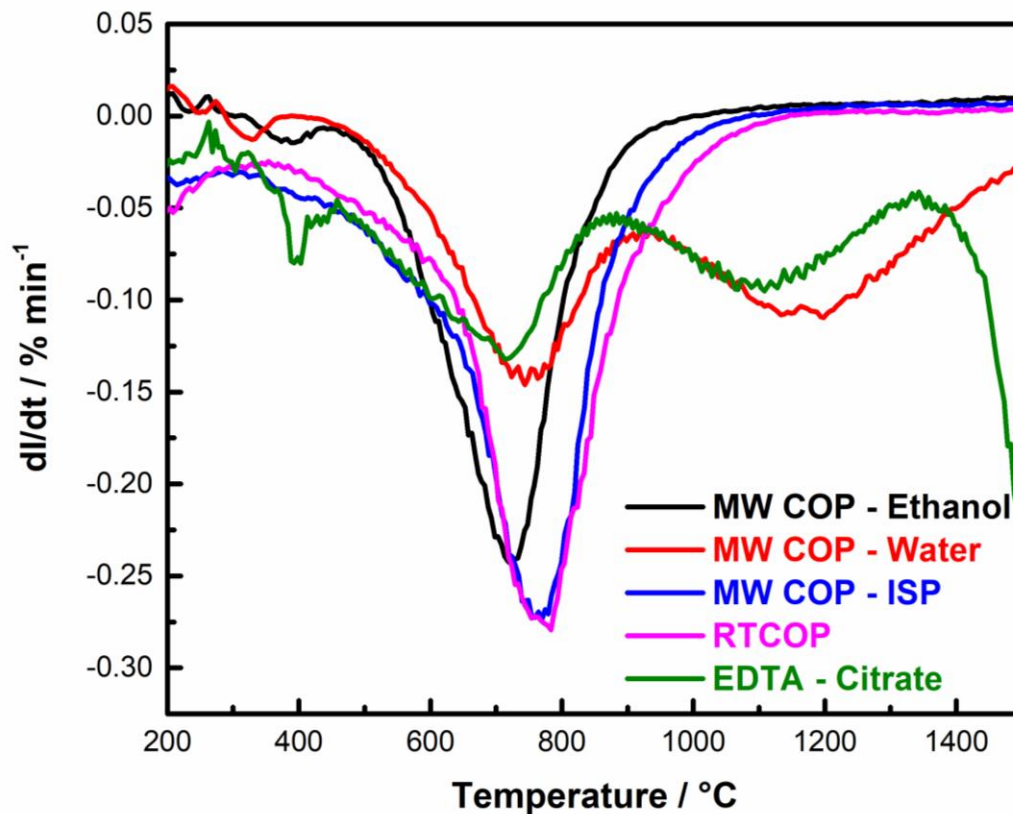
Figure 5.6: Shrinkage rate of PDC green pellets from 200°C to 1500°C

It can be seen from **Table 5.2**, that the temperature of the maximum shrinkage rate was lowered from ~1200ºC for MWCOP- Water to less than ~800ºC for MWCOP- ISP, MWCOP- Ethanol and RTCOP. The decrease in the sintering temperature range of MWCOP- ISP indicates an increase in grain boundary cation diffusion by solid state sintering.

The density achieved for the MWCOP- ISP in the present study was superior to that of the density obtained by the earlier experiment (EDTA- Citrate method) in our previous work (Shajahan et al. 2018b). The high surface area of MWCOP- ISP and RTCOP provide the driving force for sintering and result in an increase in the shrinkage rate (Selvaraj et al. 2019). During the sintering process, PDC sample synthesised by MWCOP- ISP exibited maximum shrinkage. However, it is likely that the high sinterability of as-prepared MWCOP- ISP suggest the feasibility of using PDC as an electrolyte material for IT-SOFCs and hence PDC synthesised by micowave assisted co-precipitation method using iso-propyl alcohol has been chosen for studying the sintering mechanism and kinetic parameters, which is discussed in detail in section 3.4.

5.1.6. X-Ray Diffraction (XRD) Analysis of Sintered Pellets

Figure 5.7 shows the XRD pattern of MWCOP- Ethanol, MWCOP- ISP and RTCOP sample sintered at 1100°C/ 2h and MWCOP- Water and EDTA- Citrate sintered at 1450°C/ 2h. The sintering temperature is fixed from the results obtained for dilatometer studies (please see **Figure 5.5** and **Figure 5.6**). It can be seen that the peaks of the sintered samples become narrower when compared to the calcined samples due to the increase in the mean crystalline size with the increase in the heat treatment temperature (XU et al. 2015). It can be seen from the figure, that with the increase in the sintering temperature the width of the XRD peaks gradually decreases.
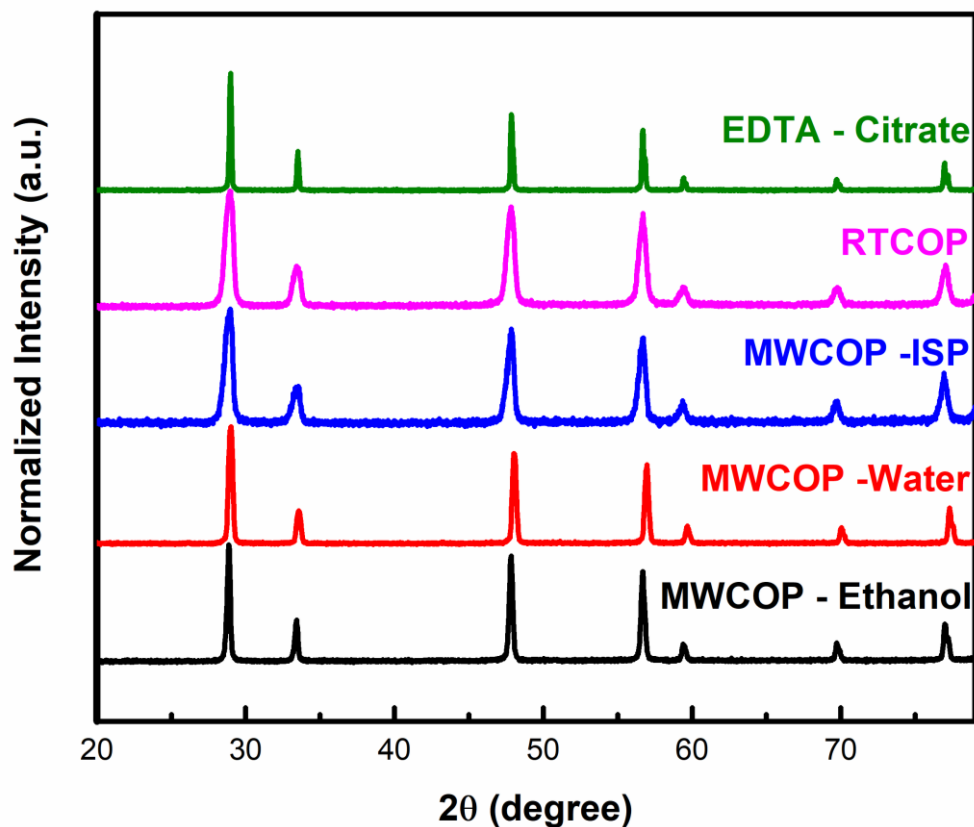
Figure 5.7: XRD pattern of sintered PDC pellet synthesised by MWCOP (Ethanol, Water and ISP), RTCOP and EDTA-citrate method sintered at 1100°C, 1450°C, 1100°C, 1100°C and 1450°C

5.1.7. Scanning Electron Micoscopy (SEM) Analysis of Sintered Pellets

The SEM images of sintered pellets obtained at 1100°C/ 2h from MWCOP- Ethanol, MWCOP- ISP and RTCOP sample; and 1450°C/ 2h from MWCOP- Water and EDTA-Citrate are shown in **Figure 5.8 (a)–(e)**. PDC synthesised by MWCOP- ISP **(Figure 5.8 (c))** exhibit a better sintering properties with a relative density of 94% at a lower temperature of 1100°C/ 2h compared to MWCOP- Ethanol **(Figure 5.8 (a))** and RTCOP **(Figure 5.8 (d))** sintered at the same temperature and are in good agreement with the relative density measured through Archimedes' principle mentioned in **Table 5.2**. The difference in the relative density can be due to the difference in the synthesis method and

the microstructural changes which can be observed from **Figure 5.8**. As seen, the SEM morphology of the PDC sample synthesised by MWCOP- Water (**Figure 5.8 (b))** and EDTA- Citrate method (**Figure 5.8 (e))** confirmed a lower densification and the density was around 90% even after sintering at 1450°C/ 2h due to the incomplete sintering or due to the residual porosity. Meanwhile, the amount of porosity decreased with the effect of synthesis methods was very pronounced and no micro-cracks or macro-cracks are found in any of the sintered samples of MWCOP-Ethanol, MWCOP-ISP and RTCOP but in the case of MWCOP-Water and EDTA-Citrate sample even after sintering to a higher temperature of 1450°C resulted in a porous sample.

MWCOP- ISP appear quite dense without any noticeable connected pores with a very uniform microstructure compared to the other samples which indicate the formation of a typical sintered ceramic compact/ dense bulk PDC material and these results further supports the linear shrinkage behaviour (See **Figure 5.5**). Eventually, it was hard to find pores on MWCOP- ISP sample sintered at 1100°C; whereas many pores still existed in the samples sintered at 1450°C. The calculated relative densities from Archimedes method for the PDC sintered pellet from MWCOP-Ethanol, MWCOP-water, MWCOP-ISP, RTCOP and EDTA-citrate are 88%, 90%, 94%, 91% and 90% of the theoretical value respectively.
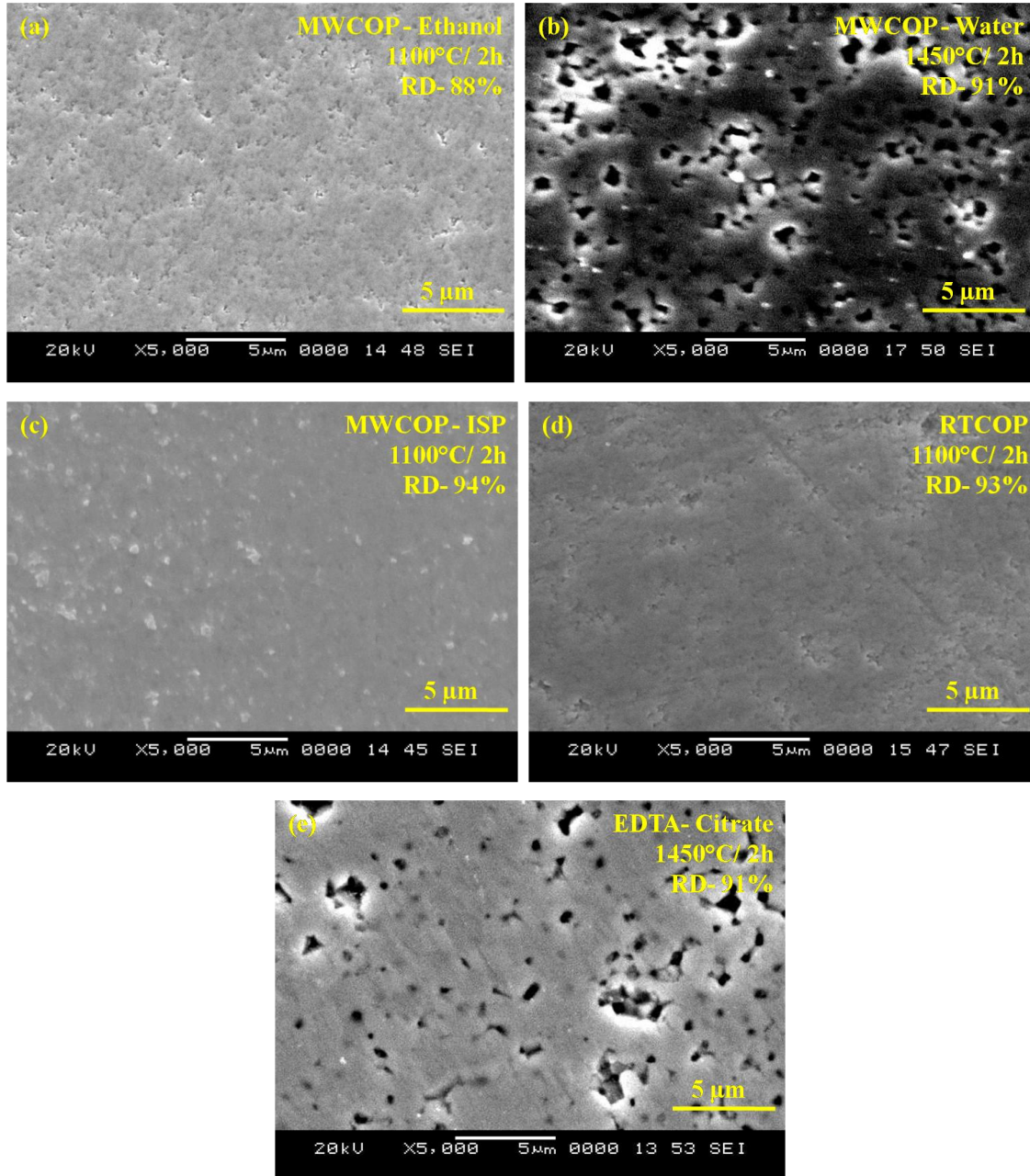
Figure 5.8: SEM micrograph of sintered PDC pellet synthesised by microwave assisted co-precipitation method, room temperature co-precipitation method and EDTA-citrate method

The density achieved for the MWCOP- ISP in the present study was superior to that of the density obtained by the earlier experiment (EDTA- Citrate method) in our previous work (Shajahan et al. 2018c). The high surface area of MWCOP-ISP and RTCOP provides the driving force for sintering and results in an increase in the shrinkage rate (Selvaraj et al. 2019). During the sintering process, PDC sample synthesised by MWCOP-ISP exibited maximum shrinkage. However, it is likely that the high sinterability of as-prepared MWCOP-ISP suggest the feasibility of using PDC as an electrolyte material for IT-SOFCs and hence PDC synthesised by micowave assisted co-precipitation method using iso-propyl alcohol has been used for studying the sintering mechanism and kinetic parameters.Therefore the obtained result indicates that MWCOP-ISP is suitable as solid electrolytes since the sintering temperature has been reduced from 1500°C (EDTA – Citrate method of the present work) to 1100°C.

5.1.8. Sintering kinetic Data Studies (CHR method)

Figure 5.9 shows the plot of the natural logarithm of $(\Delta L/L_0)$ and heating rate (C) at a particular temperature based on **Equation 3.1**. The average value of $[1/(m+1)]$ from the slope at different temperatures are listed in **Table 5.3**. The average value of m for praseodymium doped ceria has been found out to be 2.04. From the value of (m), it is evident that the sintering rate controlling mechanism in PDC is grain boundary diffusion for the initial stages of sintering. Lahiri et al (Lahiri et al. 2006) had reported that grain boundary diffusion dominates the sintering mechanism when the particle size is small in the case of ceramics and crystalline materials. As a result, the smaller particles will result in a faster neck to neck growth which is the driving force for grain boundary diffusion to takes place in the early stages of sintering.
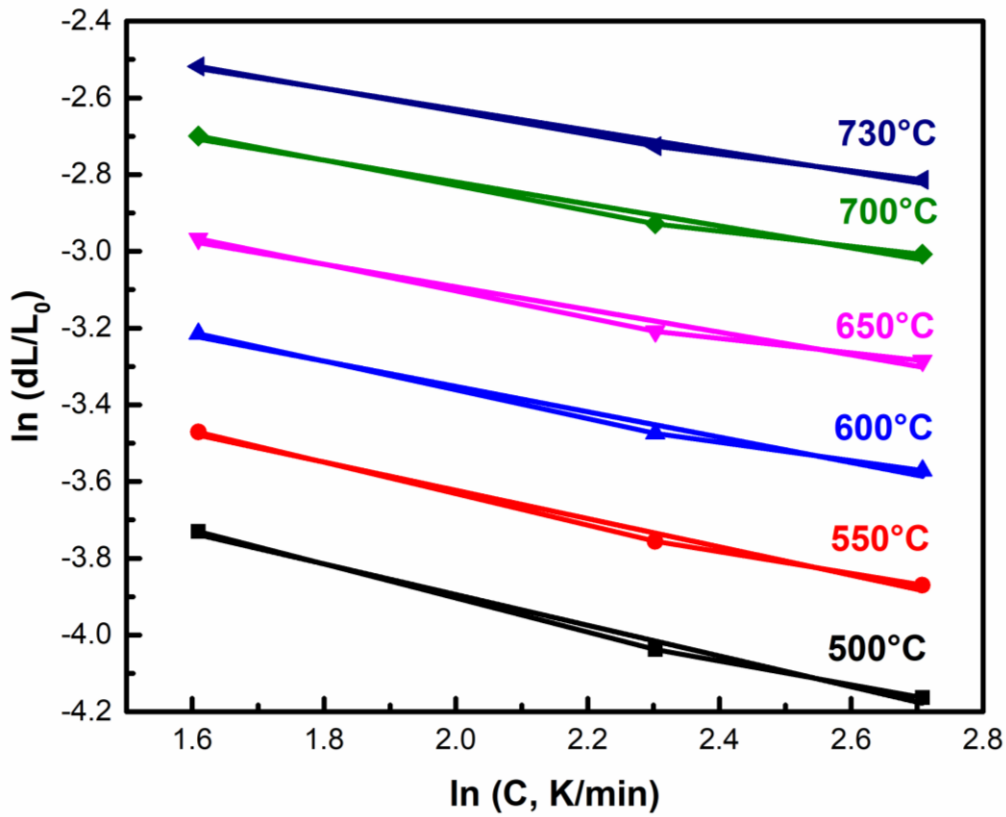
Figure 5.9: The natural logarithm of ln($\Delta L/L_0$) versus ln(C) for 10 mol% PDC of MWCOP-ISP

Table 5.3: The value of 1/(m+1) at different temperatures of MWCOP-ISP PDC pellet

MWCOP – ISP 10PDC						
Temp (ºC)	500	550	600	650	700	730
[1/ (m+1)]	0.399	0.368	0.331	0.295	0.287	0.285

The apparent activation energy of the PDC material synthesied by microwave assisted co-precipitation method using iso-propyl alcohol as solvent has been calculated from the plot of $\ln((\Delta L/L_0)/T)$ vs. $(1/T)$ by taking the average of the three slopes is shown in **Figure 5.10**. The interval of the shrinkage (relative shrinkage from 1.5 to 8.5%) has been taken for linear parts of the curves which indicates only one sintering mechanism during the early stages of sintering (Tianshu et al. 2002). The apparent activation energy of the 10 mol% PDC material synthesised by microwave assisted co-precipitation method using iso-propyl alcohol as solvent is found to be 116 kJ/mol. The activation energy obtained for 10 PDC for the early stage of sintering is much lower than that of gadolinium doped ceria in reducing atmosphere (290±20 kJ/mol) (He et al. 2010).
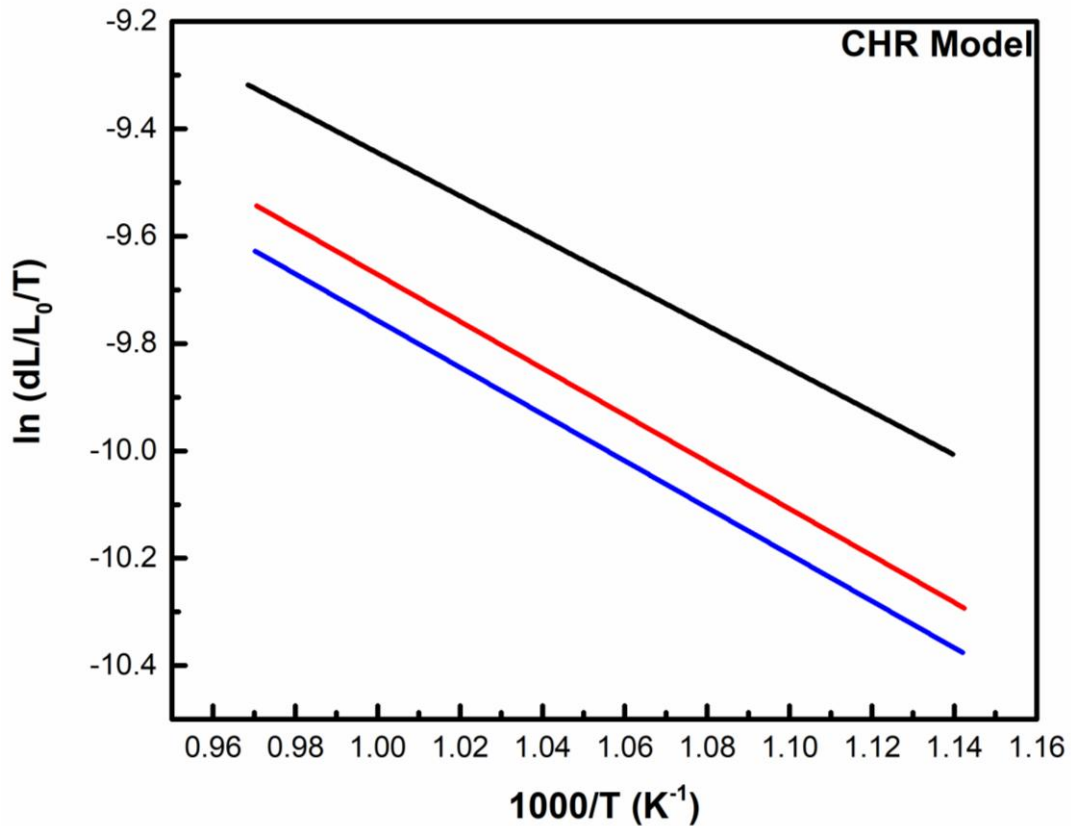
Figure 5.10: Plot of ln (($\Delta L/L_0$)/T) versus 1/T for 10 mol% PDC of MWCOP-ISP

Chen et al. (1997) had reported that grain boundary diffusion governs the densification of pure ceria (Chen and Chen 1997) whereas, He et al. (2010) reported that in a reducing atmosphere lattice diffusion dominate the early stage sintering of gadolinium doped ceria (10 GDC) (He et al. 2010). The formation of oxygen vacancies in reducing atmosphere (Ce^{4+} to Ce^{3+}) is the reason for acceleration of the densification process at a lower temperature which facilitates the movement of oxygen ions through the lattice. In the present work, PDC material exhibited the same sintering mechanism on the densification as that reported by Chen et al. (1997) for pure ceria.

5.1.9. Sintering Kinetic Data Studies (Dorn Method)

The isothermal shrinkage to calculate the apparent activation energy from the Dorn method was done in the interval of 550 – 750ºC at 50°C interval. In this method, the apparent activation energy for the initial stage of sintering was determined by giving a rapid heating rate from one isothermal range to another isothermal range so that the microstructure of the sample remains the same (BACMANN and CIZERON 1968). The Dorn method when compared to other methods to calculate the sintering mechanism and activation energy gives a direct access to the activation energy by a series of isothermal heating range. This method suits the initial stages of sintering as the microstructural changes are very negligible during this stage of sintering. The **Equation 3.4** is used to determine the apparent activation energy.

The Dorn method gives the value of activation energy at each thermal stage and the activation energy varied slightly at each thermal step varying from 165 – 180 kJ/mol. The activation energy of PDC material synthesised by microwave assisted co-precipitation method using iso-propyl alcohol as solvent was calculated using **Equation 3.4** and the average apparent actvation energy was found to be 176 kJ/mol.

5.2 CONCLUSION

Praseodymium-doped ceria-based electrolyte materials for SOFCs were prepared and studied by different synthesis methods such as microwave assisted co-precipitation method using ethanol, water and isopropyl alcohol as solvents, room temperature co-precipitation method using isopropyl alcohol and EDTA citrate method. In $Ce_{0.9}Pr_{0.1}O_2$, the solid solution solubility of Pr in CeO_2 extends to 1000ºC. All the samples exhibited a cubic fluorite-type crystal structure of CeO_2 from XRD analysis. The crystallite size of PDC material was in the range of 6 - 12nm. In comparison to other synthesis methods, PDC synthesised by MWCOP- ISP exhibited better sintering activity with a temperature of maximum shrinkage rate at the temperature of ~765ºC. The sintering temperature obtained for the electrolyte material synthesised by microwave assisted co-precipitation method using iso-propyl alcohol ($Ce_{0.9}Pr_{0.1}O_2$) as solvent has been decreased from 1500ºC (PDC synthesised by EDTA-Citrate method) of our previous work. This result showed that $Ce_{0.9}Pr_{0.1}O_2$, the sintering temperature of PDC material can be further reduced to use as an electrolyte material in low operating temperature SOFC electrolytes. In order to further decrease the sintering temperature of MWCOP- ISP, co-doping of PDC with transition metal oxides could be an alternative to reduce the sintering temperature oxides to a lower value than that obtained by the present synthesis method (Microwave assisted co-precipitation method using iso-propyl alcohol as solvent, <1100ºC).

Two different sintering models (CHR/ Dorn method) have been used to study the kinetics and the sintering parameters of MWCOP- ISP system. The activation energy for the initial stages of sintering was in the range of 116 kJ/mol (CHR model) and 176 kJ/mol (Dorn Method). It has been identified that grain boundary diffusion is the dominating mechanism for early stages of sintering. The results suggest that PDC based material prepared by MWCOP –ISP may be a better electrolyte material with a less sintering temperature for IT-SOFCs.

The next chapter focuses on the effect of sintering additives on the sintering kinetic behaviour of the PDC material synthesised by microwave assisted co-precipitation method using iso-propyl alcohol as solvent. The chapter also discusses the positive and negative effect of the addition of sintering additives on the PDC pellet. The linear shrinkage, shrinkage rate and mechanism and the activation energy for the initial stages of sintering has also been discussed in detail in the next chapter. The result of the coefficient of thermal expansion for the as-prepared PDC samples has also reported in the next chapter.

CHAPTER 6

EFFECT OF SINTERING AIDS ON SINTERING KINETIC BEHAVIOUR OF PRASEODYMIUM DOPED CERIA

The present study investigates the effect of sintering additives (Li, Co, Fe, and Mg) on the sintering kinetic behavior of the praseodymium-doped-ceria (PDC) electrolyte of solid oxide electrolyzer cell. 3Li-PDC, 3Co-PDC, 3Fe-PDC, and 3 Mg-PDC pellets were obtained from the synthesis of PDC nano-powder by microwave-assisted co-precipitation method using isopropyl alcohol as a solvent and followed by sintering additive wetness impregnation method. Linear shrinkage and shrinkage rate data suggest a positive sintering effect for 3Li-PDC and 3Co-PDC pellets and a negative sintering effect for 3 Mg-PDC and 3Fe-PDC pellets than compared to PDC pellets alone. The addition of lithium as a sintering additive (3Li-PDC) had reduced the sintering temperature of PDC from 1100°C to 850°C. For PDC, 3Li-PDC, 3Co-PDC, 3Fe-PDC and 3 Mg-PDC pellets sintered at 1100°C, 850°C, 1000°C, 1200°C, 1100°C for 2 h resulted in a relative density of 93.60 ± 0.25, 95.80 ± 0.45, 95.0 ± 0.20, 92.70 ± 0.10, and $94.5 \pm 0.10\%$, respectively. The XRD patterns of the sintered PDC pellets suggested a secondary phase formation (PrO_2) in 3Co-PDC, 3Fe-PDC, and 3Mg-PDC pellets indicating that the addition of these sintering aids results in poor solubility limit of Pr in CeO_2. On the other hand, XRD patterns of PDC and Li-PDC sintered pellets displayed no secondary peak indicating good solid-solution formation. The activation energy of the 3Li- PDC pellet is obtained from CHR and Dorn methods and was found to be 182 kJ/mol and 196 kJ/mol. From the CHR method, for the 3Li-PDC pellet, the initial sintering behavior is by the grain boundary diffusion mechanism (m = ~2).

6.1. EFFECT OF SINTERING AIDS ON SINTERING KINETIC BEHAVIOUR OF PRASEODYMIUM DOPED CERIA

The high sintering temperature (>1500°C) of ceria based materials are one of the major drawbacks of these electrolyte materials to obtain dense product. The two main approaches to reduce the sintering temperature of ceria based materials are (1) altering the synthesis methods enhance the homogeneity and improve the sintering ability of the powder and (2) addition of sintering aids to nanopowder. Praseodymium doped ceria synthesised by microwave assisted co-precipitation method was sintered to 94% of the theoretical density at 1100°C for 2h.

Kleinlogel et al. (2001) has reported that by adding small amount of Co, Fe, Mn, Cu and Ni reduced the sintering temperature of gadolinium doped ceria and was reported that the rapid densification is due to the melting of the dopants in the neck region (Kleinlogel and Gauckler 2001). It was reported that in the case of Co_3O_4, the improved sintering behavior at a lower temperature is due to the formation of a thin amorphous layer across the grain boundary; promotes the diffusion along the surface/ lattice. However, studies on the addition of sintering promoters to CeO_2 - PrO_2 system remain lacking and this motivated us to elucidate the shrinkage behaviour of PDC with the addition of sintering additives for further investigations.

Previous studies has reported that small amount of liquid additives are effective in promoting the densification of ceria based materials and was reported that 3 mol% of the dopant reduced the sintering temperature of gadolinium doped ceria material by 800°C (Nicholas and De Jonghe 2007). Based on the findings from literature, a dopant concentration of 3 mol% has been used in the present study to examine the sintering behaviour of praseodymium doped ceria based materials.

This chapter report the dilatometer results of various liquid additives (Li, Co, Fe and Mg) as co-dopants to praseodymium doped ceria at up to 3 mol% were synthesised by

microwave assisted co-precipitation method using iso-propyl alcohol as solvent. The samples were denoted as 3Li-PDC, 3Co-PDC, 3Fe-PDC and 3Mg-PDC respectively in the following sections. The structure, morphology and sintering behaviour of the electrolytes will be characterized by X- ray diffraction (XRD), Raman spectroscopy and dilatometer studies. The shrinkage behaviour of the as-synthesized samples was studied and compared with the singly doped ceria electrolyte $Ce_{0.9}Pr_{0.1}O_2$ synthesised by microwave assisted co-precipitation using iso-propyl alcohol as solvent. Furthermore, the activation energy of the as-synthesized powder has been investigated, and the effect of sintering additives on the sintering behavior of PDC has been studied for IT-SOFCs.

The use of sintering aid to doped ceria based materials results in a larger shrinkage rate and a lower sintering temperature. Therefore it is necessary to investigate the effect of sintering additives on the sintering behavior of praseodymium doped ceria solid-solutions doped at 3 mol% with four cations (Li, Fe, Mg, and Co). Zhang et al. (Tianshu et al. 2002) has reported that the early stage sintering mechanism of Fe doped CeO_2 and MnO_2 doped CeO_2 and was reported that the early stage sintering mechanism changes from volume diffusion to viscous flow in the case for pure CeO_2 and Fe/Mn-doped CeO_2, respectively. Based on these findings from the literature, in the present study, the activation energy for the initial stages of sintering of 3Li-PDC was calculated by the Constant heating rate (CHR) method and the Dorn Method. The obtained results are illustrated and discussed in further in the following sections.

Furthermore, the effect of 1 mol% lithium doping on PDC has also been investigated and has been compared with that of 3 mol% doping of lithium on PDC. The obtained results are also discussed in the following sections.

6.1.1. Dilatometer Studies

Figure 6.1 depicts the linear shrinkage of PDC and 3mol% sintering additives (Li, Co, Mg, and Fe) doped PDC green pellets. When compared to PDC pellet, 3Li-PDC and 3Co-PDC pellets showed better linear shrinkage at lower temperatures (850°C, 1000°C) and 3Mg-PDC, 3Fe-PDC pellet exhibited linear shrinkage at a higher temperature (1100°C, 1200°C).

The maximum linear shrinkage (%) of PDC, 3Li-PDC, 3Co-PDC, 3Mg-PDC and 3Fe-PDC is 12.3, 16.6, 12.6, 11.8, and 13.3%, respectively. Therefore, the doping of 3 mol% of Lithium and Cobalt confirmed the sintering temperature of $Ce_{0.9}Pr_{0.1}O_2$ to less than 850°C and 1000°C respectively. The sintering temperature has been reduced from 1100°C to 850°C with the addition of Lithium as a sintering additive to the PDC synthesized by microwave-assisted co-precipitation method.

Figure 6.2 depicts the shrinkage rate data of the prepared PDC pellets. All the prepared pellets showed only one-shrinkage maxima at different temperatures indicating a uni-modal pore distribution (Hari Prasad et al. 2010; Prasad et al. 2010a; b). The appearance of only one shrinkage maxima indicates the good homogeneity of the green compact with a uniform pore size distribution (Hari Prasad et al. 2010). The larger pores require a longer time and higher temperature for closing the pores, where smaller pores need lesser time and lower temperature to close the same (Prasad et al. 2010a).
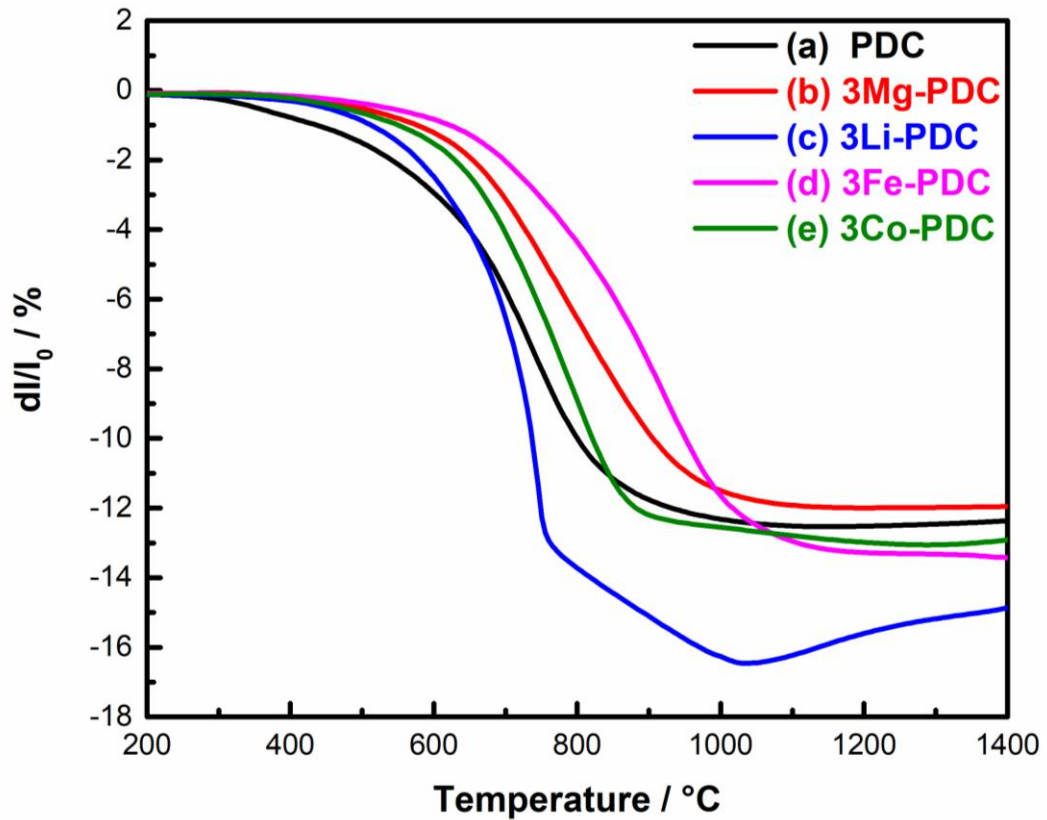
Figure 6.1: Linear Shrinkage behaviour of PDC and 3mol% sintering additives doped PDC green pellets sintered at 1100°C/2h (10 PDC, Mg-PDC), 850°C/2h (Li-PDC), 1200°C/2h (Fe-PDC) and 1000°C/2h (Co-PDC)
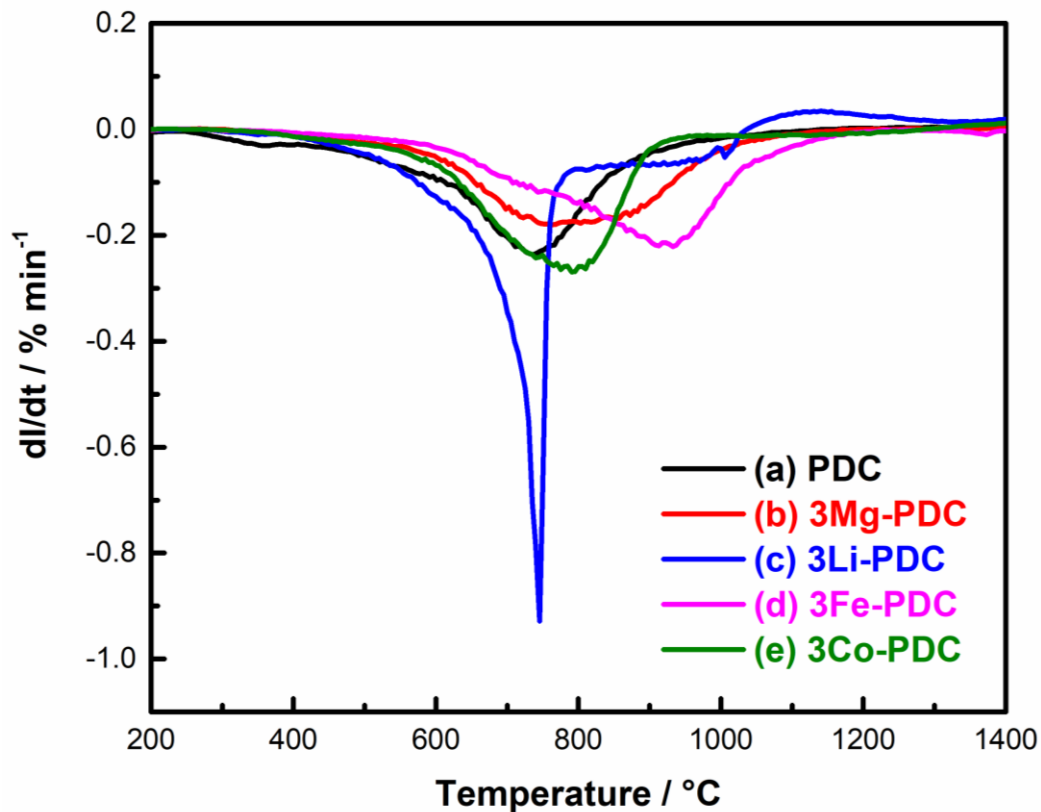
Figure 6.2: Shrinkage rate behaviour of PDC and 3mol% sintering additives doped PDC green pellets sintered at 1100°C/2h (10 PDC, Mg-PDC), 850°C/2h (Li-PDC), 1200°C/2h (Fe-PDC) and 1000°C/2h (Co-PDC)

6.1.1.1. Mg-doped PDC

The effect of 3 mol% Mg doping on the sintering behaviour of praseodymium doped ceria is shown in **Figure 6.1 (b)** and **Figure 6.2 (b)**. The linear shrinkage rate of 3 mol% Mg in PDC is shown to exhibit single shrinkage maxima at 800°C. The introduction of Mg oxide sintering aid inhibits the densification process slightly when compared to that of undoped PDC material, i.e.; PDC synthesised by MWCOP-ISP. That is MgPDC increased the sintering temperature slightly when compared to that of undoped PDC. The poor sintering activity of Mg may be due to the replacement of Ce or Pr cations by Mg as diffusion limiting species. The result of the present study agrees well with the literature report by Chen et al (Chen and Chen 1996), who has reported that Mg inhibit the grain

growth if the dopant concentration is greater than 1 mol% by a solute drag effect which in turn inhibit the sintering temperature. Nicholas et al (Nicholas and De Jonghe 2007) has also reported that Mg doping increases the sintering temperature of gadolinium doped ceria very slightly. It can be seen from the **Figure 6.1 (b)**, that MgPDC attained maximum density by ~1100°C which is less than sintering temperature of the conventionally prepared PDC material (1500°C).

Figure 6.2 (b) shows the linear shrinkage rate as a function of temperature for liquid additives dopants in PDC. The linear shrinkage curve of MgPDC exhibited uni-modal behaviour with single shrinkage maxima. The single maxima in the figure confirm the homogenous pore size distribution in the MgPDC green compact sample. The onset of the sintering temperature has been increased from 450°C (MWCOP-ISP) to 600°C. However in the present study Mg as a co-dopant has failed to influence the sintering in a positive direction.

6.1.1.2. Li-doped PDC

Figure 6.1 (c) and **Figure 6.2 (c)** shows the linear shrinkage and shrinkage rate behaviour of 3 mol% Fe in PDC at a constant heating rate of 5 K/min. it can be seen from the figure that compared to other pellets, 3Li-PDC exhibited a larger shrinkage and shrinkage rate. The shrinkage has been increased significantly when compared to other samples at 760°C and the densification process was completed within a temperature range of 150°C. This could be due to the presence of another sintering mechanism in LiPDC compared to that of undoped sample.

The PDC pellet showed a single shrinkage maximum at 760°C, and when compared to PDC pellet, only 3Li-PDC showed a single shrinkage maximum less than PDC pellet at 740°C. Whereas the result of the present study indicates that among the four dopants, Li and Co reduces the $Ce_{0.9}Pr_{0.1}O_2$ sintering temperature, while Mg has a little effect, and Fe increases the sintering temperature. The quick densification at lower temperature

occurred in the PDC sample doped with Li could be due to the formation of the liquid phase in the grain boundaries of the sample which may be due to the diffusion of the liquid phase under capillary action along with the rearrangement of the grains during the sintering process (Zhang et al. 2006). The linear shrinkage rate of Li-PDC is about 4 times as that of undoped PDC sample. The densification process of the sample has attained the saturation with a temperature range of 150°C which indicates liquid phase sintering to be the most predominant and in case of undoped PDC sample the densification process is terminated with in a temperature range of 250°C indicating a solid state sintering process to be dominant.

In the case of Li as the sintering aid, Lithium nitrate starts melts at around 247.4°C and decomposes at around 485°C, and lithium oxide is formed at around 650°C. In the present study, the calcination temperature was fixed to 400°C in all the doped samples. Therefore, all the nitrates are not converted to oxides. As a result, during the sintering process, a thin liquid layer of Ce-Pr-Li-O is formed on the surface of 10PDC grains. The formation of a liquid phase during sintering creates a capillary force that closes the porosity, compact the particles, and also increases the diffusivity in the material. Zhang et al. (Zhang et al. 2011) have reported that lithium can improve the solid state diffusion of the PDC through an undersized dopant effect at the grain boundaries. This could be another possibility for the lower sintering temperature and a higher shrinkage rate of the Li-PDC sample.

From **Figure 6.1 (c)** and **Figure 6.2 (c),** it can be seen that the 3Li-PDC pellet showed slightly different shrinkage behavior than compared to the other pellets. 3Li-PDC showed a three-stage (Stage 1: 475°C to 755°C; Stage 2: 755°C to 1040°C and Stage 3: 1040°C to 1500°C) linear shrinkage behavior (**Figure 6.1**(3Li-PDC)). Stage 1 of the linear shrinkage is reflected with shrinkage rate maxima at 740°C (Figure 6.2), where the maximum densification occurs, and the linear shrinkage rate of 3Li-PDC is about four times as that of pure PDC pellet. The results indicate a good homogeneity of the powder

is achieved with uniform pore/ size distribution) (Hari Prasad et al. 2012). The shrinkage has been increased significantly when compared to other samples at 740°C, and the densification process was completed within a temperature range of 150°C. Stage 2 of the linear shrinkage is slow when compared to Stage 1, and it is important to notice that there are no shrinkage rate maxima in **Figure 6.2** (3 Li-PDC) indicating that the Stage 2 linear shrinkage is not related to the closure of larger inter-granular pores than compared to Stage 1.

Therefore, further investigation is required to find out the reasons for such a kind of behavior, and 1Li-PDC is prepared, and the results are depicted in **Figure 6.3** (will be discussed later in the section 6.1.2). In Stage 3, instead of linear shrinkage, there is an expansion in the 3Li-PDC pellet, and similar behavior is noticed in shrinkage rate behavior (**Figure 6.2** (3Li-PDC)). The reason for such a kind of behaviour can be due to the over sintering and expansion of the 3Li-PDC pellet. Similar results were also observed by C. Kleinlogel and L. J. Gauckler (Kleinlogel et al. 1999) for copper liquid additive in GDC pellet where the density of the pellet is decreased over the sintering temperature of 1000°C. Instead of linear shrinkage, the expansion happening in 3Li-PDC is related to the thermal expansion of the material and implies that the process of sintering has been ended (Zając et al. 2009). Therefore, the comparison of 3Li-PDC and 1 Li-PDC has been discussed in detail in the section 6.1.2.

6.1.1.3. Fe-doped PDC

The linear shrinkage and shrinkage rate of Fe-doped PDC pellet is shown in **Figure 6.1 (d)** and **Figure 6.2 (d)**. The 3Fe-PDC pellet showed single shrinkage maxima at 950°C. The absence of second maxima at higher temperatures indicates the absence of the larger inter-granular pores, which requires much higher sintering temperatures. Unlike Li-PDC and Co-PDC, Fe doping increased the sintering temperature of PDC material. Zhang et al has reported that the small addition of iron oxide results in the reduction of sintering temperature by 200°C to 1300°C for gadolinium doped ceria, when compared to that of

undoped sample. This is due to the viscous flow mechanism which leads to the rapid densification at a lower temperature of 1300°C and promotes the mass diffusivity of the matrix and resulted in an improved densification with the increase in the sintering temperature (Zhang et al. 2004).

In the present study, the sintering temperature of PDC sample has been reduced to 1100°C and due to the high melting point of Fe dopant, the rearrangement/ the densification process takes place at a higher temperature could be the reason for the increase in the sintering temperature. It was reported in the literature that Fe doping showed no effect on sintering due to the high melting point of Fe_2O_3 (1596°C) and for the particular temperature range of 33 – 1500°C, Fe_2O_3 cannot become a liquid phase (Tianshu et al. 2002). In the present case, the densification takes place at a much higher temperature in 3Fe-PDC than compared to PDC pellet. As a result 3Fe-PDC has a negative effect on the sintering temperature of PDC pellet.

6.1.1.4. Co-doped PDC

The sintering of praseodymium doped ceria with cobalt oxide added in the concentration of 3 mol% is shown in **Figure 6.1 (e)** and **Figure 6.2 (e)**. It can be seen from the figure that the sintering end temperature has been reduced to less than 1000°C and the Co dopant is found to be effective in reducing the sintering temperature of PDC. The improved sintering behaviour of Co-doped PDC is due to the formation of a thin cobalt rich grain boundary film and this layer melt at a temperature of 900°C and facilitates the densification by liquid phase sintering. **Figure 6.2 (e)** shows the linear shrinkage rate as a function of temperature for cobalt dopant in PDC. The linear shrinkage curve of Co-PDC exhibited uni-modal behaviour with single shrinkage maxima. The single maxima in the figure confirm the homogenous pore size distribution in the Co-PDC green compact sample. The addition of Co-PDC did not improve the shrinkage rate maxima peak temperature of undoped PDC because PDC can be sintered at a lower sintering temperature due to the high surface area of the as-synthesized sample which is the driving

force for the sintering in PDC sample. Also, the as-synthesized PDC sample already reached maximum shrinkage rate temperature at a lower temperature. The shrinkage rate maxima peak temperature of PDC (760°C) is better than that of Co-PDC (790°C) but the closing end temperature of Co-PDC (1000°C) is lower than that of the PDC sample (1100°C) even though the linear shrinkage of the PDC and Co-PDC samples showed almost similar linear shrinkage (%) (~12%).

As a result, the lower end sintering temperature for Co-PDC was due to the presence of a low melting point of cobalt oxides. The melting point of the material decreases with the decrease in particle size. The melting point of the particle decreases as the particle size decreases. The sintering temperature decreases from 1100°C to 1000°C with the Co addition and achieves > 95% relative density. The reduction in the sintering end temperature of Co-PDC is due to the formation of liquid phase sintering (Kondakindi and Karan 2009). As shown in Figure 6.1, by doping $Ce_{0.9}Pr_{0.1}O_2$ with 3 mol% Co, it is possible to sinter $Ce_{0.9}Pr_{0.1}O_2$ to 1000°C for 2h to a density of 95% whereas, the PDC sample sintered at 1100°C showed a relative density of 94% (See Table 6.1). The single maxima in the figure confirm the homogenous pore size distribution in the 3Co-PDC green compact sample. The result shows that cobalt doping in PDC has a positive effect on densification when compared to that of 3Mg-PDC and 3Fe-PDC pellets.

Table 6.1 shows the information related to the initial sintering temperature, sintering end temperatures of the prepared pellets. Among the sintering additives, 3Li-PDC (475°C) showed the least initial sintering temperature, and 3Fe-PDC (610°C) showed highest initial sintering temperature indicating that Li additive has a positive effect on sintering and Fe additive has a negative effect in decreasing the sintering temperature of PDC pellet. The sintering temperature of the PDC is decreased from 1100°C to 850°C with the addition of Lithium as a sintering additive. The Li-PDC pellet sintered at 850°C for 2h showed a relative density of 95.8±0.45% and is higher than all the PDC pellets at their final sintering temperatures (>1000°C).

Table 6.1: Comparison of sintering data for 10 mol% PDC and Co-doped PDC material at a heating rate of 5K/min

Material	Calcination Temperature (°C)	Relative Density of Green Pellet (%)	Initial sintering temperature (ºC)	Sintering end temperature (ºC)	Maximum shrinkage rate temperature (ºC)	Sintering Temperature (°C)/ 2h	Relative Density of Sintered Pellet (%)
10 PDC (MWCOP- ISP)	350°C/2h	58 ± 0.33	430	955	760	1100	93.6±0.25
3Mg-PDC	400°C/2h	59 ± 0.21	550	1085	820	1100	94.5±0.10
3Li-PDC	400°C/2h	57 ± 0.88	475	1000	740	850	95.8±0.45
3Fe-PDC	400°C/2h	60 ± 0.18	610	1200	950	1200	92.7±0.10
3Co-PDC	400°C/2h	57 ± 0.31	480	980	790	1000	95.0±0.20

6.1.2. Comparison of dilatometer studies of 1Li-PDC and 3Li-PDC pellets

To find out the reason for the expansion behavior of 3Li-PDC, 1Li-PDC has been prepared**. Figure 6.3** shows the linear shrinkage and shrinkage rate of the 1Li-PDC and 3Li-PDC pellets. With the decrease of the Li content, there is a slight change in the sintering behavior in the 1Li-PDC pellet than compared to the 3Li-PDC pellet. The starting sintering temperature is slightly high in the 1Li-PDC pellet than the 3Li-PDC Pellet indicating that 3 mol% Li played a critical role in rearranging the powder compact for the initial stage sintering.
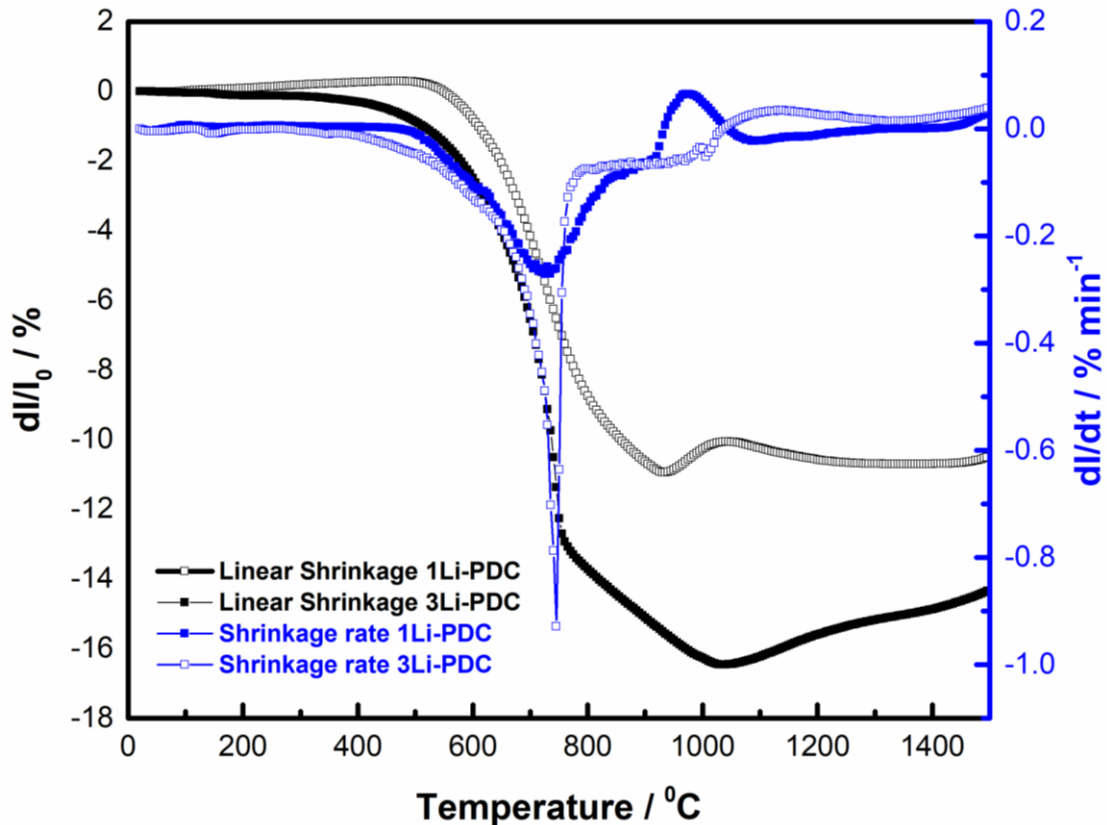

Figure 6.3: Linear shrinkage and shrinkage rate of the 1Li-PDC and 3Li-PDC pellets sintered at 950°C/2h and 850°C/2h

Stage 1 sintering temperature is almost the same in both the pellets, followed by the corresponding shrinkage rate at 745°C. The slope of Stage 2 linear shrinkage is decreased in 1Li-PDC than compared to 3Li-PDC Pellet. It is interesting to note that, for both samples, there was no peak in the shrinkage rate corresponding to Stage 2 linear shrinkage indicating that in both the cases, the linear shrinkage in Stage 2 is not related to the closure of the larger inter-granular pores than compared to Stage 1. In Stage 3 of linear shrinkage behavior, 1Li-PDC pellet also displayed an expansion in pellet behavior, and the corresponding peak is displayed in shrinkage rate temperature range of 885 to 1125°C. A further investigation is required to understand such a kind of sintering behavior that is observed in Li-PDC pellets.

6.1.3. Linear Shrinkage behaviour of sintered PDC pellets

Figure 6.4 displays the linear shrinkage of the PDC, 3Li-PDC, 3Co-PDC, 3Fe-PDC and 3Mg-PDC pellets sintered up to 1100°C, 850°C, 1000°C, 1200°C and 1100°C temperatures (heating rate 15°C/min) and with a dwell time of 2h. The end temperature of the sample obtained from the linear shrinkage vs. temperature curve (see Figure 6.1) is the key for selecting the final shrinkage temperature, i.e., from Figure 6.1, for PDC sample the shrinkage curve became flattened at ~1100ºC. Therefore the sintering temperature of PDC has been fixed to 1100ºC. Similarly for the other pellets sintering temperature has been fixed.

As a result, based on the results of Figure 6.1 and Figure 6.2, the end sintering temperatures of the PDC, 3Li-PDC, 3Co-PDC, 3Fe-PDC, and 3Mg-PDC pellets, the sintering temperature has been fixed to 1100°C, 850°C, 1000°C, 1200°C and 1100°C respectively. Compared to all other pellets 3Li-PDC pellet showed maximum shrinkage of 16%. The obtained pellets were collected, and the corresponding relative density information is given in **Table 6.1**. All the PDC pellets displayed a relative density of over ~92%, and the Li-PDC pellet showed a maximum relative density of ~95%.
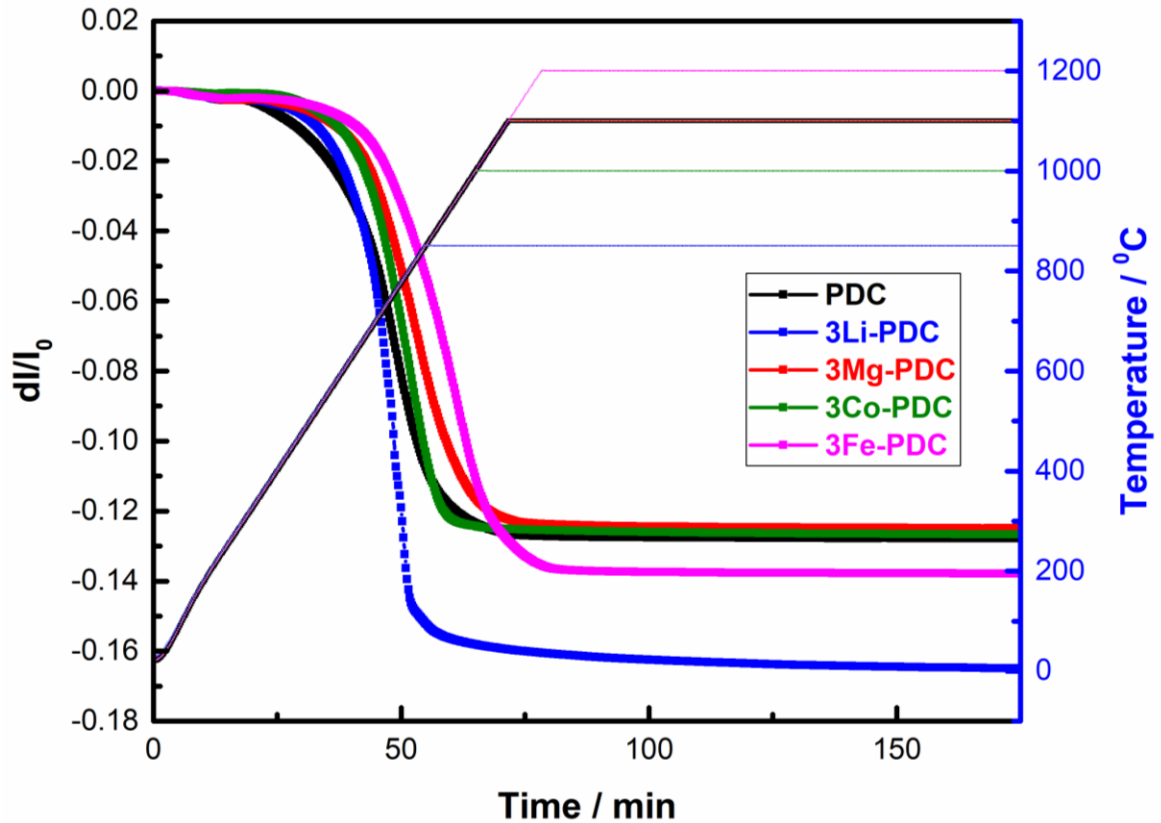
Figure 6.4: Linear shrinkage of PDC, 3Li-PDC, 3Co-PDC, 3Fe-PDC and 3Mg-PDC pellets sintered at 1100°C, 850°C, 1000°C, 1200°C and 1100°C/ 2h

6.1.4. X-ray Diffraction (XRD) Analysis of Sintered Pellets

Figure 6.5 shows the XRD patterns of all the PDC pellets sintered at various temperatures (as depicted in **Figure 6.4**). From **Figure 6.5**, apart from the peaks that were observed for the PDC pellet, an additional peak was seen for 3Fe-PDC, 3Co-PDC, 3Mg-PDC pellets, and this peak correspond to PrO_2 phase (Dogra et al. 2014). 1Li-PDC pellet, which is sintered at 1500°C, showed XRD patterns similar to PDC pellet, which is sintered at 1100°C indicating that the presence of Li controlled the phase stability in Praseodymium doped Ceria without any secondary phase (PrO_2), and the addition of sintering additives like Fe, Co, and Mg resulted in phase separation in Praseodymium-Ceria system. It can be seen that the peaks of the sintered samples become narrower when

compared to the calcined samples due to the increase in the mean crystalline size with the increase in the heat treatment temperature (XU et al. 2015). It can be seen from the figure that with the increase in the sintering temperature the width of the XRD peaks gradually decreases.

The present results indicate that the phase stability of PDC can be controlled by adding suitable sintering additives like Lithium and, at the same time, decrease the sintering temperature. Sintering kinetic studies were further studied on 3Li-PDC pellet to find the initial stages of the sintering mechanism and apparent activation energy calculated from CHR and Dorn methods.
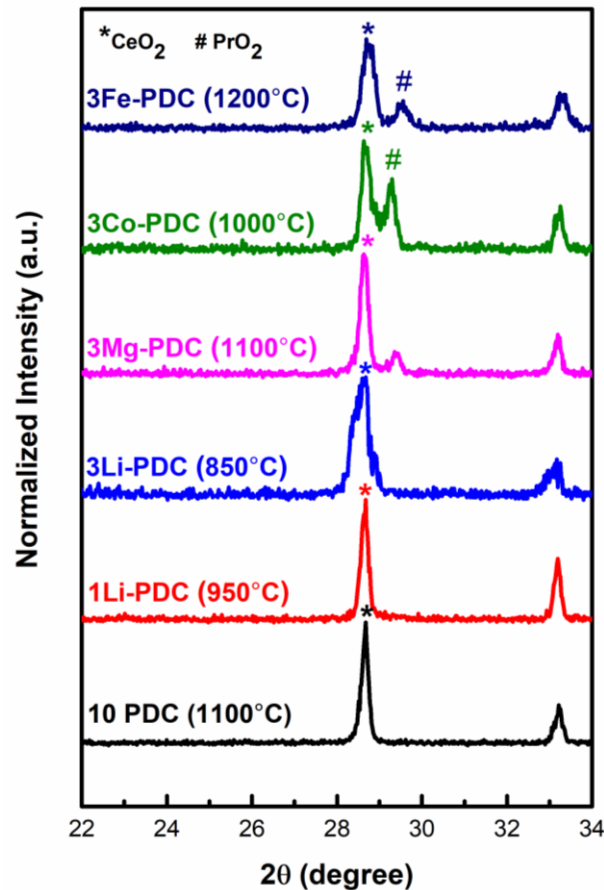
Figure 6.5: XRD patterns of all the PDC pellets sintered at 1100°C, 1500°C, 850°C, 1000°C, 1200°C and 1100°C/ 2h

6.1.5. Sintering Kinetic Data Studies

Figure 6.6 and **Figure 6.7** shows the plot of $\ln(dL/L_0)$ versus $\ln(C)$ and $\ln(dL/L_0/T)$ versus $1/T$ respectively for the 3Li-PDC pellets. The pellets were heated at different heating rates (say 5K/min, 10K/min, 15K/min) to calculate the activation energy and the sintering mechanism (m), which is discussed in detail in the section 3.2. The calculated activation energy for the 3Li-PDC pellet is ~182 kJ/mol.
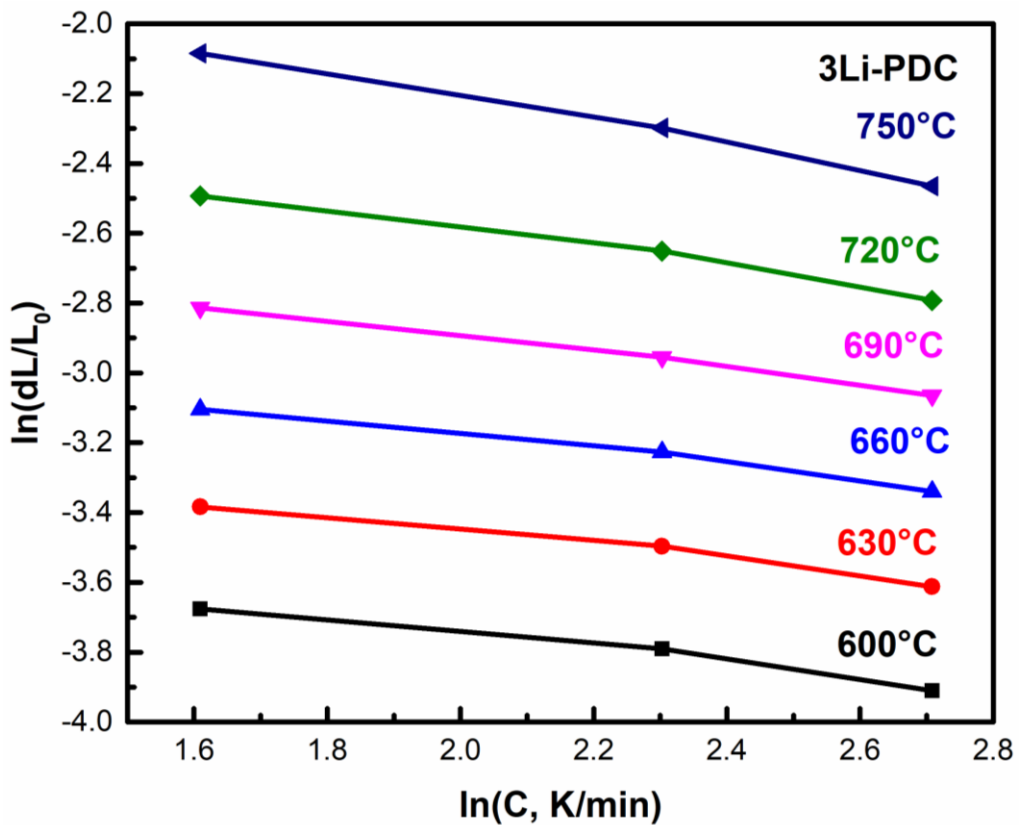
Figure 6.6: The natural logarithm of $\ln(\Delta L/L_0)$ versus $\ln(C)$ for 3Li-PDC pellet

The average value of (m) for 3Li-PDC from the slope of **Figure 6.6** at different temperatures has been found out to be ~2, which indicates that the grain boundary diffusion mechanism is the dominating mechanism in the early stage sintering of 3Li-PDC sample. Jud et al. (Jud et al. 2005) have reported that the small addition of the

sintering additives increases the diffusion rate through the grain boundary by the formation of a thin grain boundary layer.
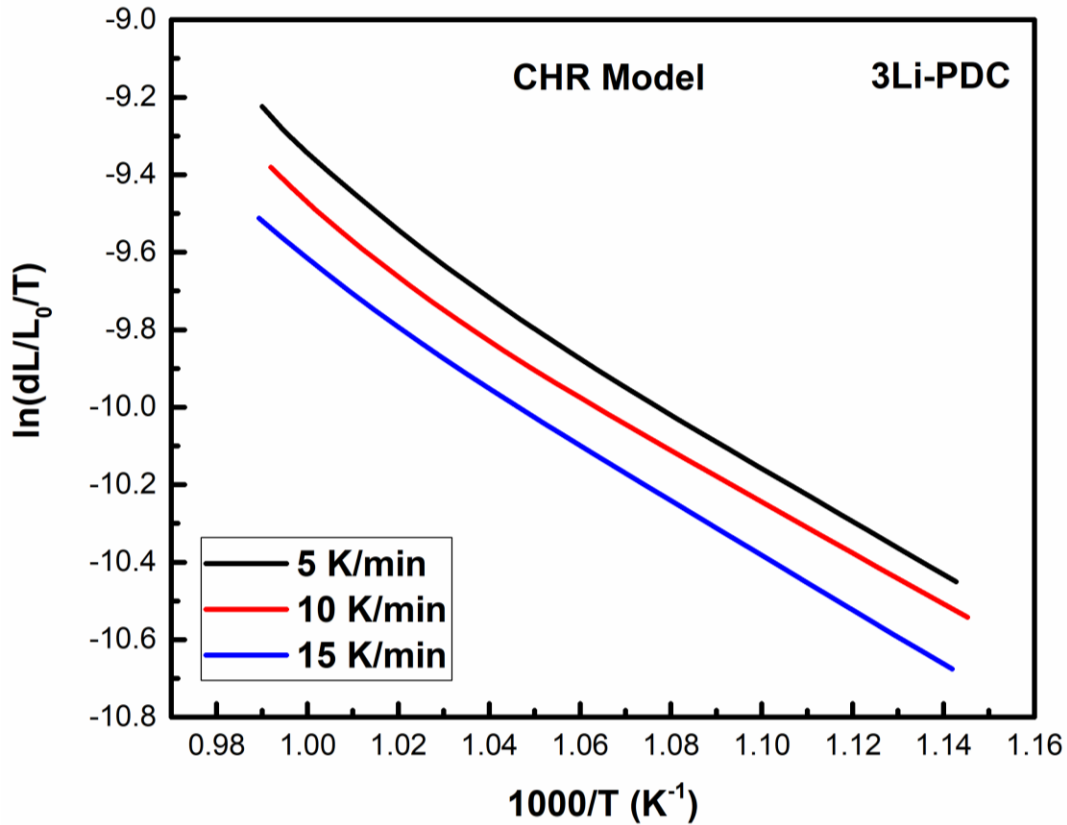
Figure 6.7: Plot of ln ((ΔL/L$_0$)/T) versus 1/T for 3Li-PDC pellet

According to Zhang et al. (Tianshu et al. 2002), the viscous flow mechanism, which causes a reduction in the inter-particle friction, was identified as the dominating mechanism in the early stage sintering of Fe doped CeO_2. Whereas the densification of Co-doped GDC is governed by the rearrangement, and the grain boundary diffusion and increased activation energy were noticed for Co-doped GDC when compared to undoped sample by Jud et al. (Jud and Gauckler 2005). It was reported that the presence of intergranular layer was the reason for such higher activation energy in doped samples, which in turn increases the diffusion of the atoms along the grain boundary. An increase in the activation energy of the densification for doped samples has been observed in

several systems such as Fe doped CeO_2 (Tianshu et al. 2002), ZrO_2 doped Al_2O_3 (Wang and Raj 1990) and Li_2O doped SDC (Le et al. 2013) and the increase is due to the presence of a liquid phase in the grain boundary.

In the present work, 3Li-PDC exhibited the same mechanism (grain boundary diffusion with a thin layer of sintering/ liquid additive over the PDC particles in the pellet) on the densification, as reported by Jud et al. (Jud and Gauckler 2005) and Le et al. (Le et al. 2013) for Co-doped CeO_2 and Li_2O doped SDC respectively.

The apparent activation energy was calculated by the Dorn method for the isothermal shrinkage in the range of 600–730°C at an interval of 50°C. The activation energy of 3Li-PDC material was found out to be 196 KJ/mol. The sintering temperature has been reduced from 1100°C to 850°C with the addition of Lithium as a sintering additive to the PDC synthesized by microwave-assisted co-precipitation method.

6.1.6. Thermal Expansion Co-efficient Studies

Figure 6.8 shows the thermal expansion behaviour of the as-synthesised PDC sintered pellets from 100 to 800°C and the calculated coefficient of thermal expansion (CTE) values of 10PDC, 1Li-PDC, 3Li-PDC, 3Co-PDC, 3Fe-PDC and 3Mg-PDC are 15.3×10^{-6} / °C, 18.2×10^{-6} / °C, 14×10^{-6} / °C 15.2×10^{-6} / °C, 13.8×10^{-6} / °C, 15.7×10^{-6} / °C respectively. Ceria based materials exhibited a CTE value around 11 – 12 / °C (Bochentyn et al. 2020; Cheng et al. 2017; Venkataramana et al. 2020). Larramendi et al. (2011) has reported that for $Ce_{0.8}Pr_{0.2}O_2$ electrolyte material exhibited a CTE value of 22.1×10^{-6} K^{-1} in the temperature range of 400 – 1000°C. (Ruiz De Larramendi et al. 2011). It can be observed from the thermal expansion behaviour study of the present work that the CTE of as-prepared PDC based electrolyte materials are lesser than that reported by Larramendi et al. (2011). The addition of lithium and iron as sintering additive has a positive effect on PDC material. Therefore, the as-prepared PDC pellets can be further investigated for the use of electrolyte material for IT - SOFCs.
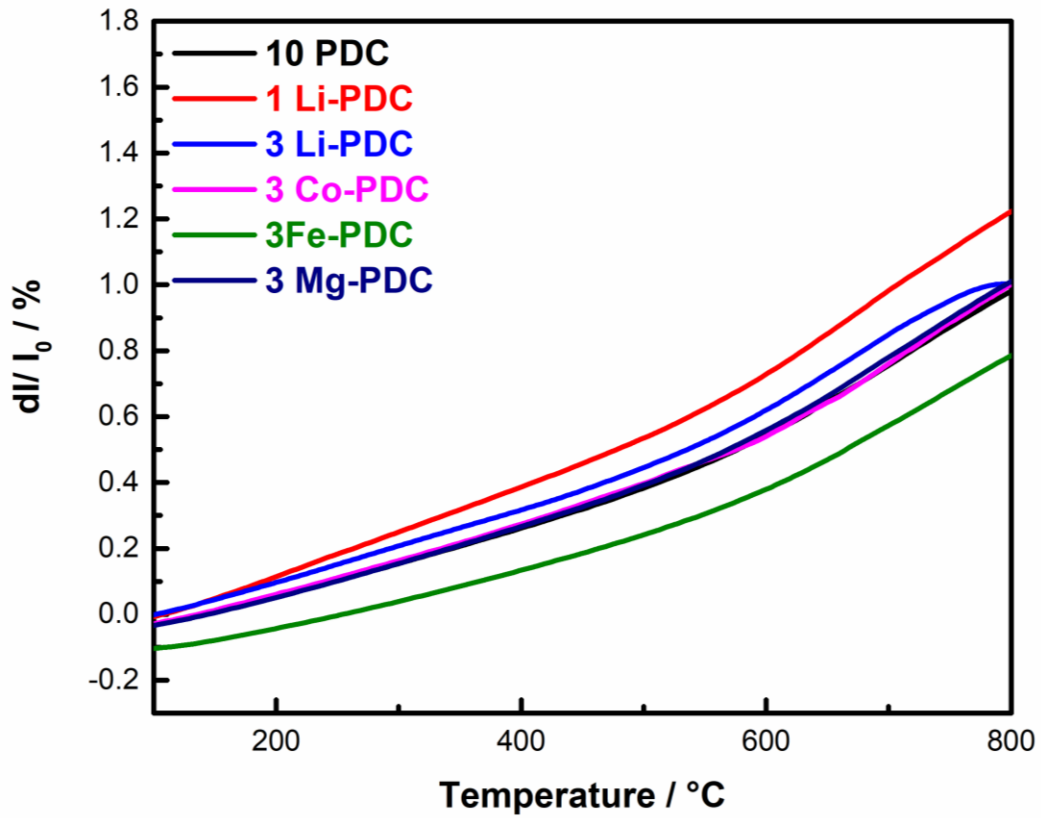
Figure 6.8: Thermal Expansion behaviour of sintered PDC pellets from 100°C to 800°C

6.2. CONCLUSION

The sintering behaviour of praseodymium doped ceria (synthesised by microwave assisted co-precipitation method using iso-propyl alcohol as solvent) with Magnesium, Lithium, Iron and Cobalt as co-dopants were investigated. The densification kinetics are characterised by the nature of the dopant and the amount of the dopant addition. In the present study, small amount of 3 mol% of the dopant is used and the result indicates that magnesium and iron has a very little effect on the sintering behaviour of doped ceria, while the sintering temperature of the PDC is decreased from 1100°C to 850°C with the addition of lithium as a sintering additive. It was noted that for lithium as a sintering additive, an expansion was observed after 1000°C. The reason for this could be exceeding the sintering temperature to 98% density leads to over-sintering and expansion of the doped sample.

The improved sintering behaviour of co-doped PDC was observed and this is due to the formation of a thin cobalt rich grain boundary film and this layer melt at a temperature of 900°C and facilitates the densification by liquid phase sintering. For PDC, 3Li-PDC, 3Co-PDC, 3Fe-PDC and 3Mg-PDC pellets sintered at 1100°C, 850°C, 1000°C, 1200°C, 1100°C for 2h resulted in a relative density of 93.6±0.25, 95.8±0.45, 95.0±0.20, 92.7±0.10, and 94.5±0.10 %, respectively. The 3Li-PDC pellet sintered at 850°C for 2h showed a relative density of 95.8±0.45% and is higher than all the PDC pellets at their final sintering temperatures (>1000°C). Unlike the Co-PDC, Fe-PDC, and Mg-PDC pellets, the XRD peaks of Li-PDC pellets resembled PDC pellets without any secondary phase (PrO_2).

The sintering kinetic studies over 3Li-PDC pellets showed that the initial sintering mechanism followed the grain-boundary diffusion mechanism with m~2 obtained from the CHR method. The activation energy is calculated using CHR and Dorn Methods and was around 182 and 196 kJ/mol.

The coefficient of thermal expansion (CTE) values in the range of 100 – 800°C of 10PDC, 1Li-PDC, 3Li-PDC, 3Co-PDC, 3Fe-PDC and 3Mg-PDC are 15.3×10^{-6} / °C, 18.2×10^{-6} / °C, 14×10^{-6} / °C, 15.2×10^{-6} / °C, 13.8×10^{-6} / °C, 15.7×10^{-6} / °C respectively.

CHAPTER 7

SUMMARY AND CONCLUSIONS

7.1. SUMMARY

The summary drawn from the research with respect to the effect of synthesis methods/ doping on praseodymium doped ceria-based metal oxides on the sintering activity is discussed in this section.

Praseodymium doped ceria as electrolyte material for IT-SOFCs has been evaluated. The effect of EDTA – Citrate synthesis method on praseodymium doped ceria-based electrolyte material has also been explored.

- XRD and Raman spectroscopy analysis confirms that the calcined sample displayed a cubic fluorite structure. The bands at 457 cm^{-1} and 550 cm^{-1} in the Raman spectroscopy results confirmed the formation of PDC solid solution, which is in good agreement with the XRD data.

- From XRD, BET, and TEM analysis it can be observed that the calcined sample exhibited a crystallite/particle size of 5–10 nm, and from particle size analyser, it is found that the sample displayed an agglomerate size 3.06 μm.

- From dilatometer studies, multi-step shrinkage behaviour is noticed for the PDC green pellet, a linear shrinkage up to −18% is noticed below 1500 °C.

- At 700°C, the sample displayed conductivity of 1.213×10^{-3} S cm^{-1} and with an activation energy of 1.28 eV. Instead of a single fluorite structure, XRD of sintered PDC pellet showed multiple structures (Fluorite structure (CeO_2) and cubic structure (PrO_2).

To study the effect of synthesis methods on the dilatometer studies of PDC based material and to develop praseodymium doped ceria based metal oxides with low sintering temperature.

- Praseodymium-doped ceria-based electrolyte materials for SOFCs were prepared and studied by different synthesis methods such as microwave-assisted co-precipitation method using ethanol, water, and isopropyl alcohol as solvents, room temperature co-precipitation method using isopropyl alcohol, and EDTA citrate method.

- All the samples exhibited a cubic fluorite-type crystal structure of CeO_2 from XRD analysis. The crystallite size of PDC material was in the range of 6–12 nm.

- Compared to other synthesis methods, PDC synthesized by MWCOP- ISP exhibited better sintering activity with a temperature of maximum shrinkage rate at ~765°C.

- Two different sintering models (CHR/Dorn method) have been used to study the kinetics and the sintering parameters of the MWCOP- ISP system.

- The activation energy for the initial stages of sintering was in the range of 116 kJ/mol (CHR model) and 176 kJ/mol (Dorn Method). It has been identified that grain boundary diffusion is the dominating mechanism for the early stages of sintering.

To study the effect of sintering aids on sintering kinetic behaviour of praseodymium doped ceria based electrolyte material for solid oxide cells and to develop praseodymium doped ceria-based metal oxides based on the results obtained from the effect of synthesis methods on PDC metal oxides.

- 3Li-PDC and 3Co-PDC showed a decrease in sintering temperature, and 3Fe-PDC and 3Mg-PDC showed an increase in sintering temperature than compared to PDC pellets alone.

- The sintering temperature of the PDC is decreased from 1100°C to 850°C, with the addition of lithium as a sintering additive.

- The 3Li-PDC pellet sintered at 850°C for 2h showed a relative density of 95.8 ± 0.45% and is higher than all the PDC pellets at their final sintering temperatures (>1000°C).

- Unlike the 3Co-PDC, 3Fe-PDC, and 3Mg-PDC pellets, the XRD peaks of 3Li-PDC pellets resembled PDC pellets without any secondary phase (PrO_2).

- The sintering kinetic studies over 3Li-PDC pellets showed that the initial sintering mechanism followed the grain-boundary diffusion mechanism with m~2 obtained from the CHR method. The activation energy is calculated using CHR and Dorn Methods and was around 182 and 196 kJ/mol.

- The calculated coefficient of thermal expansion (CTE) values of 10PDC, 1Li-PDC, 3Li-PDC, 3Co-PDC, 3Fe-PDC and 3Mg-PDC from 100 to 800°C are 15.3×10^{-6} / °C, 18.2×10^{-6} / °C, 14×10^{-6} / °C, 15.2×10^{-6} / °C, 13.8×10^{-6} / °C, 15.7×10^{-6} / °C respectively.

7.2. CONCLUSIONS

Praseodymium-doped ceria ($Ce_{0.9}Pr_{0.1}O_2$, PDC), as an electrolyte material for IT-SOFCs, is investigated to the effect of the synthesis method, and a detailed analysis was carried out to understand the effect on crystallite size, morphology, specific surface area and sintering behaviour. The various synthesis routes such as microwave-assisted co-precipitation method (using ethanol, water and isopropyl alcohol as solvents), room temperature co-precipitation method using isopropyl alcohol as a solvent and EDTA-citrate complexing method was adopted for the synthesis of praseodymium doped ceria-based nano-materials. In $Ce_{0.9}Pr_{0.1}O_2$, the solid solution solubility of Pr in CeO_2 extends to 1000°C. All the samples exhibited a cubic fluorite-type crystal structure of CeO_2 from XRD analysis. PDC synthesised by microwave-assisted co-precipitation method using isopropyl alcohol as solvent exhibited better sintering activity, reduced the sintering temperature and promoted the densification rate when compared to other synthesis methods with uni-model shrinkage behaviour with shrinkage maxima at 765°C. Therefore, by altering the synthesis method, the sintering temperature has been drastically reduced from 1500°C (EDTA – Citrate) to 1100°C (MWCOP – ISP). Based on two sintering models (CHR/Dorn method), the initial stage sintering mechanism was investigated in the present study and confirmed that the grain boundary diffusion (m ~ 2) as the dominant mechanism and the activation energy was found to be 116 kJ/mol (CHR model) and 176 kJ/mol (Dorn Method) for initial stages of sintering for PDC material synthesised by microwave-assisted co-precipitation method using isopropyl alcohol as the solvent. The effect of sintering additives (Li, Co, Fe, and Mg) on the sintering kinetic behavior of the praseodymium-doped-ceria (PDC) electrolyte of solid oxide cells were further studied. The addition of lithium as a sintering additive (3Li-PDC) had reduced the sintering temperature of PDC from 1100°C to 850°C. The initial sintering behavior of the 3Li-PDC sample was found out to be is by the grain boundary diffusion mechanism (m

~2) with an activation energy of 182 kJ/mol (CHR Method). The thermal expansion behaviour of the as-synthesised PDC sintered pellets from 100 to 800°C has been studied and the calculated coefficient of thermal expansion (CTE) values of 10PDC, 1Li-PDC, 3Li-PDC, 3Co-PDC, 3Fe-PDC and 3Mg-PDC are $15.3x10^{-6}$ / °C, $18.2x10^{-6}$ / °C, $14x10^{-6}$ / °C, $15.2x10^{-6}$ / °C, $13.8x10^{-6}$ / °C, $15.7x10^{-6}$ / °C respectively.

7.3. SCOPE OF THE WORK

- 10PDC, 3Li-PDC, 3Co-PDC, 3Fe-PDC and 3Mg-PDC synthesised by microwave assisted co-precipitation method can be tested for electrical conductivity measurements.

- Multi dopants, such as rare earth metals, can be added to analyze the electrical conductivity of the samples and to understand the sintering kinetic behaviour.

- Alternative suitable electrode materials based on synthesised PDC electrolyte material can be further developed.

- Fuel cell can be fabricated using 10PDC, 3Li-PDC, 3Co-PDC, 3Fe-PDC and 3Mg-PDC and can be tested for power generation.

APPENDIX- I

Study on Praseodymium Doped Ceria Based (PDC) Electrolyte Materials For IT-SOFCs
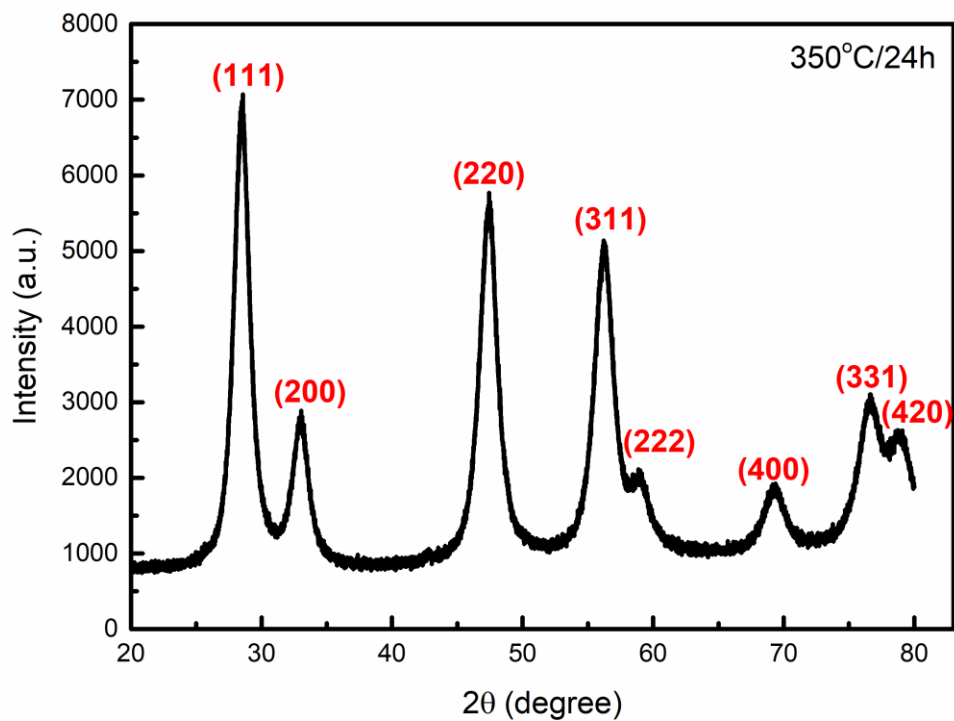
Figure S4.1: XRD pattern of PDC samples calcined at 350°C/ 24h
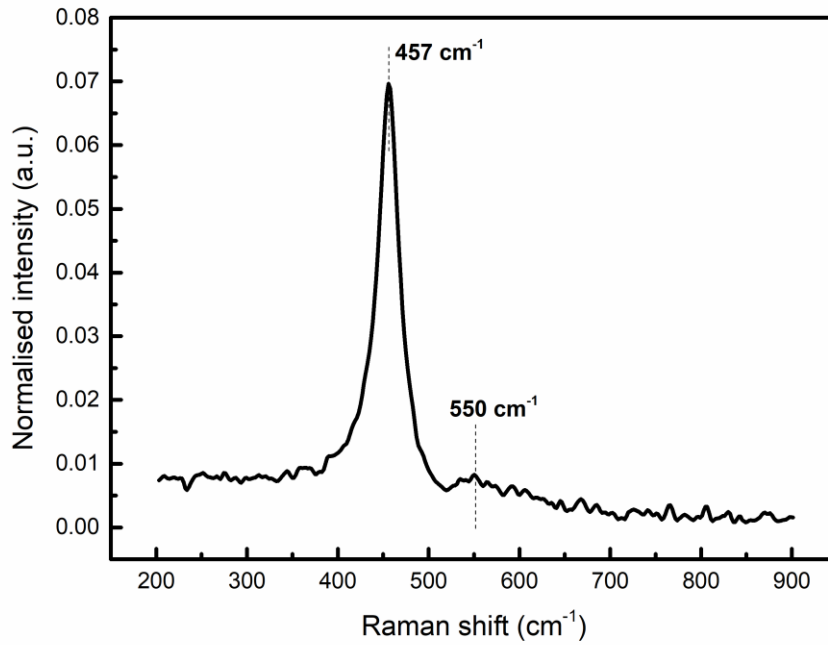
Figure S4.2: Raman spectra of PDC samples calcined at 350°C/ 24h
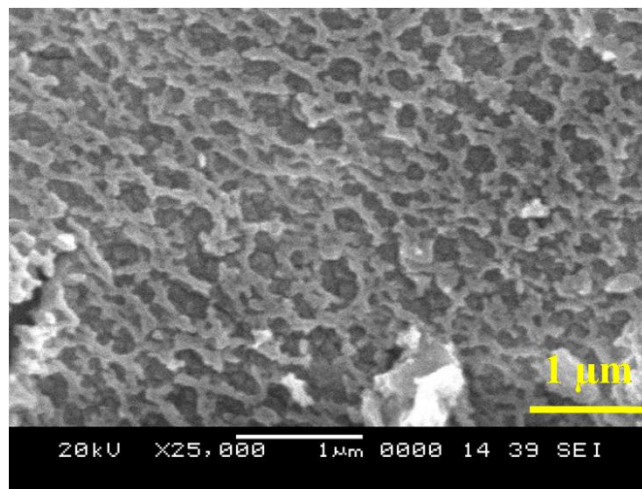
Figure S4.3: SEM micrograph of PDC samples calcined at 350°C/ 24h
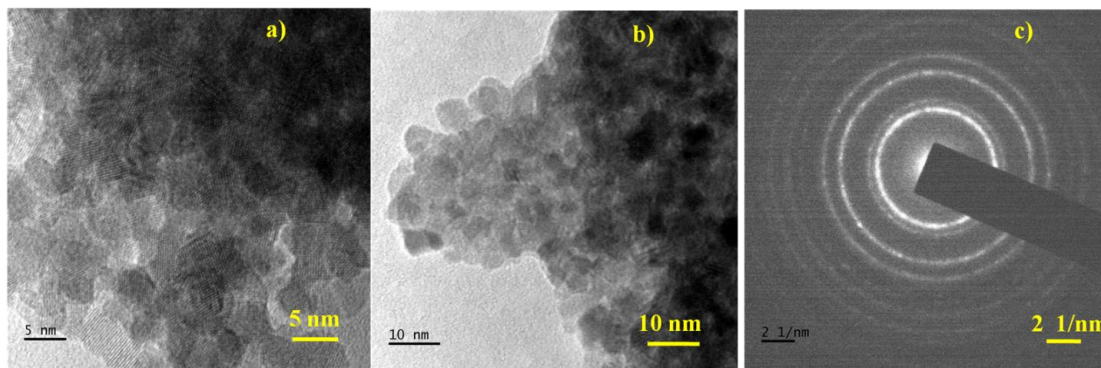
Figure S4.4: (a) and (b) TEM micrographs of the calcined PDC powder (350°C/24 h) and (c) SAED patterns for calcined PDC nanopowder
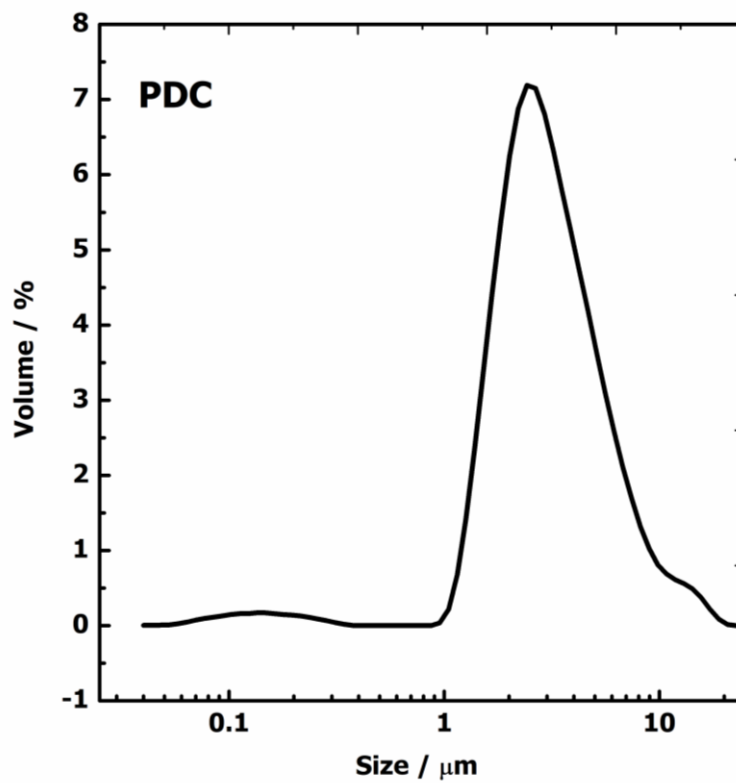
Figure S4.5: Particle size distribution of calcined PDC
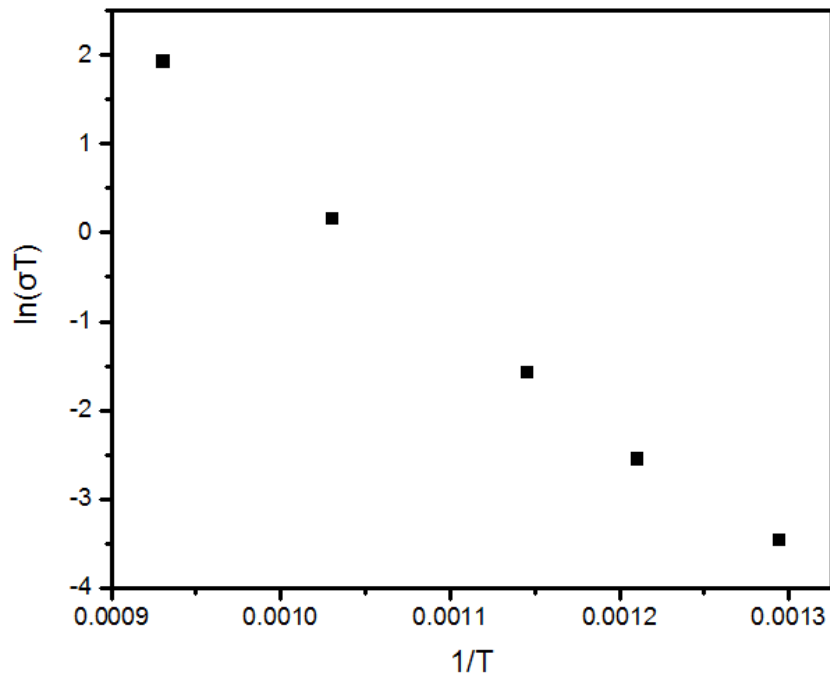
Figure S4.6: Electrical conductivity of PDC pellet sintered at 1500°C/5 h
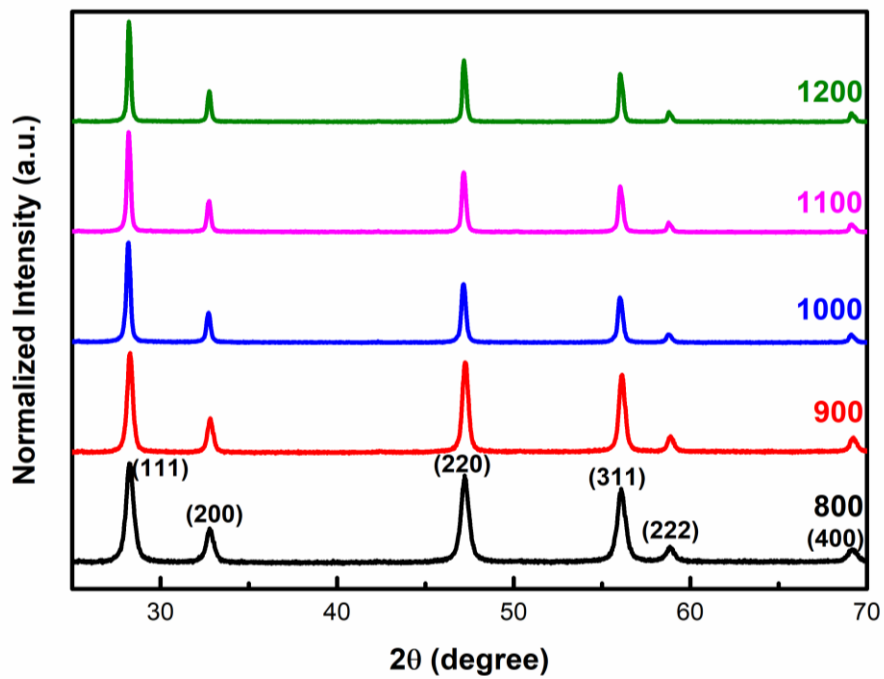
Figure S4.7: XRD pattern of PDC sample sintered at 800, 900, 1000, 1100 and 1200°C/ 5h
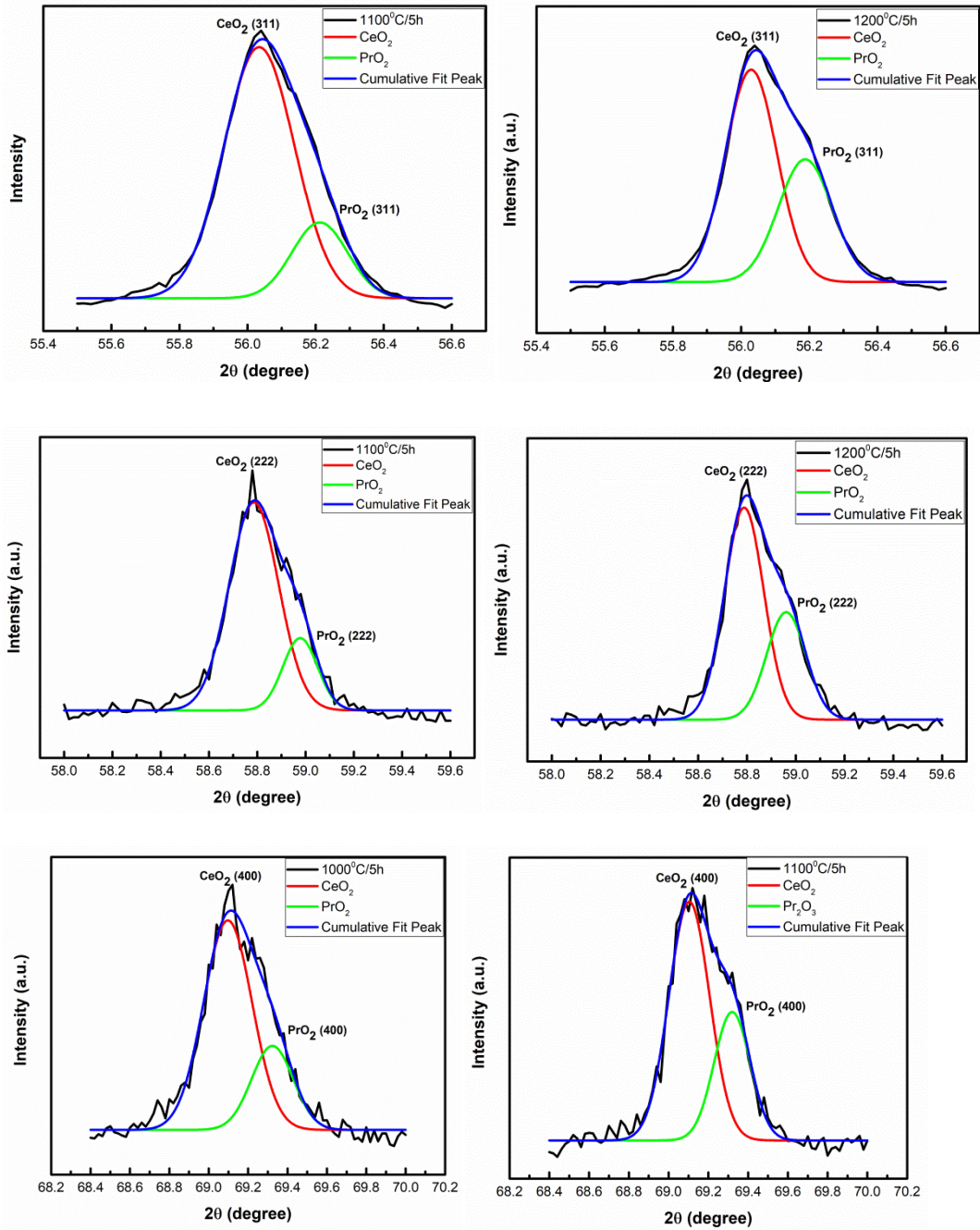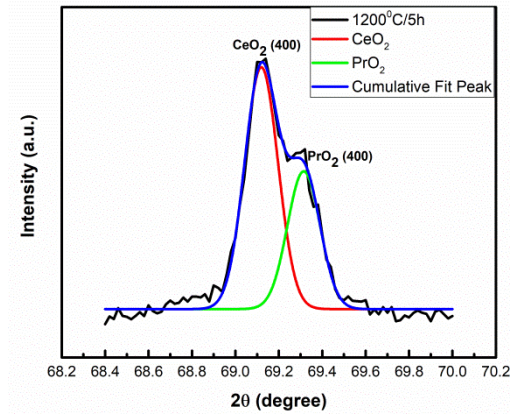
Figure S4.8: XRD pattern corresponding to peak splitting of (311), (222), (400) peaks of sintered PDC sample

Table S4.1: Crystallographic data, lattice strain and BET surface area of PDC sample sintered at 800, 900, 1000, 1100 and 1200ºC/5h

Sintering Temperature (ºC)	Crystallite size, nm	Lattice Strain (%)	Particle Size, nm	Lattice parameter (Aº)	BET Surface area, m²/g
800	15.857	0.0049	53.32	5.44	15.65
900	21.62	0.0035	75.12	5.44	11.11
1000	28.38	0.0029	118.21	5.45	7.06
1100	31.21	0.0026	237.78	5.45	3.51
1200	34.64	0.0024	309.11	5.46	2.70

REFERENCES

Abbas, Z., Surendran, M., Anjana, P. A., Jidev, P. K., Dasari, H., Sudhakar Naidu, N., Anandhan, S., Bhat, K. U., Bhaskar Babu, G. U., and Prasad Dasari, H. (2017). "Solubility Limits of Ceria-Zirconia-Lanthana Solid-Solutions." *Mater. Today Proc.*, 4(9), 9360–9364.

Adler, S. B. (1998). "Mechanism and kinetics of oxygen reduction on porous $La_{1-x}Sr_xCoO_{3-\delta}$ electrodes." *Solid State Ionics*, 111(1–2), 125–134.

Ahn, K., Yoo, D. S., Prasad, D. H., Lee, H., Chung, Y., and Lee, J. (2012). "Role of Multivalent Pr in the Formation and Migration of Oxygen Vacancy in Pr-Doped Ceria: Experimental and First-Principles Investigations." *Chem. Mater.*, 24, 4261−4267.

An, B., Zhou, W., Guo, Y., Ran, R., and Shao, Z. (2010). "A composite oxygen-reduction electrode composed of $SrSc_{0.2}Co_{0.8}O_{3-\delta}$ perovskite and $Sm_{0.2}Ce_{0.8}O_{1.9}$ for an intermediate-temperature solid-oxide fuel cell." *Int. J. Hydrogen Energy*, 35(11), 5601–5610.

Arabacı, A., and Öksüzömer, M. F. (2012). "Preparation and characterization of 10 mol% Gd doped CeO_2(GDC) electrolyte for SOFC applications." *Ceram. Int.*, 38(8), 6509–6515.

Arsalis, A. (2008). "Thermoeconomic modeling and parametric study of hybrid SOFC-gas turbine-steam turbine power plants ranging from 1.5 to 10 MWe." *J. Power Sources*, 181(2), 313–326.

Arunkumar, P., Meena, M., and Babu, K. S. (2012). "A review on cerium oxide-based electrolytes for ITSOFC." *Nanomater. Energy*, 1(5), 288–305.

Ayastuy, J. L., Gurbani, A., González-Marcos, M. P., and Gutiérrez-Ortiz, M. A. (2010). "CO oxidation on $Ce_XZr_{1-X}O_2$-supported CuO catalysts: Correlation between activity and support composition." *Appl. Catal. A Gen.*, 387(1–2), 119–128.

Ayawanna, J., Wattanasiriwech, D., Wattanasiriwech, S., and Aungkavattana, P. (2009). "Effects of cobalt metal addition on sintering and ionic conductivity of Sm(Y)-doped ceria solid electrolyte for SOFC." *Solid State Ionics*, 180(26–27), 1388–1394.

BACMANN, J. J., and CIZERON, G. (1968). "Dorn Method in the Study of Initial Phase of Uranium Dioxide Sintering." *J. Am. Ceram. Soc.*, 51(4), 209–212.

Badwal, S. P. S., and Foger, K. (1996). "Solid Oxide Electrolyte Fuel cell Review." *Ceram. Int.*, 22(95), 257–265.

Barbir, F. (2013). *Fuel Cell Electrochemistry. PEM Fuel Cells*.

Bellon, O., Sammes, N. M., and Staniforth, J. (1998). "Mechanical properties and electrochemical characterisation of extruded doped cerium oxide for use as an electrolyte for solid oxide fuel cells." *J. Power Sources*, 75, 116–121.

Bishop, S. R., Marrocchelli, D., Chatzichristodoulou, C., Perry, N. H., Mogensen, M. B., Tuller, H. L., and Wachsman, E. D. (2014). "Chemical Expansion: Implications for Electrochemical Energy Storage and Conversion Devices." *Annu. Rev. Mater. Res.*, 44(1), 205–239.

Bochentyn, B., Błaszczak, P., Gazda, M., Fuerte, A., Wang, S. F., and Jasiński, P. (2020). "Investigation of praseodymium and samarium co-doped ceria as an anode catalyst for DIR-SOFC fueled by biogas." *Int. J. Hydrogen Energy*, 5, 0–11.

Bonamartini Corradi, A., Bondioli, F., Ferrari, A. M., and Manfredini, T. (2006). "Synthesis and characterization of nanosized ceria powders by microwave-hydrothermal method." *Mater. Res. Bull.*, 41(1), 38–44.

Bondioli, F., Corradi, A. B., Manfredini, T., Leonelli, C., and Bertoncello, R. (2000). "Nonconventional synthesis of praseodymium-doped ceria by flux method." *Chem. Mater.*, 12(2), 324–330.

Camilo de Souza, E. C., and Muccillo, E. N. (2019). "Low Sintering Temperature and

Electrical Properties of Samarium-Doped Ceria." *ECS Trans.*, 25(2), 1643–1649.

Chakraborty, U. K. (2018). "Reversible and irreversible potentials and an inaccuracy in popularmodels in the fuel cell literature." *Energies*, 11(7).

Chen, M.-J., Cheng, S., Wang, F.-Y., Lee, J. F., and Tai, Y. L. (2007). "Study of Pr-doped Ceria-based Electrolytes for ITSOFC." *ECS Trans.*, 7(1), 2245–2252.

Chen, P. L., and Chen, I. W. (1996a). "Sintering of Fine Oxide Powders: I, Microstructural Evolution." *J. Am. Ceram. Soc*, 79(12), 3129–41.

Chen, P. L., and Chen, I. W. (1996b). "Grain growth in CeO_2: Dopant effects, defect mechanism, and solute drag." *J. Am. Ceram. Soc.*

Chen, P. L., and Chen, I. W. (1997). "Sintering of Fine Oxide Powders: II, Sintering Mechanisms." *J. Am. Ceram. Soc.*, 80(3), 637–645.

Cheng, J. G., Zha, S. W., Huang, J., Liu, X. Q., and Meng, G. Y. (2003). "Sintering behavior and electrical conductivity of $Ce_{0.9}Gd_{0.1}O_{1.95}$ powder prepared by the gel-casting process." *Mater. Chem. Phys.*, 78(3), 791–795.

Cheng, S., Chatzichristodoulou, C., Søgaard, M., Kaiser, A., and Hendriksen, P. V. (2017). " Ionic/Electronic Conductivity, Thermal/Chemical Expansion and Oxygen Permeation in Pr and Gd Co-Doped Ceria Pr_x $Gd_{0.1}$ $Ce_{0.9-x}$ $O_{1.95-\delta}$." *J. Electrochem. Soc.*, 164(13), F1354–F1367.

Christie, G., and Berkel, F. P., Van. (1996). "Microstructure — ionic conductivity relationships in ceria-gadolinia electrolytes." *Solid State Ionics*, 83(1–2), 17–27.

Ding, D., Liu, B., Gong, M., Liu, X., and Xia, C. (2010). "Electrical properties of samaria-doped ceria electrolytes from highly active powders." *Electrochim. Acta*, 55(15), 4529–4535.

Dogra, S., Singh, J., Dilawar Sharma, N., Samanta, K., Poswal, H. K., Sharma, S. M., and Bandyopadhyay, A. K. (2014). "Phase progression via phonon modes in lanthanide

A Study On Sintering Behaviour Of Praseodymium Doped Ceria Based SOFC Electrolytes

dioxides under pressure." *Vib. Spectrosc.*, 70, 193–199.

Dong, Q., Du, Z. H., Zhang, T. S., Lu, J., Song, X. C., and Ma, J. (2009). "Sintering and ionic conductivity of 8YSZ and CGO10 electrolytes with small addition of Fe_2O_3: A comparative study." *Int. J. Hydrogen Energy*, 34(19), 7903–7909.

Dong, Y., Hampshire, S., Lin, B., Ling, Y., and Zhang, X. (2010). "High sintering activity Cu-Gd co-doped CeO_2 electrolyte for solid oxide fuel cells." *J. Power Sources*, 195(19), 6510–6515.

Dong, Y., Hampshire, S., Zhou, J. E., and Meng, G. (2011). "Synthesis and sintering of Gd-doped CeO2 electrolytes with and without 1 at.% CuO dopping for solid oxide fuel cell applications." *Int. J. Hydrogen Energy*, 36(8), 5054–5066.

Dudek, M., Rapacz-Kmita, A., Mroczkowska, M., Mosiałek, M., and Mordarski, G. (2010). "Co-doped ceria-based solid solution in the CeO_2-M_2O_3-CaO, M = Sm, Gd system." *Electrochim. Acta*, 55(14), 4387–4394.

Esposito, V., Fonseca, F. C., Florio, D. Z. De, Žunić, M., Muccillo, R., and E, V. (2007). "Fabrication of $Ce_{1-x}Gd_xO_{2-0.5x}$ Electrolytes with Tunable Dense Microstructures for IT-SOFC Applications." *ECS Trans.*, 7(1), 2093–2101.

Esposito, V., Zunic, M., and Traversa, E. (2009). "Improved total conductivity of nanometric samaria-doped ceria powders sintered with molten $LiNO_3$ additive." *Solid State Ionics*, 180(17–19), 1069–1075.

Esther Jeyanthi, C., Siddheswaran, R., Kumar, P., Karl Chinnu, M., Rajarajan, K., and Jayavel, R. (2015). "Investigation on synthesis, structure, morphology, spectroscopic and electrochemical studies of praseodymium-doped ceria nanoparticles by combustion method." *Mater. Chem. Phys.*, 151(March), 22–28.

Fergus, J. W. (2006). "Electrolytes for solid oxide fuel cells." *J. Power Sources*, 162(1), 30–40.

Fergus, W. J., Hui, R., Li, X., Wilkinson, P. D., and Zhang, J. (Eds.). (2009). *Solid Oxide Fuel Cells Materials Properties and Performance*. New York.

Ftikos, C., Nauer, M., and Steele, B. C. H. (1993). "Electrical conductivity and thermal expansion of ceria doped with Pr, Nb and Sn." *J. Eur. Ceram. Soc.*, 12(6), 267–270.

Gadonneix, P., Pacific, A., Asia, S., Kim, Y. D., Meyers, K., Ward, G., Statham, B., and Frei, C. (2013). "2013 World Energy Issues Monitor."

German, R. M., Suri, P., and Park, S. J. (2009). "Review: Liquid phase sintering." *J. Mater. Sci.*, 44(1), 1–39.

Ghosh, A., Suri, A. K., Rao, B. T., and Ramamohan, T. R. (2008). "Synthesis of nanocrystalline sinteractive 3Y-TZP powder in presence of ammonium sulphate and poly ethylene glycol." *Adv. Appl. Ceram.*, 108(3), 183–188.

Gil, V., Tartaj, J., Moure, C., and Durán, P. (2006). "Sintering, microstructural development, and electrical properties of gadolinia-doped ceria electrolyte with bismuth oxide as a sintering aid." *J. Eur. Ceram. Soc.*, 26(15), 3161–3171.

Godinho, M. J., Gonçalves, R. F., S Santos, L. P., Varela, J. A., Longo, E., and Leite, E. R. (2007). "Room temperature co-precipitation of nanocrystalline CeO_2 and $Ce_{0.8}Gd_{0.2}O_{1.9-\delta}$ powder." *Mater. Lett.*, 61(8–9), 1904–1907.

Gondolini, A., Mercadelli, E., Sanson, A., Albonetti, S., Doubova, L., and Boldrini, S. (2013). "Effects of the microwave heating on the properties of gadolinium-doped cerium oxide prepared by polyol method." *J. Eur. Ceram. Soc.*, 33(1), 67–77.

Guo, M., Lu, J., Wu, Y., Wang, Y., and Luo, M. (2011). "UV and Visible Raman Studies of Oxygen Vacancies in Rare-Earth-Doped Ceria." 3872–3877.

Gupta, T. K. (1971). "Sintering of MgO: Densification and grain growth." *J. Mater. Sci.*, 6(1), 25–32.

Hari Prasad, D., Kim, H. R., Park, J. S., Son, J. W., Kim, B. K., Lee, H. W., and Lee, J.

H. (2010b). "Superior sinterability of nano-crystalline gadolinium doped ceria powders synthesized by co-precipitation method." *J. Alloys Compd.*, 495(1), 238–241.

Hari Prasad, D., Kim, H. R., Son, J. W., Kim, B. K., Lee, H. W., and Lee, J. H. (2009). "Superior compositional homogeneity and long-term catalytic stability of Ni-$Ce_{0.75}Zr_{0.25}O_2$ cermets prepared via glycine nitrate process." *Catal. Commun.*, 10(9), 1334–1338.

Hari Prasad, D., Park, S. Y., Ji, H., Kim, H. R., Son, J. W., Kim, B. K., Lee, H. W., and Lee, J. H. (2012). "Cobalt oxide co-doping effect on the sinterability and electrical conductivity of nano-crystalline Gd-doped ceria." *Ceram. Int.*, 38(SUPPL. 1), 497–500.

He, Z., Yuan, H., Glasscock, J. A., Chatzichristodoulou, C., Phair, J. W., Kaiser, A., and Ramousse, S. (2010). "Densification and grain growth during early-stage sintering of $Ce_{0.9}Gd_{0.1}O_{1.95-\delta}$ in a reducing atmosphere." *Acta Mater.*, 58(11), 3860–3866.

Herle, J. Van, Horita, T., Kawada, T., Sakai, N., Yokokawa, H., and Dokiya, M. (1996). "Low temperature fabrication of (Y,Gd,Sm)-doped ceria electrolyte." *Solid State Ionics*, 86–88(96), 1255–1258.

Herring, C. (1950). "Effect of change of scale on sintering phenomena." *J. Appl. Phys.*, 21(4), 301–303.

Himri, A. El, Haboubi, K., Himri, M. El, Dimane, F., Jeffali, F., and Hanafi, I. (2016). "Fuel cell technology : Synthesis and electrical properties of electrolyte for intermediate temperature." 7(12), 4672–4681.

Huang, W., Shuk, P., and Greenblatt, M. (1997). "Properties of sol-gel prepared $Ce_{1-x}Sm_xO_{2-x/2}$ solid electrolytes." *Solid State Ionics*, 100(1–2), 23–27.

Hui, S. (Rob), Roller, J., Yick, S., Zhang, X., Deces-Petit, C., Xie, Y., Maric, R., and Ghosh, D. (2007). "A brief review of the ionic conductivity enhancement for selected oxide electrolytes." *J. Power Sources*, 172(2), 493–502.

Hwang, N., and Barron, An. R. (1987). *Connexions BET Surface Area Analysis of Nanoparticles*.

Inaba, H., and Tagawa, H. (1996). "Ceria-based solid electrolytes." *Solid State Ionics*, 83(1–2), 1–16.

Ishihara, T., Tabuchi, J., Ishikawa, S., Yan, J., Enoki, M., and Matsumoto, H. (2006). "Recent progress in LaGaO$_3$ based solid electrolyte for intermediate temperature SOFCs." *Solid State Ionics*, 177(19-25 SPEC. ISS.), 1949–1953.

Jamshidijam, M., Mangalaraja, R. V, Akbari-fakhrabadi, A., Ananthakumar, S., and Chan, S. H. (2014). "Effect of rare earth dopants on structural characteristics of nanoceria synthesized by combustion method." *Powder Technol.*, 253, 304–310.

Ji, Y., Liu, J., He, T., Wang, J., and Su, W. (2005). "The effect of Pr co-dopant on the performance of solid oxide fuel cells with Sm-doped ceria electrolyte." *J. Alloys Compd.*, 389(1–2), 317–322.

Jiang, S. P. (2008). "Development of lanthanum strontium manganite perovskite cathode materials of solid oxide fuel cells : a review." *J. Mater. Sci.*, 43(21), 6799–6833.

Jiang San Ping, and Hwa Chan, S. (2004). "A review of anode materials development in solid oxide fuel cells." *J. Mater. Sci.*, 39, 4405– 4439 A.

Jiang, Y. (1998). "Electrochemical reduction of oxygen on a strontium doped lanthanum manganite electrode." *Solid State Ionics*, 110(1–2), 111–119.

Joh, W. D., Rath, K. M., Park, W. J., Park, H. J., Cho, H. K., Lee, S., Yoon, joong K., Lee, J.-H., and Lee, T. K. (2016). "Sintering behavior and electrochemical performances of nano-sized gadolinium-doped ceria via ammonium carbonate assisted co-precipitation for solid oxide fuel cells." *J. Alloys Compd.*, 682(May), 188–195.

Jud, E., and Gauckler, L. J. (2005). "Sintering behavior of cobalt oxide doped ceria powders of different particle sizes." *J. Electroceramics*, 14, 247–253.

Jud, E., Huwiler, C. B., and Gauckler, L. J. (2005). "Sintering analysis of undoped and cobalt oxide doped ceria solid solutions." *J. Am. Ceram. Soc.*, 88(11), 3013–3019.

Jung, G. B., Huang, T. J., Huang, M. H., and Chang, C. L. (2001). "Preparation of samaria-doped ceria for solid-oxide fuel cell electrolyte by a modified sol-gel method." *J. Mater. Sci.*, 36(24), 5839–5844.

Kalra, P., Garg, R., and Kumar, A. (2015). "Modelling of a High Temperature Solid Oxide Fuel Cell." *J. Energy Technol. Policy*, 5(2), 76–84.

Kharton, V. V., Figueiredo, F., Navarro, L., Naumovich, E., Kovalevsky, A., Yaremchenko, A., Viskup, A., Carneiro, a, Marques, F., and Frade, J. (2001). "Ceria-based materials for solid oxide fuel cells." *J. Mater. Sci.*, 36(5), 1105–1117.

Kharton, V. V., Marques, F. M. B., and Atkinson, A. (2004). "Transport properties of solid oxide electrolyte ceramics: a brief review." *Solid State Ionics*, 174(1–4), 135–149.

Kleinlogel, C., and Gauckler, L. J. (2000). "Sintering and properties of nanosized ceria solid solutions." *Solid State Ionics*, 135(1–4), 567–573.

Kleinlogel, C., and Gauckler, L. J. (2001). "Sintering of Nanocrystalline CeO$_2$ Ceramics." *Adv. Mater.*, 13(14), 1081–1085.

Kleinlogel, C., Gauckler, L. J., and Materials, N. (1999). "NANO SIZED CERIA SOLID SOLUTIONS FOR INTERMEDIATE TEMPERATURE SOLID OXIDE FUEL CELLS." *Electrochem. Soc.*, 99(19), 225–232.

Koh, J. H., Yoo, Y. S., Park, J. W., and Lim, H. C. (2002). "Carbon deposition and cell performance of Ni-YSZ anode support SOFC with methane fuel." *Solid State Ionics*, 149(3–4), 157–166.

Kondakindi, R. R., and Karan, K. (2009). "Characterization of Fe- and Mn-doped GDC for low-temperature processing of solid oxide fuel cells." *Mater. Chem. Phys.*, 115(2–3), 728–734.

Kuczynski, G. . (1956). "The mechanism of densification during sintering of metallic particles." *Acta Metall.*, 4(1), 58–61.

Kuru, Y., Bishop, S. R., Kim, J. J., Yildiz, B., and Tuller, H. L. (2011). "Chemomechanical properties and microstructural stability of nanocrystalline Pr-doped ceria : An in situ X-ray diffraction investigation." *Solid State Ionics*, 193(1), 1–4.

Lahiri, D., Rao, S. V. R., Rao, G. V. S. H., and Srivastava, R. K. (2006). "Study on sintering kinetics and activation energy of UO_2 pellets using three different methods." *J. Nucl. Mater.*, 357(1–3), 88–96.

Laosiripojana, N., Wiyaratn, W., Kiatkittipong, W., Arpornwichanop, A., Soottitantawat, A., and Assabumrungrat, S. (2009). "Reviews on solid oxide fuel cell technology." *Eng. J.*, 13(1), 65–83.

Le, S., Zhu, S., Zhu, X., and Sun, K. (2013a). "Densification of $Sm_{0.2}Ce_{0.8}O_{1.9}$ with the addition of lithium oxide as sintering aid." *J. Power Sources*, 222, 367–372.

Lewis, G. S., Atkinson, A., and Steele, B. C. H. (2001). "Cobalt additive for lowering the sintering temperature of yttria-stabilized zirconia." *J. Mater. Sci. Lett.*, 20(12), 1155–1157.

Li, H. G., Ikegami, T., Wang, Y. R., and Mori, T. (2002). "Reactive ceria nanopowders via carbonate precipitation." *J. Am. Ceram. Soc.*, 85(9), 2376–2378.

Li, S. P., Lu, J. Q., Fang, P., and Luo, M. F. (2009). "Effect of oxygen vacancies on electrical properties of $Ce_{0.8}Sm_{0.1}Nd_{0.1}O_{2-\delta}$ electrolyte: An in situ Raman spectroscopic study." *J. Power Sources*, 193(1), 93–98.

Liu, Y., Fan, L., Cai, Y., Zhang, W., Wang, B., and Zhu, B. (2017). "Superionic Conductivity of Sm^{3+}, Pr^{3+}, and Nd^{3+} Triple-Doped Ceria through Bulk and Surface Two-Step Doping Approach." *ACS Appl. Mater. Interfaces*, 9, 23614−23623.

Lu, C., Worrell, W. L., Wang, C., Park, S., Kim, H., Vohs, J. M., and Gorte, R. J. (2002).

"Development of solid oxide fuel cells for the direct oxidation of hydrocarbon fuels." *Solid State Ionics*, 152–153, 393–397.

Ma, J., Zhang, T. S., Kong, L. B., Hing, P., and Chan, S. H. (2004). "$Ce_{0.8}Gd_{0.2}O_{2-\delta}$ ceramics derived from commercial submicron-sized CeO_2 and Gd_2O_3 powders for use as electrolytes in solid oxide fuel cells." *J. Power Sources*, 132, 71–76.

Machado, M., Moraes, L. P. R., Rodrigues, L. N., Tabanez, M., Ferrazoli, M., Fonseca, F. C., and N. (2019). "Evaluation of Fe-doped CGO Electrolyte for Application in IT-SOFCs." *ECS Trans.*, 91(1), 1209–1216.

Mario Birkholz. (2006). *Principles of X-ray Diffraction. Thin Film Anal. by X-Ray Scatt.*

McBride, J. R., Hass, K. C., Poindexter, B. D., and Weber, W. H. (1994). "Raman and x-ray studies of Ce1-xRExO2-y, where RE= La, Pr, Nd, Eu, Gd, and Tb." *J. Appl. Phys.*, 76(4), 2435–2441.

Medisetti, S., Ahn, J., Patil, S., Goel, A., Bangaru, Y., Sabhahit, G. V., Babu, G. U. B., Lee, J.-H., and Dasari, H. P. (2017a). "Synthesis of GDC electrolyte material for IT-SOFCs using glucose & fructose and its characterization." *Nano-Structures & Nano-Objects*, 11, 7–12.

Mukherjee, D., Rao, B. G., and Reddy, B. M. (2017). "Characterization of Ceria-Based Nano-Oxide Catalysts by Raman Spectroscopy." *Top. Catal.*, 60(19–20), 1673–1681.

Murray, E. P., Tsai, T., and Barnett, S. A. (1998). "Oxygen transfer processes in $(La,Sr)MnO_3/Y_2O_3$-stabilized ZrO_2 cathodes: an impedance spectroscopy study." *Solid State Ionics*, 110(3–4), 235–243.

Nauer, M., and Steele, B. C. H. (1994a). "An Evaluation of Ce-Pr Oxides and Ce-Pr-Nb Oxides Mixed Conductors for Cathodes of Solid Oxide Fuel Cells : Structure , Thermal Expansion and Electrical Conductivity." *J. Electrochem. Soc.*, 14, 493–499.

Nicholas, J. D., and Jonghe, L. C. De. (2007). "Prediction and evaluation of sintering aids

for Cerium Gadolinium Oxide." *Solid State Ionics*, 178(19–20), 1187–1194.

Peng, C., and Zhang, Z. (2007). "Nitrate – citrate combustion synthesis of $Ce_{1-x}Gd_xO_{2-x/2}$ powder and its characterization." *Ceram. Int. 33*, 33(3), 1133–1136.

Pérez-Coll, D., Sánchez-López, E., and Mather, G. C. (2010). "Influence of porosity on the bulk and grain-boundary electrical properties of Gd-doped ceria." *Solid State Ionics*, 181(21–22), 1033–1042.

Pikalova, E. Y., Maragou, V. I., Demina, A. N., Demin, A. K., and Tsiakaras, P. E. (2008). "The effect of co-dopant addition on the properties of $Ln_{0.2}Ce_{0.8}O_{2-\delta}$(Ln = Gd, Sm, La) solid-state electrolyte." *J. Power Sources*.

Pound, B. G. (1992). "The characterization of doped CeO_2 electrodes in solid oxide fuel cells." *Solid State Ionics*, 52, 183–188.

Prakash, B. S., Kumar, S. S., and Aruna, S. T. (2014). "Properties and development of Ni / YSZ as an anode material in solid oxide fuel cell : A review." *Renew. Sustain. Energy Rev.*, 36, 149–179.

Prasad, D. H., Ji, H. I., Kim, H. R., Son, J. W., Kim, B. K., Lee, H. W., and Lee, J. H. (2011). "Effect of nickel nano-particle sintering on methane reforming activity of Ni-CGO cermet anodes for internal steam reforming SOFCs." *Appl. Catal. B Environ.*, 101(3–4), 531–539.

Prasad, D. H., Lee, J. H., Lee, H. W., Kim, B. K., and Park, J. S. (2010a). "Correlation between the powder properties and sintering behaviors of nano-crys-talline gadolinium-doped ceria." *J. Ceram. Process. Res.*, 11(5), 523–526.

Prasad, D. H., Park, S. Y., Ji, H., Kim, H. R., Son, J. W., Kim, B. K., Lee, H. W., and Lee, J. H. (2012a). "Effect of steam content on nickel nano-particle sintering and methane reforming activity of Ni-CZO anode cermets for internal reforming SOFCs." *Appl. Catal. A Gen.*, 411–412, 160–169.

Prasad, D. H., Park, S. Y., Oh, E., Ji, H., Kim, H., Yoon, K., Son, J., and Lee, J. (2012b). "Synthesis of nano-crystalline La$_{1-x}$ Sr$_x$ CoO$_{3-\delta}$ perovskite oxides by EDTA – citrate complexing process and its catalytic activity for soot oxidation." *Appl. Catal. A Gen.*, 447–448, 100–106.

Prasad, D. H., Son, J. W., Kim, B. K., Lee, H. W., and Lee, J. H. (2008). "Synthesis of nano-crystalline Ce$_{0.9}$Gd$_{0.1}$O$_{1.95}$ electrolyte by novel sol-gel thermolysis process for IT-SOFCs." *J. Eur. Ceram. Soc.*, 28(16), 3107–3112.

Prasad, H. D., Son, J., Kim, B., Lee, H., and Lee, J. (2010b). "A significant enhancement in sintering activity of nanocrystalline Ce$_{0.9}$Gd$_{0.1}$O$_{1.95}$ powder synthesized by a glycine-nitrate-process." *Ceram. Process. Res.*, 11(2), 176–183.

Purohit, R. D., Saha, S., and Tyagi, A. K. (2006). "Powder characteristics and sinterability of ceria powders prepared through different routes." *Ceram. Int.*, 32, 143–146.

Rahaman, M. N. (1996). "Ceramic processing and sintering." *Int. Mater. Rev.*, 41(1), 36–37.

Ravi Chandran, P., and Arjunan, T. V. (2015). "A review of materials used for solid oxide fuel cell." *Int. J. ChemTech Res.*, 7(1), 489–498.

Reddy, B. M., Thrimurthulu, G., and Katta, L. (2011). "Design of Efficient Ce$_x$M$_{1-x}$O$_{2-\delta}$ (M = Zr, Hf, Tb and Pr) Nanosized Model Solid Solutions for CO Oxidation." *Catal. Letters*, 141(4), 572–581.

Reddy, B. M., Thrimurthulu, G., Katta, L., and Park, S. (2009a). "Structural Characteristics and Catalytic Activity of Nanocrystalline Ceria - Praseodymia Solid Solutions." *J. Phys. Chem. C*, 113(36), 15882–15890.

Reis, S. L., Souza, E. C. C., and Muccillo, E. N. S. (2011). "Solid solution formation, densification and ionic conductivity of Gd- and Sm-doped ceria." *Solid State Ionics*,

192(1), 172–175.

Ruiz-Morales, J. C., Marrero-López, D., Canales-Vázquez, J., and Irvine, J. T. S. (2011). "Symmetric and reversible solid oxide fuel cells." *RSC Adv.*, 1, 1403–1414.

Ruiz De Larramendi, I., Ortiz-Vitoriano, N., Acebedo, B., Jimenez De Aberasturi, D., Gil De Muro, I., Arango, A., Rodríguez-Castellón, E., Ruiz De Larramendi, J. I., and Rojo, T. (2011). "Pr-doped ceria nanoparticles as intermediate temperature ionic conductors." *Int. J. Hydrogen Energy*, 36(17), 10981–10990.

Sadykov, V. A., Kuznetsova, T. G., Frolova-Borchert, Y. V, Alikina, G. M., Lukashevich, A. I., Rogov, V. A., Muzykantov, V. S., Pinaeva, L. G., Sadovskaya, E. M., Ivanova, Y. A., Paukshtis, E. A., Mezentseva, N. V, Batuev, L. C., Parmon, V. N., Neophytides, S., Kemnitz, E., Scheurell, K., Mirodatos, C., and Veen, A. C. van. (2006). "Fuel-rich methane combustion : Role of the Pt dispersion and oxygen mobility in a fluorite- like complex oxide support." *Catal. Today*, 117(October 2006), 475–483.

Santos, T. H., Grilo, J. P. F., Loureiro, F. J. A., Fagg, D. P., Fonseca, F. C., and Macedo, D. A. (2018). "Structure, densification and electrical properties of Gd^{3+} and Cu^{2+} co-doped ceria solid electrolytes for SOFC applications: Effects of Gd_2O_3 content." *Ceram. Int.*, 44(3), 2745–2751.

Selvaraj, T., Johar, B., and Khor, S. F. (2019). "Iron/zinc doped 8 mol% yttria stabilized zirconia electrolytes for the green fuel cell technology: A comparative study of thermal analysis, crystalline structure, microstructure, mechanical and electrochemical properties." *Mater. Chem. Phys.*, 222(October 2018), 309–320.

Setoguchi, T., Okamoto, K., Eguchi, K., and Arai, H. (1992). "Effects of Anode Material and Fuel on Anodic Reaction of Solid Oxide Fuel Cells." *J. Electrochem. Soc.*, 139(10), 2875–2880.

Shajahan, I., Ahn, J., Nair, P., Medisetti, S., Patil, S., Niveditha, V., Bhaskar, G. U., Prasad, H., and Lee, J. (2018a). "Praseodymium doped ceria as electrolyte material for

IT-SOFC applications." *Mater. Chem. Phys.*, 216(February), 136–142.

Shao, Z., and Haile, S. M. (2004). "A high-performance cathode for the next generation of solid-oxide fuel cells." *Nature*, 431(7005), 170–173.

Shao, Z., Yang, W., Cong, Y., Dong, H., Tong, J., and Xiong, G. (2000). "Investigation of the permeation behavior and stability of a $Ba_{0.5}Sr_{0.5}Co_{0.8}Fe_{0.2}O_{(3-\delta)}$ oxygen membrane." *J. Memb. Sci.*, 172(1–2), 177–188.

Shimada, H., Suzuki, T., Yamaguchi, T., Sumi, H., Hamamoto, K., and Fujishiro, Y. (2016). "Challenge for lowering concentration polarization in solid oxide fuel cells." *J. Power Sources*, 302, 53–60.

Shuk, P., and Greenblatt, M. (1999). "Hydrothermal synthesis and properties of mixed conductors based on $Ce_{1-x}Pr_xO_{2-\delta}$ solid solutions." *Solid State Ionics*, 116(3–4), 217–223.

Singhal, C. S., and Kendall, K. (Eds.). (2003). *High Temperature Solid Oxide Fuel Cells: Fundamentals, Design and Applications*. *Elsevier*, Oxford, UK.

Singhal, S. . (2000). "Advances in solid oxide fuel cell technology." *Solid State Ionics*, 135(1), 305–313.

Skinner, S. J., and Kilner, J. A. (2003). "Oxygen ion conductors." *Mater. Today*, 6(3), 30–37.

Smith, E., and Dent, G. (2005). *Modern Raman Sectroscopy - A Practical Approach*. John Wiley & Sons Ltd.

Spiridigliozzi, L., Agli, G. D., Accardo, G., Yoon, S. P., and Frattini, D. (2019). "Electro-morphological , structural , thermal and ionic conduction properties of Gd / Pr co-doped ceria electrolytes exhibiting mixed Pr^{3+} / Pr^{4+} cations." *Ceram. Int.*, 45(November), 4570–4580.

Stambouli, A. B., and Traversa, E. (2002). "Solid oxide fuel cells (SOFCs): A review of an environmentally clean and efficient source of energy." *Renew. Sustain. Energy Rev.*,

6(5), 433–455.

Steele, B. . C. H. (2000). "Appraisal of $Ce_{1-y}Gd_yO_{2-y/2}$ electrolytes for IT-SOFC operation at 500°C." *Solid State Ionics*, 129(1–4), 95–110.

Tan, L., Gu, X., Yang, L., Jin, W., Zhang, L., and Xu, N. (2003). "Influence of powder synthesis methods on microstructure and oxygen permeation performance of $Ba_{0.5}Sr_{0.5}Co_{0.8}Fe_{0.2}O_{3-\delta}$ perovskite-type membranes." *J. Memb. Sci.*, 212, 157–165.

Tian, C., and Chan, S. W. (2000). "Ionic conductivities, sintering temperatures and microstructures of bulk ceramic CeO_2 doped with Y_2O_3." *Solid State Ionics*, 134(1–2), 89–102.

Tian, R., Zhao, F., Chen, F., and Xia, C. (2011). "Sintering of Samarium-doped ceria powders prepared by a glycine-nitrate process." *Solid State Ionics*, 192(1), 580–583.

Tianshu, Z., Hing, P., and Huang, H. (2002). "Early-stage sintering mechanisms of Fe-doped CeO_2." *J. Mater. Sci.*, 37, 997– 1003.

Tok, A. I. . Y., Du, S. W., Boey, F. Y. C., and Chong, W. K. (2007a). "Hydrothermal synthesis and characterization of rare earth doped ceria nanoparticles." *Mater. Sci. Eng. A*, 466(1–2), 223–229.

Tok, A. I. Y., Luo, L. H., and Boey, F. Y. C. (2004). "Carbonate Co-precipitation of Gd_2O_3 -doped CeO_2 solid solution nano-particles." *Mater. Sci. Eng. A*, 383, 229–234.

Tok, A. I. Y., Luo, L. H., Boey, F. Y. C., and Woodhead, J. L. (2006). "Consolidation and properties of $Gd_{0.1}Ce_{0.9}O_{1.95}$ nanoparticles for solid-oxide fuel cell electrolytes." *J. Mater. Res.*, 21, 119–124.

Tsipis, E. V. E. materials and reaction mechanisms in solid oxide fuel cells: A. brief review : I. P. factors, and Kharton, V. V. (2008). "Electrode materials and reaction mechanisms in solid oxide fuel cells: A brief review." *J. Solid State Electrochem.*, 12(9), 1039–1060.

Upadhyaya, J., Peters, R. W., Fouad, F. H., Ahluwalia, R. K., Doss, E. D., and Das, T. (2004). "Environmental impact of fuel cell technology for electric power generation: An overview and case studies." *AIChE Annu. Meet. Conf. Proc.*, (January), 9389–9423.

VanHerle, J., Horita, T., Kawada, T., Sakai, N., Yokokawa, H., and Dokiya, M. (1997). "Fabrication and sintering of fine yttria-doped ceria powder." *J. Am. Ceram. Soc.*, 80(4), 933–940.

Venkataramana, K., Madhuri, C., and Reddy, C. V. (2020). "Triple-doped Ceria–Carbonate ($Ce_{0.82}La_{0.06}Sm_{0.06}Gd_{0.06}O_{2-\delta}$ − $(Li–Na)_2CO_3$) nanocomposite solid electrolyte materials for LT–SOFC applications." *Ceram. Int.*, 46(17), 27584–27594.

Venkataramana, K., Madhuri, C., Suresh Reddy, Y., Bhikshamaiah, G., and Vishnuvardhan Reddy, C. (2017). "Structural, electrical and thermal expansion studies of tri-doped ceria electrolyte materials for IT-SOFCs." *J. Alloys Compd.*, 719, 97–107.

Venugopal, A., Naveen Kumar, S., Ashok, J., Hari Prasad, D., Durga Kumari, V., Prasad, K. B. S., and Subrahmanyam, M. (2007). "Hydrogen production by catalytic decomposition of methane over Ni / SiO_2." *Int. J. Hydrogen Energy*, 32(12), 1782–1788.

Voutou, B., and Stefanaki, E.-C. (2008). *Electron Microscopy: The Basics. Phys. Adv. Mater. Winter Sch.*

Wang, J., and Raj, R. (1990). "Estimate of the Activation Energies for Boundary Diffusion from Rate-Controlled Sintering of Pure Alumina, and Alumina Doped with Zirconia or Titania." *J. Am. Ceram. Soc.*, 73(5), 1172–1175.

Wang, Y., Mori, T., Li, J.-G., and Ikegami, T. (2002). "Low-Temperature Synthesis of Praseodymium-Doped Ceria Nanopowders." *J. Am. Ceram. Soc.*, 85(12), 3105–3107.

Welaya, Y. M. A., Gohary, M. M. El, and Ammar, N. R. (2011). "A comparison between fuel cells and other alternatives for marine electric power generation." *Int. J. Nav. Archit. Ocean Eng.*, 3(2), 141–149.

Woolfrey, J. L., and Bannister, M. J. (1972). "Nonisothermal Techniques for Studying Initial-Stage Sintering." *J. Am. Ceram. Soc.*, 55(8), 390–394.

XU, L., SHUI, A., and DAI, W. (2015). "Study on the preparation and structure of nanocrystal-based Sm^{3+}-doped ceria." *J. Ceram. Soc. Japan*, 123(1437), 443–447.

Yingping, Z., Shaorong, W., Zhenrong, W., Liwei, W., and Yueming, S. (2010). "Synthesis and characterization of $Ce_{0.8}Sm_{0.2}O_{1.9}$ nanopowders using an acrylamide polymerization process." *J. Rare Earths*, 28(1), 92–95.

Yoshida, H., and Inagaki, T. (2006). "Effects of additives on the sintering properties of samaria-doped ceria." *J. Alloys Compd.*, 408–412, 632–636.

YOUNG, W. S., and CUTLER, I. B. (1970). "Initial Sintering with Constant Rates of Heating." *J. Am. Ceram. Soc.*, 53(12), 659–663.

Zaera, F., and Ma, Z. (2006). "Characterization of Heterogeneous Catalysts." *Surf. Nanomolecular Catal.*, 1–38.

Zajac, W., Suescun, L., Świerczek, K., and Molenda, J. (2009). "Structural and electrical properties of grain boundaries in $Ce_{0.85}Gd_{0.15}O_{1.925}$ solid electrolyte modified by addition of transition metal ions." *J. Power Sources*, 194(1), 2–9.

Zhang, L., Lan, R., Cowin, P. I., and Tao, S. (2011). "Fabrication of solid oxide fuel cell based on doped ceria electrolyte by one-step sintering at $800^{\circ c}$." *Solid State Ionics*, 203(1), 47–51.

Zhang, T. S., Ma, J., Kong, L. B., Chan, S. H., Hing, P., and Kilner, J. A. (2004a). "Iron oxide as an effective sintering aid and a grain boundary scavenger for ceria-based electrolytes." *Solid State Ionics 167*, 167, 203–207.

Zhang, T. S., Ma, J., Leng, Y. J., Chan, S. H., Hing, P., and Kilner, J. A. (2004b). "Effect of transition metal oxides on densification and electrical properties of Si-containing $Ce_{0.8}Gd_{0.2}O_{2-\delta}$ ceramics." *Solid State Ionics*, 168(1–2), 187–195.

Zhang, X., Decès-Petit, C., Yick, S., Robertson, M., Kesler, O., Maric, R., and Ghosh, D. (2006). "A study on sintering aids for $Sm_{0.2}Ce_{0.8}O_{1.9}$ electrolyte." *J. Power Sources*, 162(1), 480–485.

Zhen, Y. D., Tok, A. I. Y., Jiang, S. P., and Boey, F. Y. C. (2008). "Fabrication and performance of gadolinia-doped ceria-based intermediate-temperature solid oxide fuel cells." *J. Power Sources*, 178(1), 69–74.

Zheng, Y., Zhou, M., Ge, L., Li, S., Chen, H., and Guo, L. (2011). "Effect of Fe_2O_3 on Sm-doped ceria system solid electrolyte for IT-SOFCs." *J. Alloys Compd.*, 509(2), 546–550.

Zhu, T., Lin, Y., Yang, Z., Su, D., Ma, S., Han, M., and Chen, F. (2014). "Evaluation of Li_2O as an efficient sintering aid for gadolinia-doped ceria electrolyte for solid oxide fuel cells." *J. Power Sources*, 261, 255–263.

Zhu, W. Z., and Deevi, S. C. (2003). "A review on the status of anode materials for solid oxide fuel cells." *Mater. Sci. Eng. A*, 362(1–2), 228–239.

PUBLICATIONS

International Peer Reviewed Journals (From Thesis)

<u>**Accepted**</u>

1. **Irfana Shajahan**, Hari Prasad Dasari, M B Saidutta., "Effect of sintering aids on Sintering Kinetic behaviour of Praseodymium Doped Ceria based Electrolyte material for solid oxide cells.**"** *International Journal of Hydrogen Energy, 45 (2020) 25935 – 25944* **(IF 4.9)**

2. **Irfana Shajahan,** Hari Prasad Dasari, P. Govardhan., "Dilatometer studies of Praseodymium doped ceria: Effect of synthesis method on sintering behaviour."
   Materials Chemistry and Physics, 240 (2020) 122211 **(IF 3.4)**

3. **Irfana Shajahan,** Junsung Ahn, Parvathi Nair, Srikar Medisetti, Sunaina Patil, V. Niveditha, G. Uday Bhaskar Babu, Hari Prasad Dasaria, Jong-Ho Lee., "Praseodymium Doped Ceria as electrolyte material for IT-SOFC applications." *Materials Chemistry and Physics, 216 (2018) 136–142* **(IF 3.4)**

<u>**Other Publications apart from Thesis (Submitted)**</u>

4. Raksha Rao, Keerthana Kamath, Priyanka R, **Irfana Shajahan** and Hari Prasad Dasari., "Synthesis of Praseodymium Doped Ceria Based Electrolyte Material by Hydrothermal Method." Springer Nature (Book Chapter)

5. Ashmita Das, Lakhan Lal, **Irfana Shajahan,** Hari Prasad Dasari, M.B. Saidutta, and Harshini Dasari., "Dilatometer Studies on LAMOX Based Electrolyte Materials for Solid Oxide Cells.**"** *Materials Chemistry and Physics* **(IF 3.4)**

Conference Proceedings

6. **Irfana Shajahan** et al. (2020). "Dilatometer studies of praseodymium doped ceria by reverse strike co-precipitation method," on "International Conference on Electrochemistry in Industry, Health, and Environment" January 21st – 25th, 2020, Mumbai, India.

BIODATA

Name   : **Mrs. Irfana Shajahan**

PERSONAL DETAILS

Date of Birth   25/08/1990

Address   36/1516A, Parakkat House, Judges Avenue, Sebastian Road,
                        Kaloor, Kochi,Kerala
                        Pin-682017

Mobile   +91-8296060434

Email id   irfana.shajahan1990@gmail.com

EDUCATION

2016 – Till Date   **Ph.D. in Chemical Engineering**
                        National Institute of Technology Karnataka, Surathkal
                        Department of Chemical Engineering
                        Research topic: Solid Oxide Fuel cells, Electrolyte Materials for SOFCs, Solid
                        Oxide Electrolysis Cells, Nanomaterials
                        (CGPA 8.67)

2015-2013   **M-Tech in Chemical Engineering**
                        Manipal Institute of Technology Manipal
                        Department of Chemical Engineering
                        Research topic: Plant Design, Nano materials
                        (CGPA 9.53)

2008-2012   **B-Tech in Chemical Engineering**
                        T.K.M. College of Engineering, Kollam (Kerala University)
                        Department of Chemical Engineering
                        (CGPA 7.62)

PUBLICATION DETAILS

International Journals   **03 (Accepted)**

International Conference   **01**

Conference Proceedings   **01**